SAND2018-4555PE

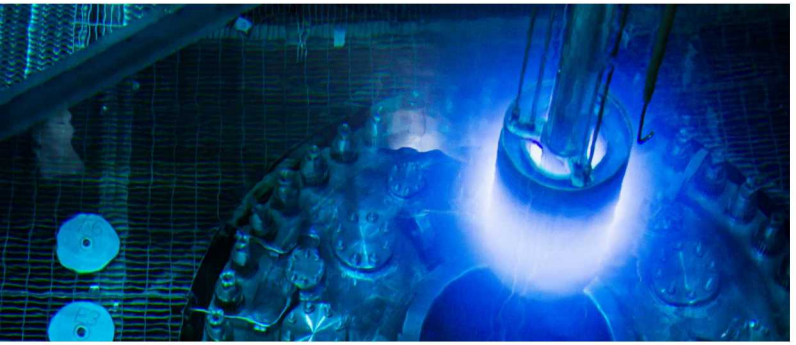
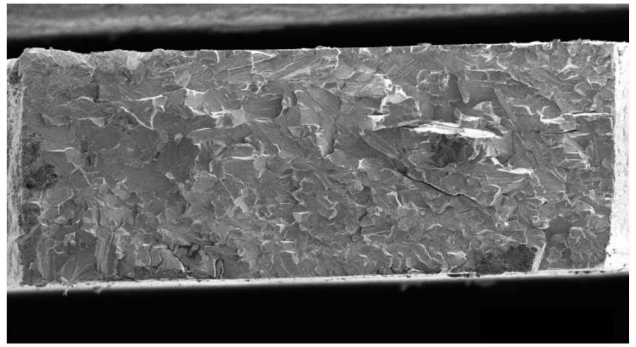
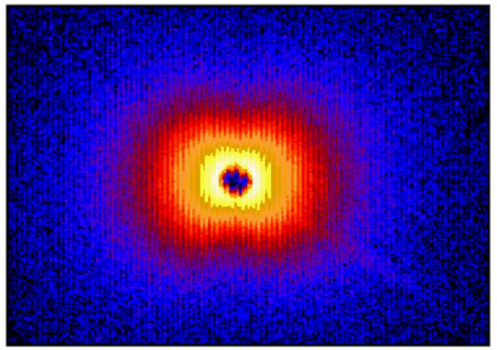
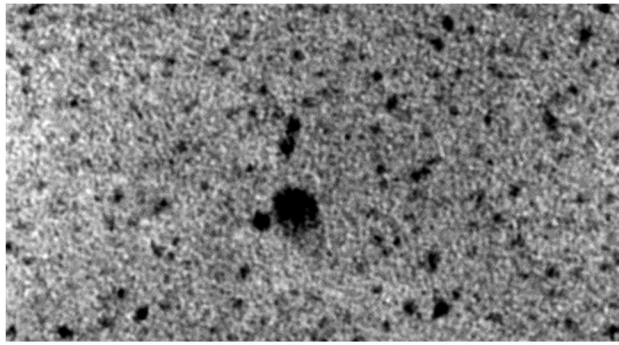

Radiation tolerance of FeCrAl alloys for light water reactor fuel cladding applications

Presented by:

Dr. Samuel A. Briggs

Sandia National Laboratories is a multimission laboratory managed and operated by National Technology and Engineering Solutions of Sandia, LLC, a wholly owned subsidiary of Honeywell International, Inc., for the U.S. Department of Energy's National Nuclear Security Administration under contract DE-NA0003525.


Dr. Todd Allen
Dr. Kumar Sridharan
PNNL
INL
Oregon State University (2007-2011)
University of Wisconsin – Madison (2011-2016)
Oak Ridge National Laboratory (2015-2016)
Sandia National Laboratories (2017-Present)
Dr. Khalid Hattar
Dr. Kevin Field
THE UNITED STATES
PHYSICAL
LAMBERT CONFORMAL CONIC PROJECTION

Reactor Materials Challenges

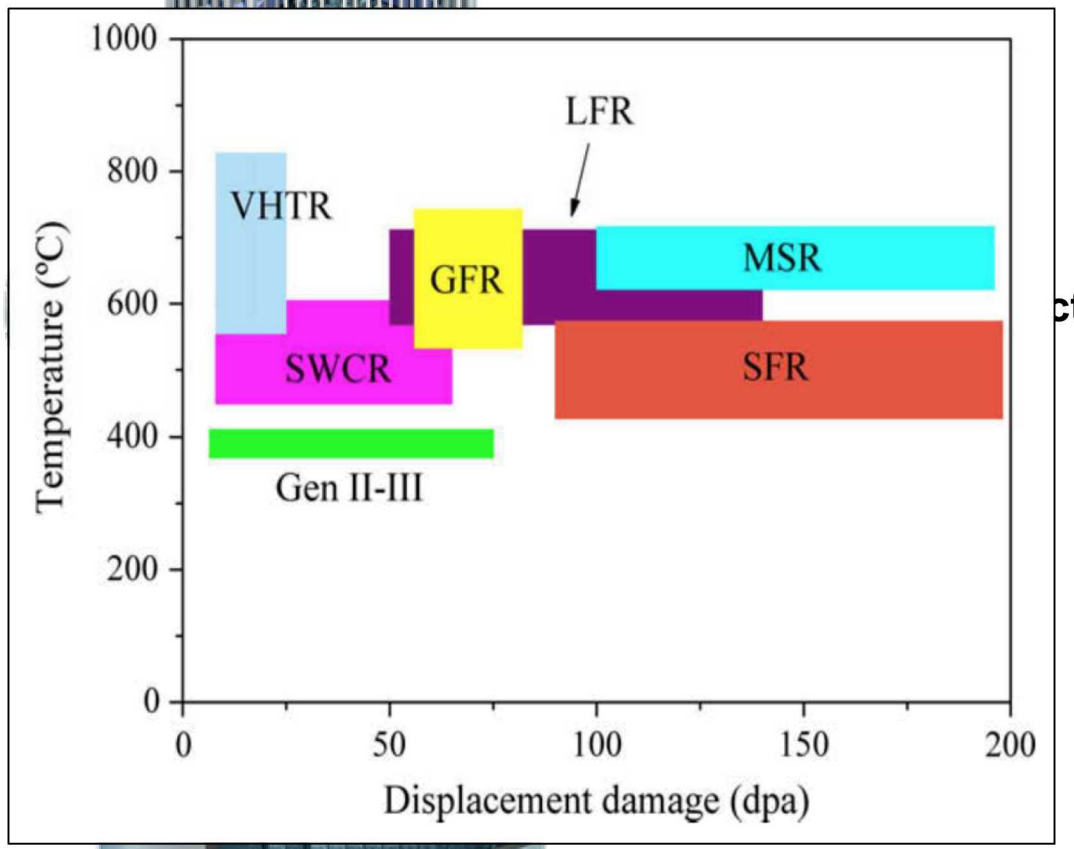

- Nuclear reactors are one of most demanding environments for materials performance
  - High temperatures
  - Corrosive coolants
  - Radiation displacement damage
  - Fission products and nuclear transmutation

- Long-term operation of next-generation reactor designs promise to push our understanding of materials degradation in these environments to its limits

[1] Lambert, T. and Nghiem, X.H., 2015. PAM Review: Energy Science & Technology, 1, pp.90-108.

Reactor Materials Challenges

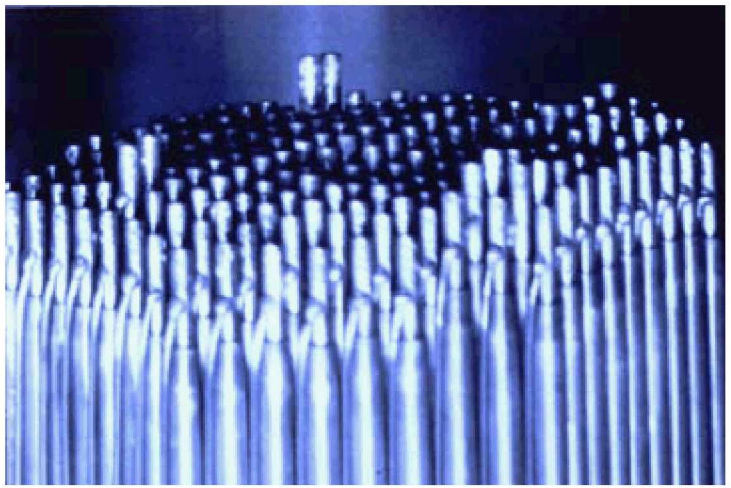

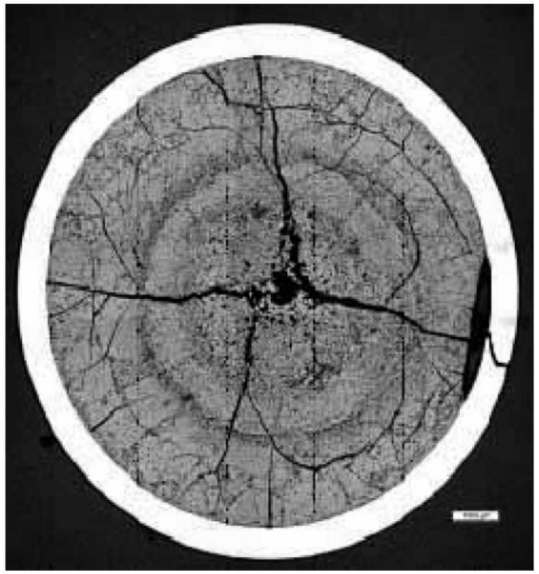

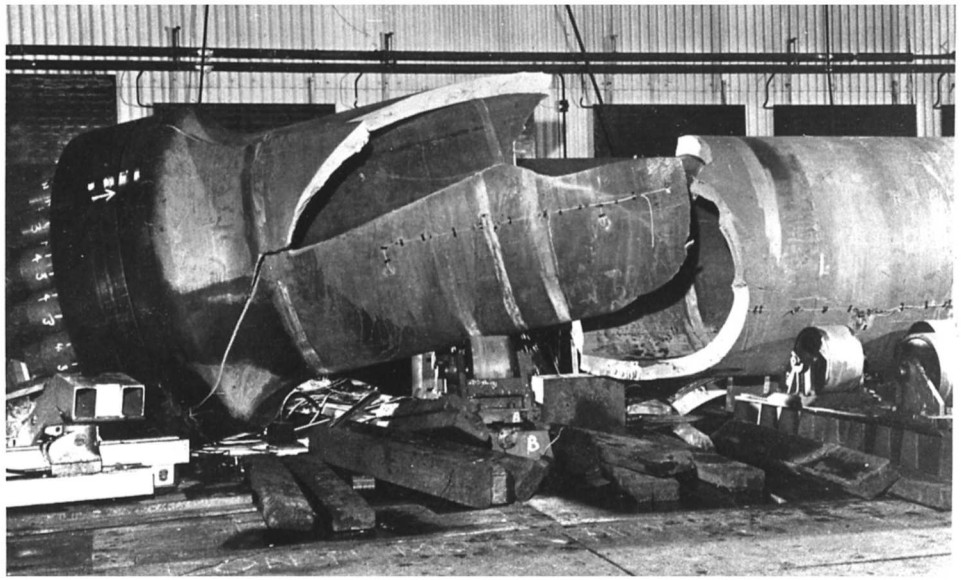

- **Changes in local microstructure and chemistry leads to macroscopic changes in properties and performance and potential failures**
  - Top left: Void swelling in a 316 SS cladding tube following irradiation to high fluences in the Fast Flux Test Facility
  - Top right: Failure of a UO_2/Zr-4 fuel rod due to stress corrosion cracking, leading to fission product release
  - Bottom: Catastrophic failure of pressure vessel during hydrostatic testing due to improper postweld heat treatment

Motivation: Accident Tolerant Fuel Forms

- Fukushima accident has demonstrated that Zircaloy cladding is detrimental in Loss of Coolant Accident (LOCA) scenarios
  - Exothermic oxidation reaction with H_2O produces H_2 gas

- DOE-NE has funded development of accident-tolerant fuel (ATF) and fuel claddings
  - **Fe-Cr-Al Claddings**
  - SiC/SiC Composite Claddings
  - SiC/Cr/MAX-phase Coatings for Zr
  - High-density/high-conductivity fuels (UN, U_3Si_2)

$$Zr + 2H_2O \rightarrow 2H_2 + ZrO_2 + Heat$$

Fe-Cr-Al Alloys for Nuclear Systems

- Why is Fe-Cr-Al attractive as a LWR cladding material?
  - Exceptional high temperature oxidation resistance due to formation of passivating Al_2O_3 (up to 1200-1475 °C)
  - High strength, with potential for oxide-dispersion strengthened variants
  - Low swelling rates in irradiation environments
  - Potential for near-term deployment

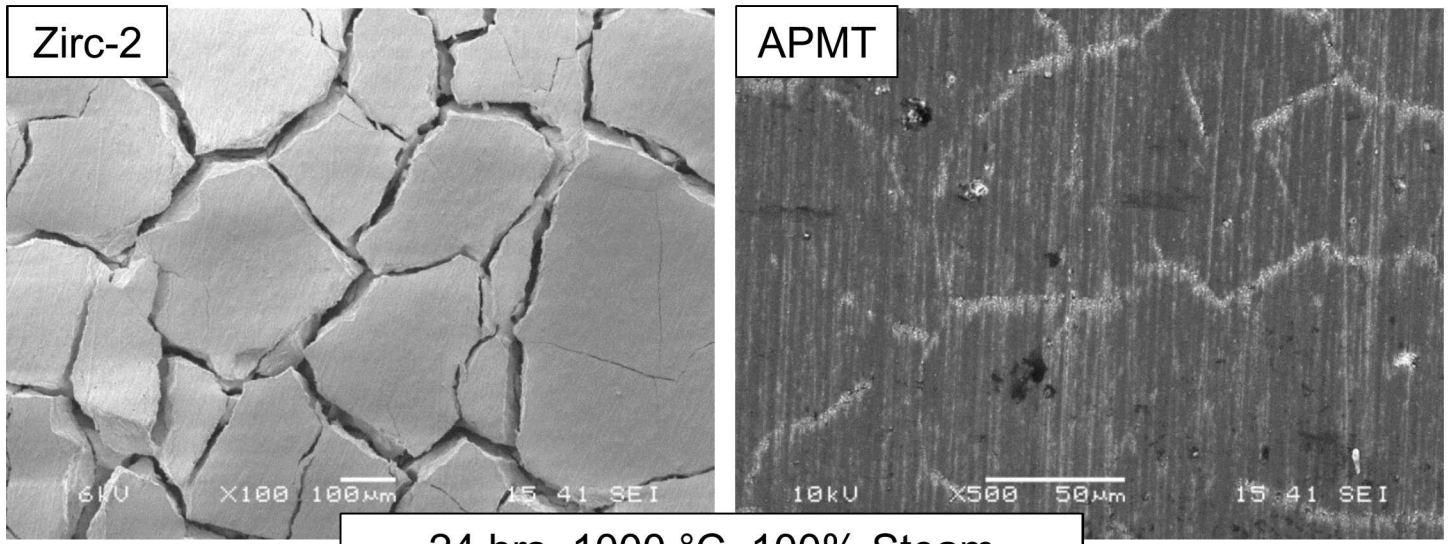

24 hrs, 1000 °C, 100% Steam

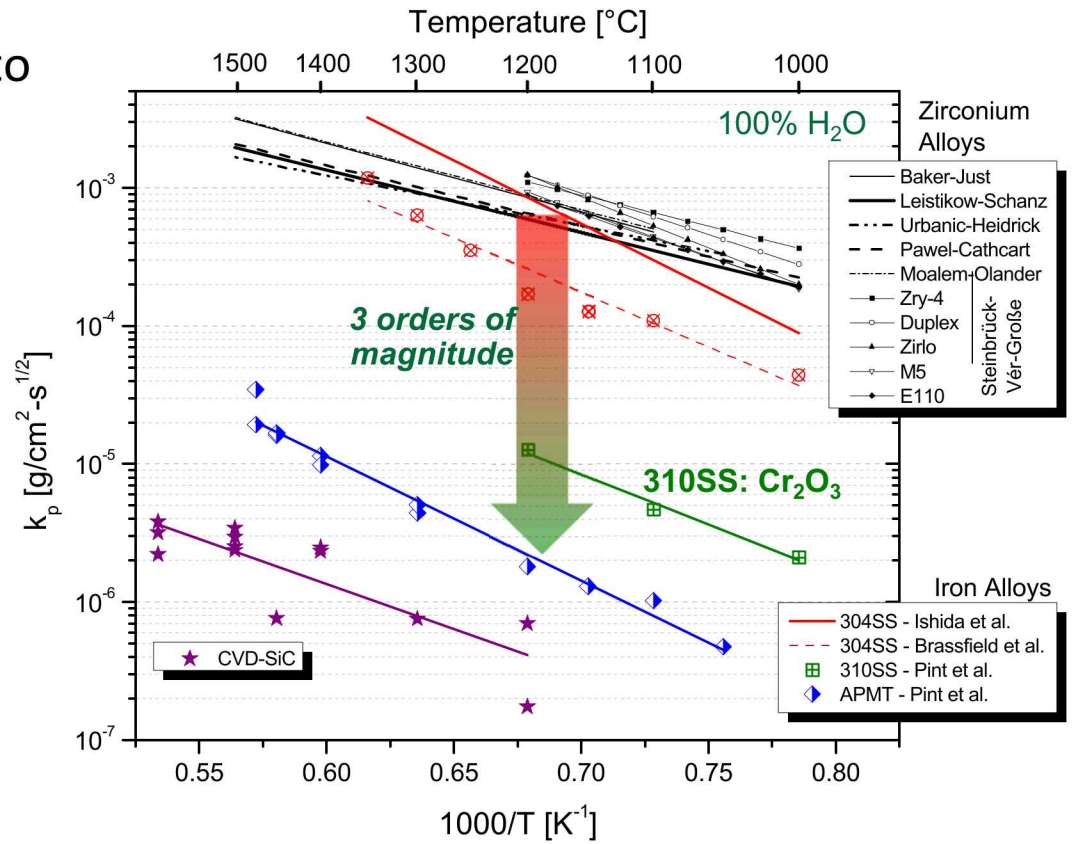

Fe-Cr-Al Cladding Design Campaign

- Multidisciplinary design problem, numerous performance metrics
- Primarily involved in assessing radiation tolerance
  - Gen. I model ternary alloys
  - Gen. II ODS variants

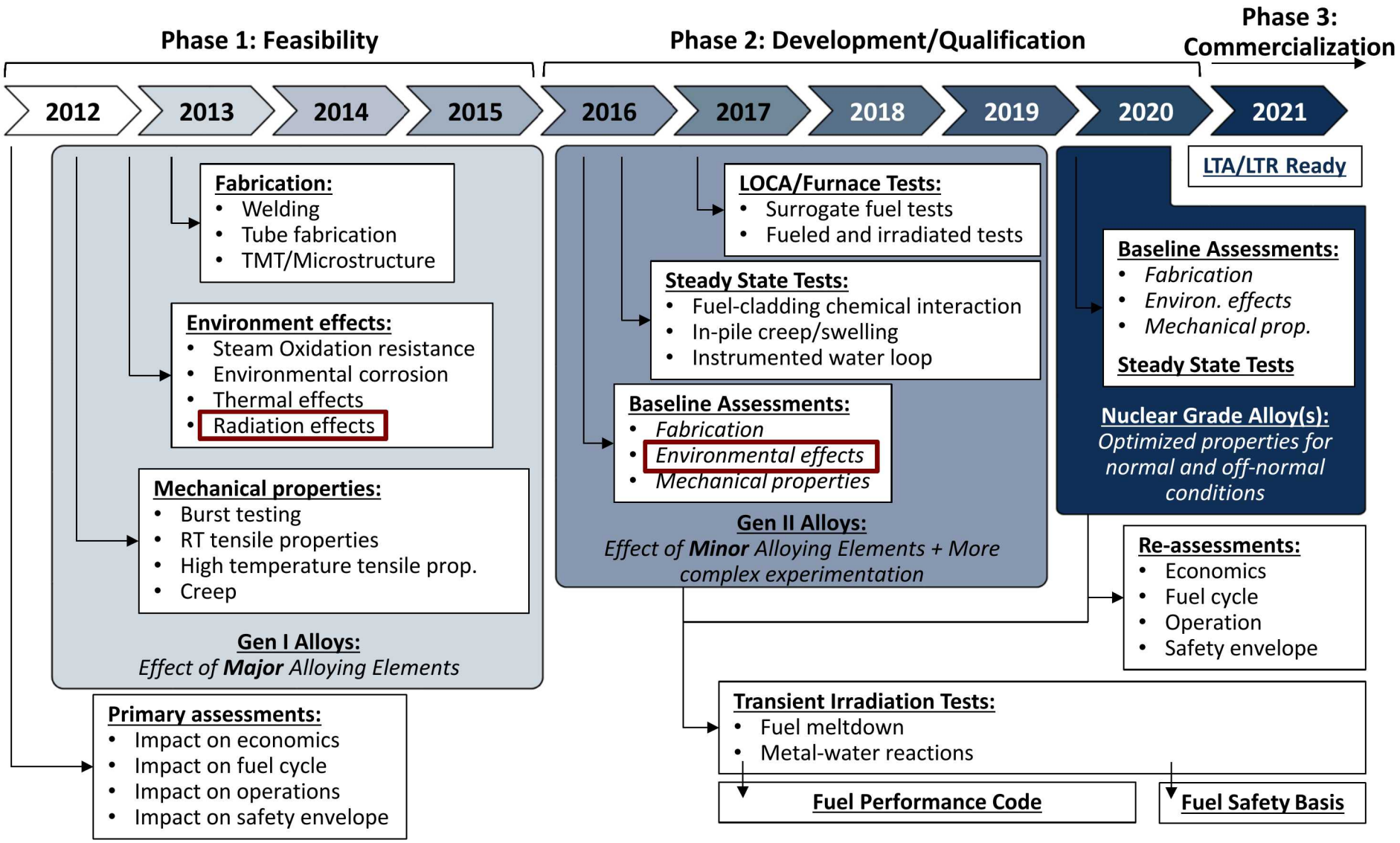

Radiation Damage in Materials

- Incident particles impart energy to lattice atoms causing a displacement damage cascade, ultimately resulting in the formation of point defects
- These point defects then diffuse and agglomerate into organized microstructural and microchemical features

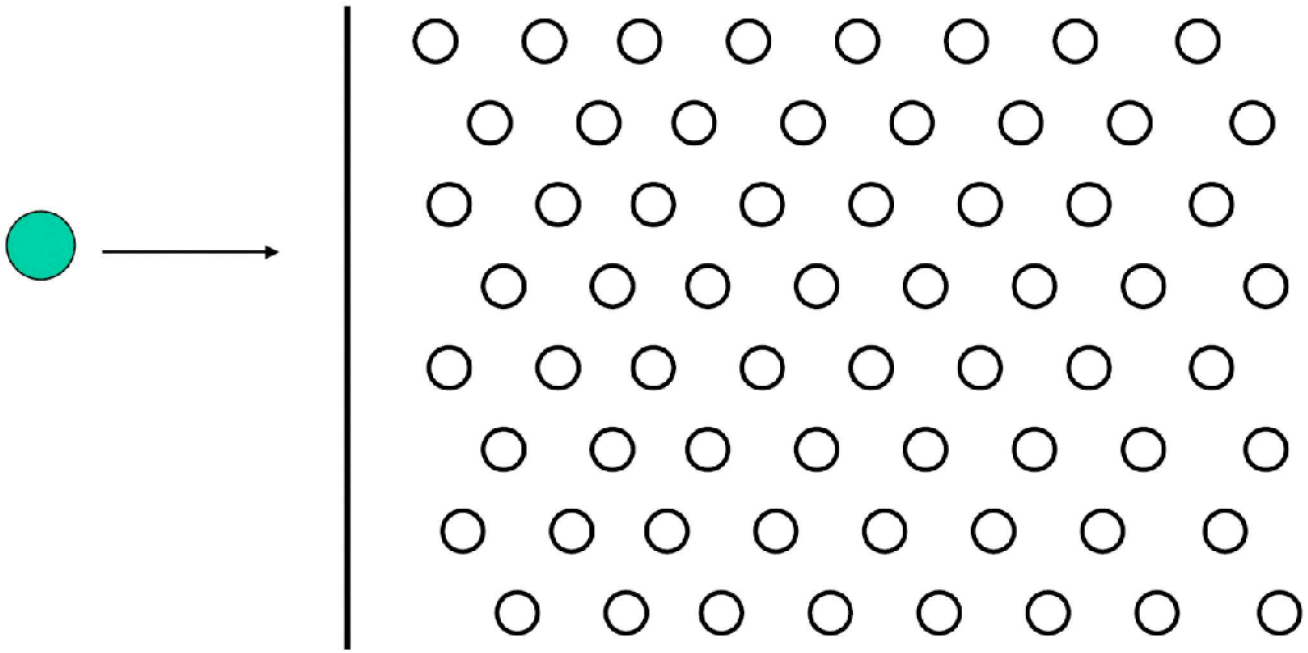

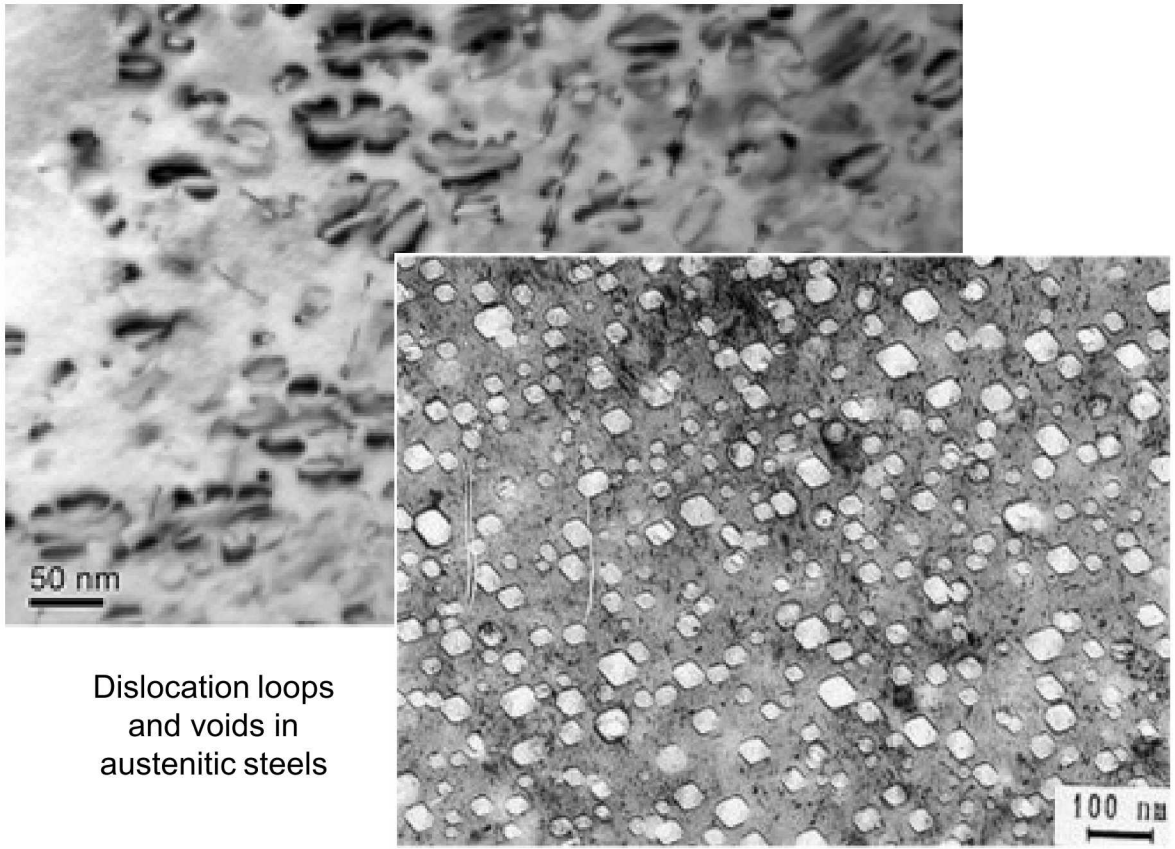

Dislocation loops and voids in austenitic steels

[1] R.W. Fuller, et al. (2016). Fatigue life predictions for irradiated stainless steels considering void swellings effects. *Engineering Failure Analysis*, 59, 79-98.
[2] Z.-C. Zheng, et al. (2017). Evolution of Dislocation Loops in AL-6XN Stainless Steels Irradiated by Hydrogen Ions. *Acta Metallurgica Sinica,* 30(1), 89-96.

Radiation Damage in High-Cr Ferritics

- While ferritic alloys are known to possess excellent swelling resistance, they have a perceived susceptibility to irradiation-induced hardening and embrittlement

- For low Cr alloys, hardening is primarily due to the formation of dislocation loops

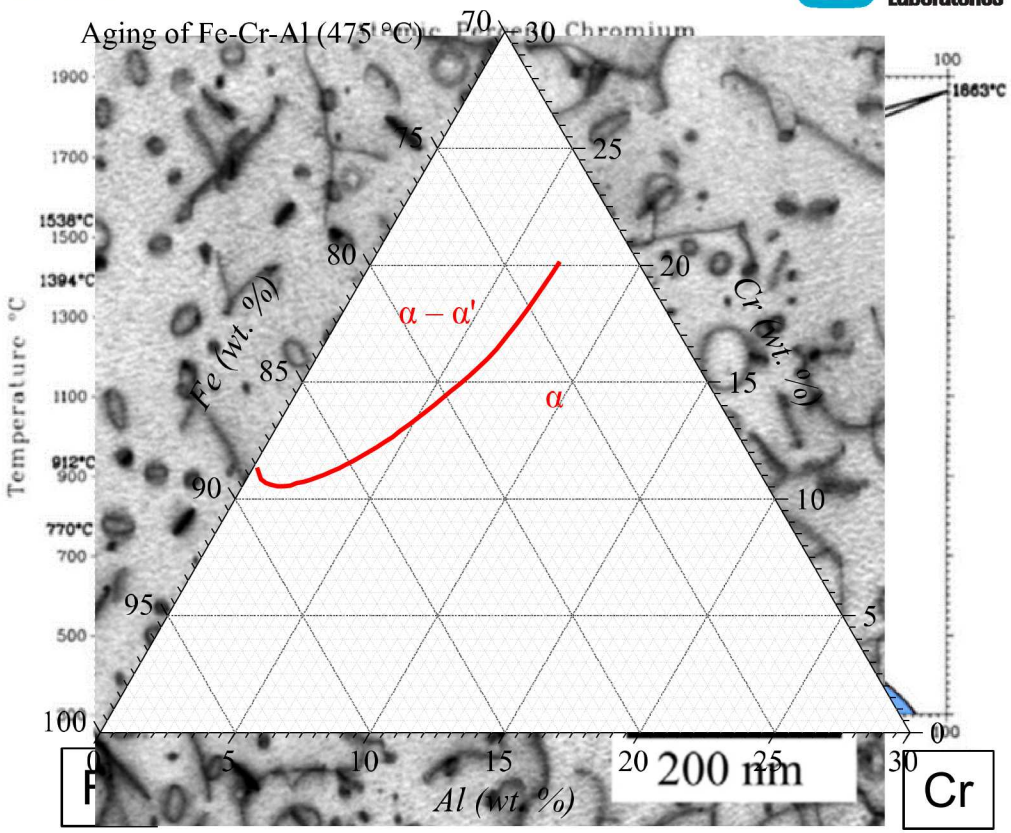

- Above 8-9 wt.% Cr, radiation-enhanced precipitation of Cr-rich α′ dominates the radiation-induced hardening and embrittlement response
  - α′ phase is stable at temperatures below ~475-500 °C
  - Irradiation-enhanced diffusion effects allow the phase to form at LWR-relevant temperatures (300-350 °C) where diffusion kinetics are typically slow

Kobayashi, S., & Takasugi, T. (2010). Mapping of 475C embrittlement in ferritic Fe-Cr-Al alloys. *Scripta Materialia*, 63(11), 1104–1107.

ODS FeCrAl Alloy Development

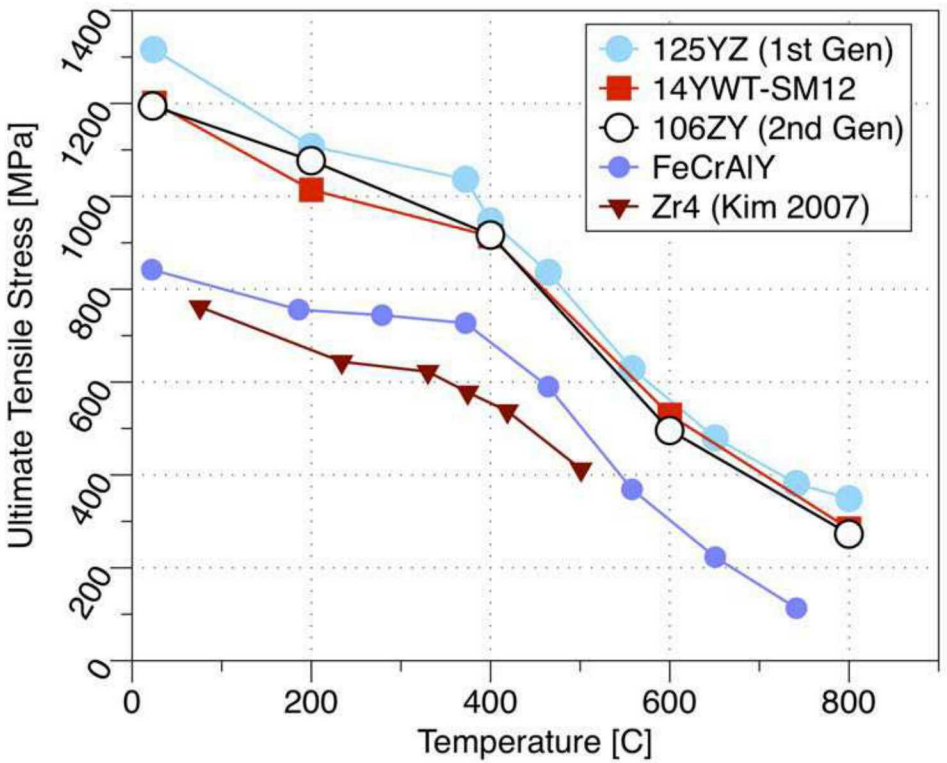

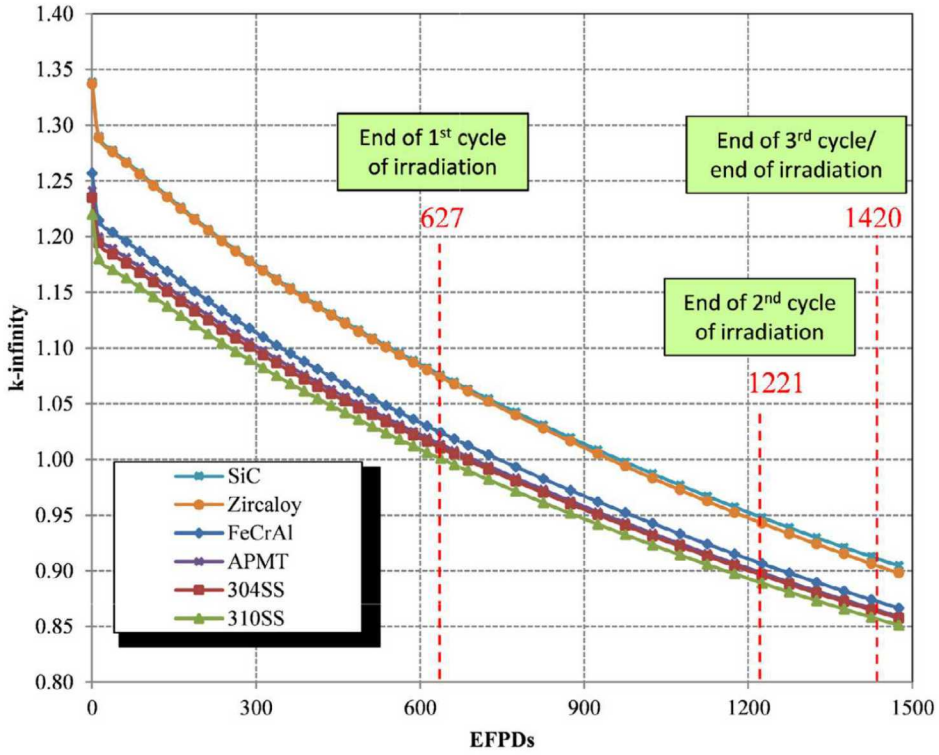

- Exhibit high strength at elevated temperatures, excellent oxidation and corrosion resistance, high thermal conductivity, low thermal expansion and good void swelling resistance
- Nanoparticles could lead to high irradiation resistance due to a higher density of defect sinks compared to wrought FeCrAl alloys
- Improved strength allows for thinner cladding wall thickness, improved neutron economy

N.M. George, et al. “Neutronic analysis of candidate accident-tolerant cladding condepts in pressurized water reactors.” Ann. Nucl. Energy **75** (2015) 703-712.

HFIR Irradiation: FCAY and FCAT Rabbits

- Alloys studied:
  1. Model alloys (M): F1C5AY, B125Y, B154Y-2, B183Y-2
  2. Engineering grade alloys (E): C06M, C35M, C36M, C37M, C35MN, C35M10TC
  3. Commercial alloys (C): Kanthal APMT™, and Alkrothal 720
  4. ODS Alloys (O): 125YF
- SS-J2 and SS-2E flat sheet tensile specimen geometries
- Design temperatures of 200-550 °C
  - Temperature monitored passively using SiC thermometry

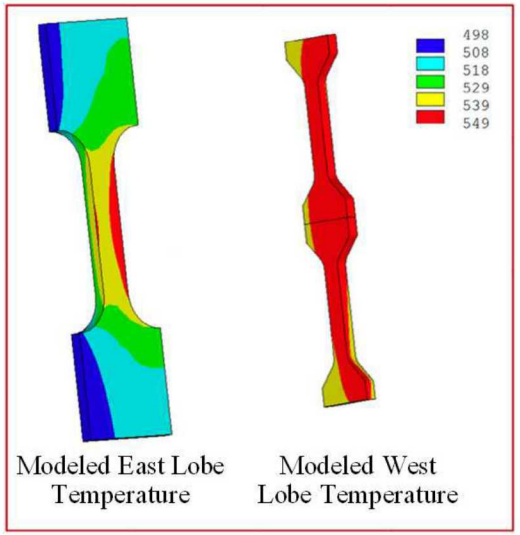

Example of specimen temperature gradients for 550°C irradiation

Capsule ID	Alloys	Exposure Time (hrs)	Neutron Fluence (n/cm^2) E > 0.1 MeV	Dose Rate (dpa/s)	Dose (dpa)	Irradiation Temperature (°C)
FCAY-01	M+C	120	3.69×10^{20}	7.7×10^{-7}	0.3	334.5 ± 0.6
FCAY-02	M+C	301	9.25×10^{20}	7.7×10^{-7}	0.8	355.1 ± 3.4
FCAY-03	M+C	614	1.95×10^{21}	8.1×10^{-7}	1.8	381.9 ± 5.4
FCAY-04	M+C	2456	7.73×10^{21}	7.9×10^{-7}	7.0	319.9 ± 10.2
FCAY-05	M+C	4914	1.55×10^{22}	7.8×10^{-7}	13.8	340.5 ± 25.7
FCAT-01	E+O	548	2.17×10^{21}	9.6×10^{-7}	1.9	194.5 ± 37.9
FCAT-02	E+O	548	2.05×10^{21}	9.1×10^{-7}	1.8	362.7 ± 21.2
FCAT-03	E+O	548	2.17×10^{21}	9.6×10^{-7}	1.9	559.4 ± 28.1

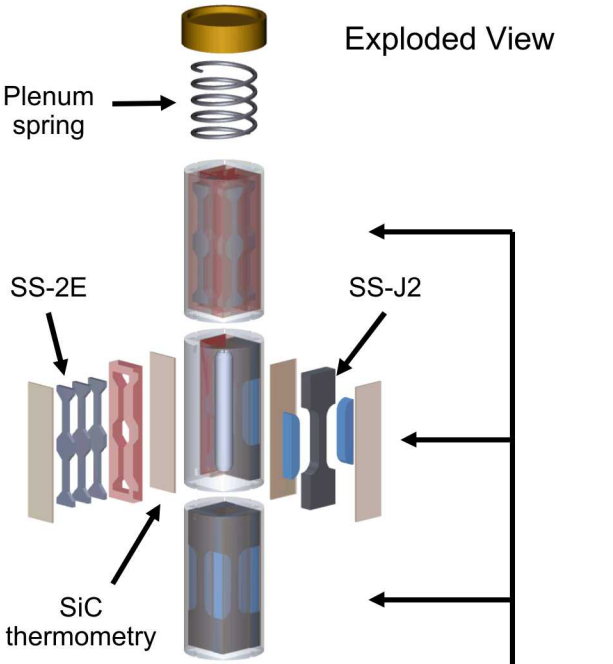

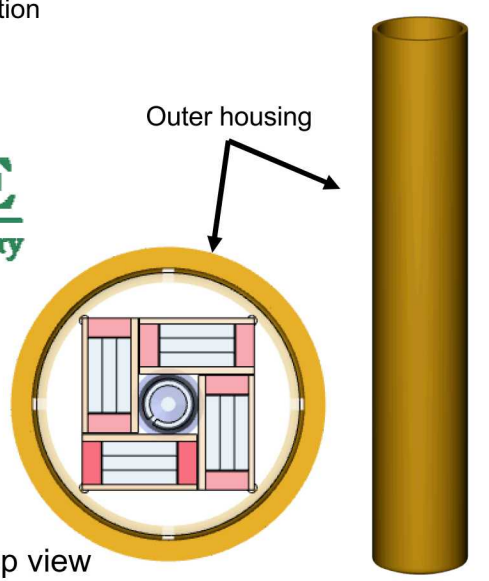

Finalized FCAT capsule design

Sample Handling Logistics

- Neutron-irradiated samples pose a significant radiological hazard
- Optimized workflow maximizes scientific yield while minimizing personnel exposure

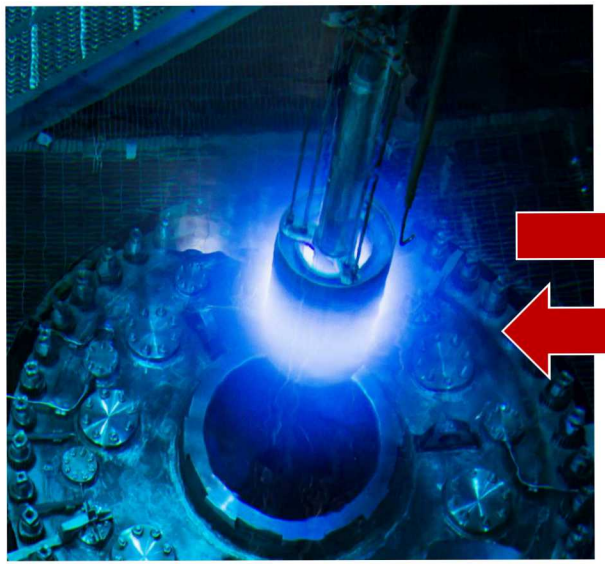

HFIR

- Sample Irradiation
- SANS

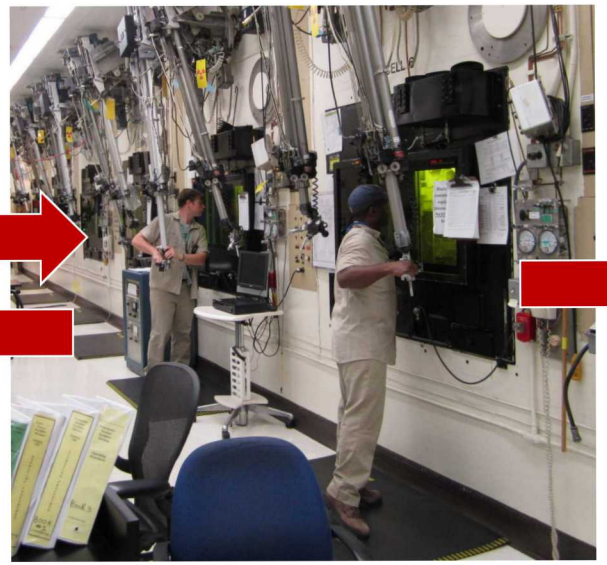

IMET Hot Cells

- Tensile Testing
- Sectioning

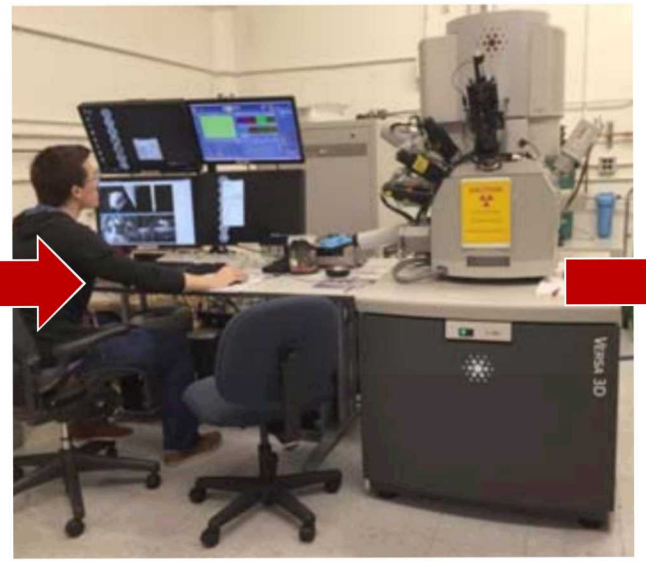

LAMDA Laboratory

- Metallography
- FIB Sample Prep

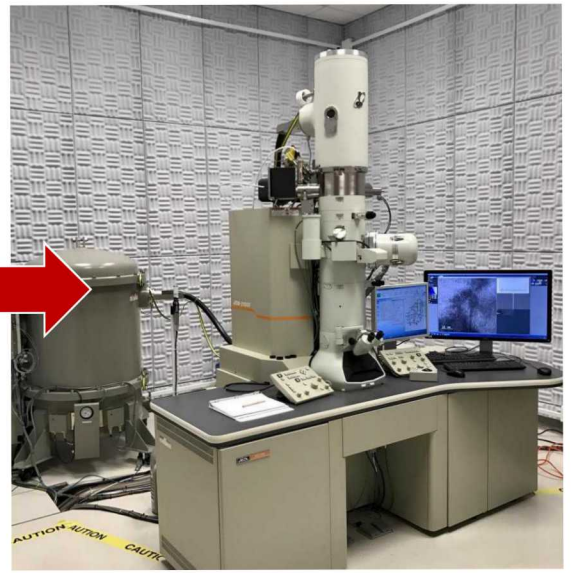

Microscopy & Analysis

- TEM/STEM
- APT

Atom Probe Tomography

- Destructive analysis – field evaporates atoms from cryo-cooled, sharp needle specimen using localized high voltage pulses coupled with focused laser pules
- Can reconstruct specimen geometry in 3D using ion time-of-flight (TOF) and position-sensitive detector – allows for detailed elemental analysis
- Most comprehensive α' analysis method – yields data regarding phase morphology, distribution and composition

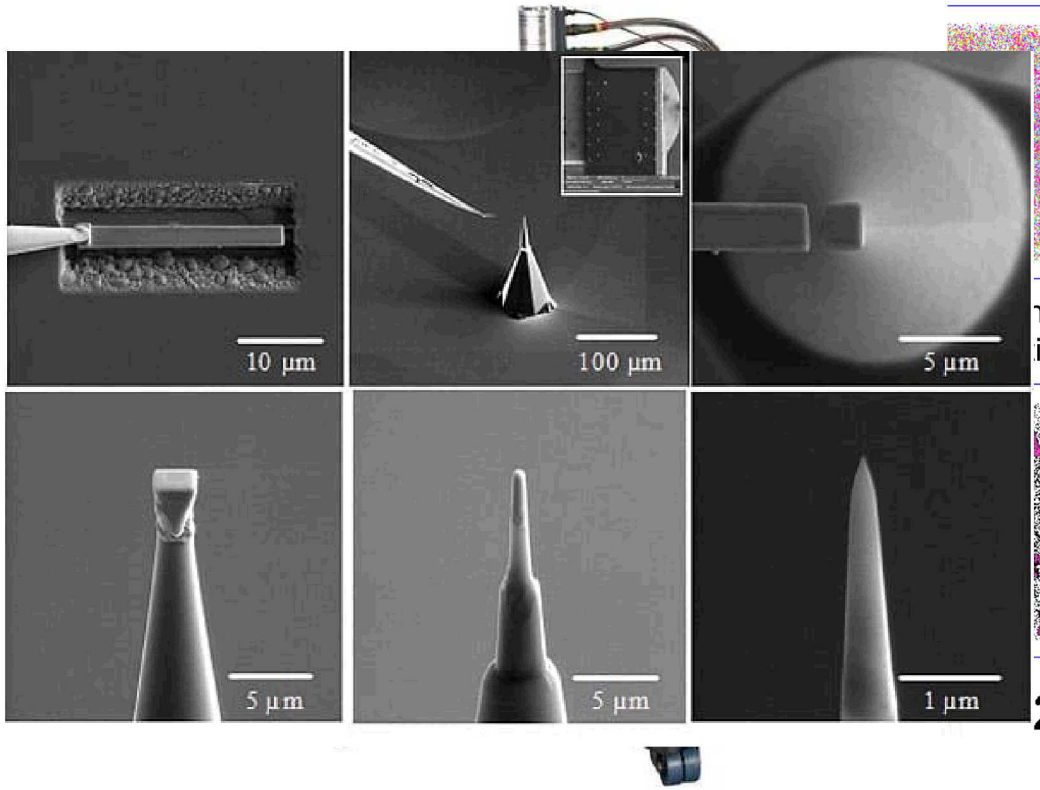

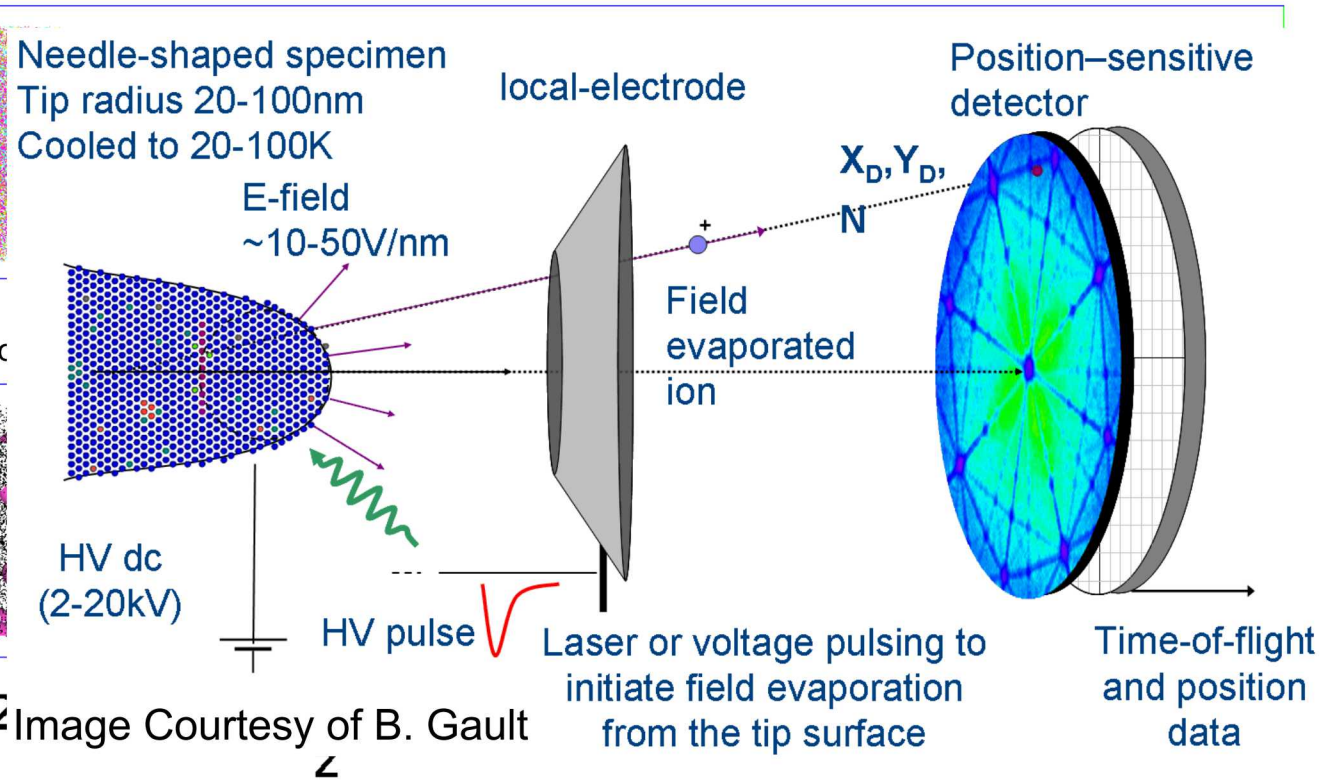

Image Courtesy of B. Gault

Small Angle Neutron Scattering

- Non-destructive analysis – incident neutron beam scatters off of nuclei in a specimen and produces a 2D diffractogram

- Analysis of diffractogram provides insight into bulk material microstructure – microstructural features of different length scales and chemistries will scatter neutrons differently

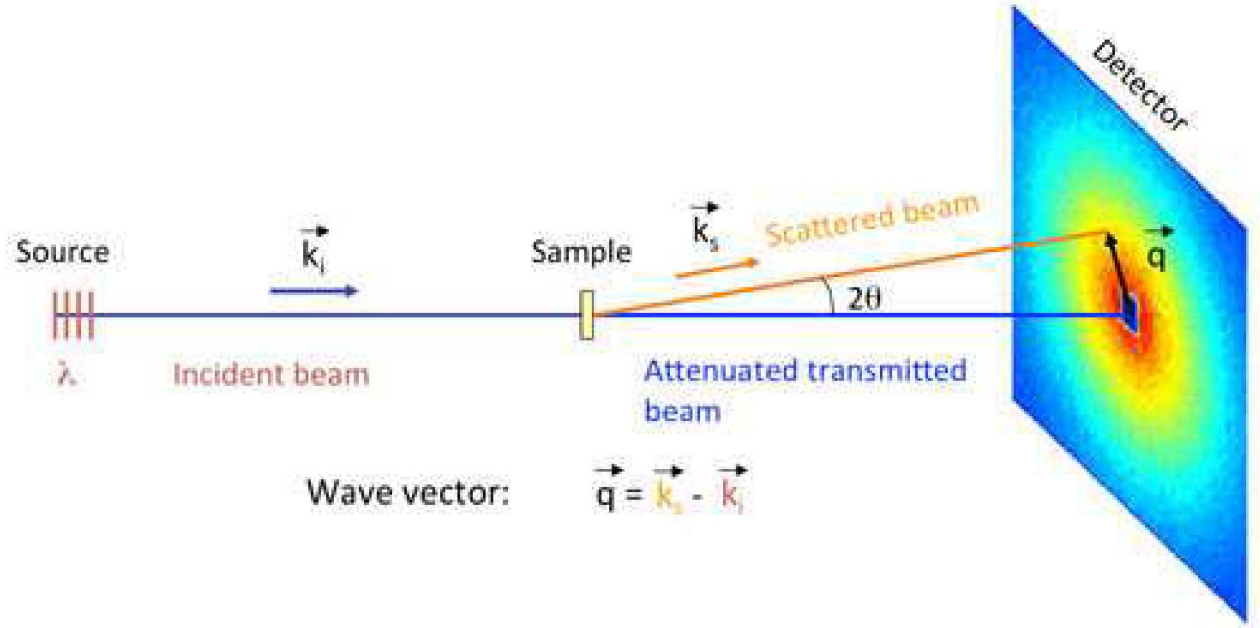

Analytical Transmission Electron Microscopy

- Incredibly flexible microanalysis technique, but requires extremely thin specimens (<100 nm)
- Works similarly to an overhead projector, but uses electrons as a “light” source
- Analysis of x-rays produced by excited atoms (EDS) or energy loss of transmitted electrons (EFTEM/EELS) provides insight into local chemistry

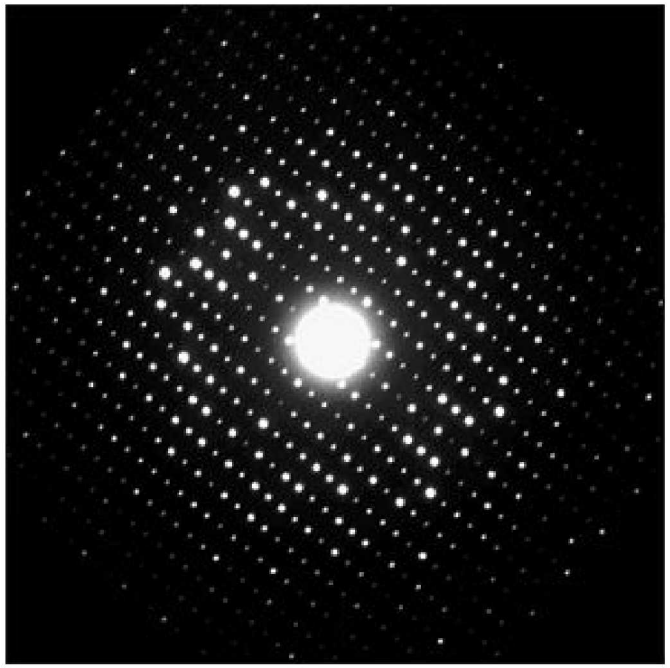

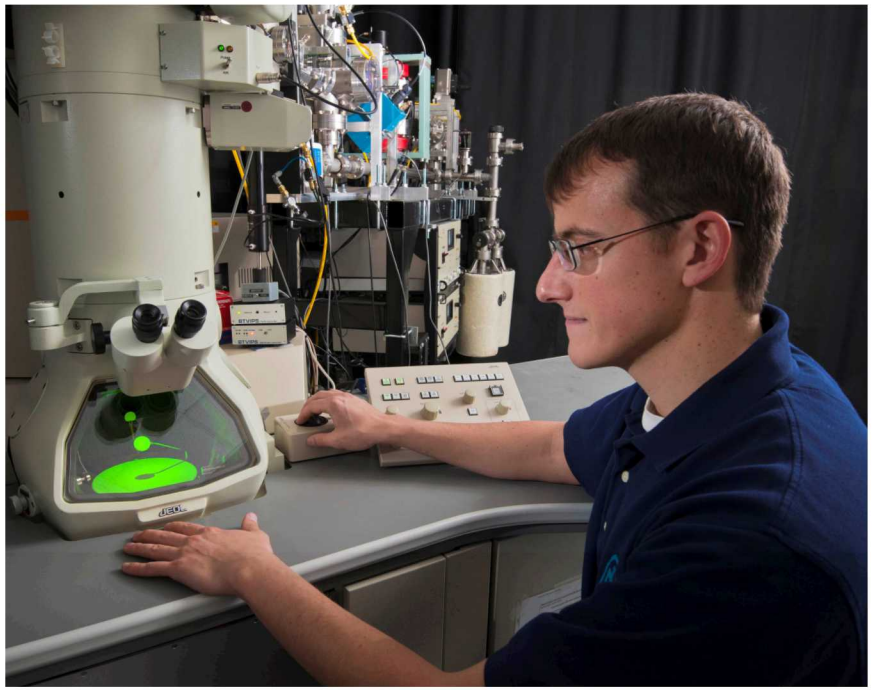

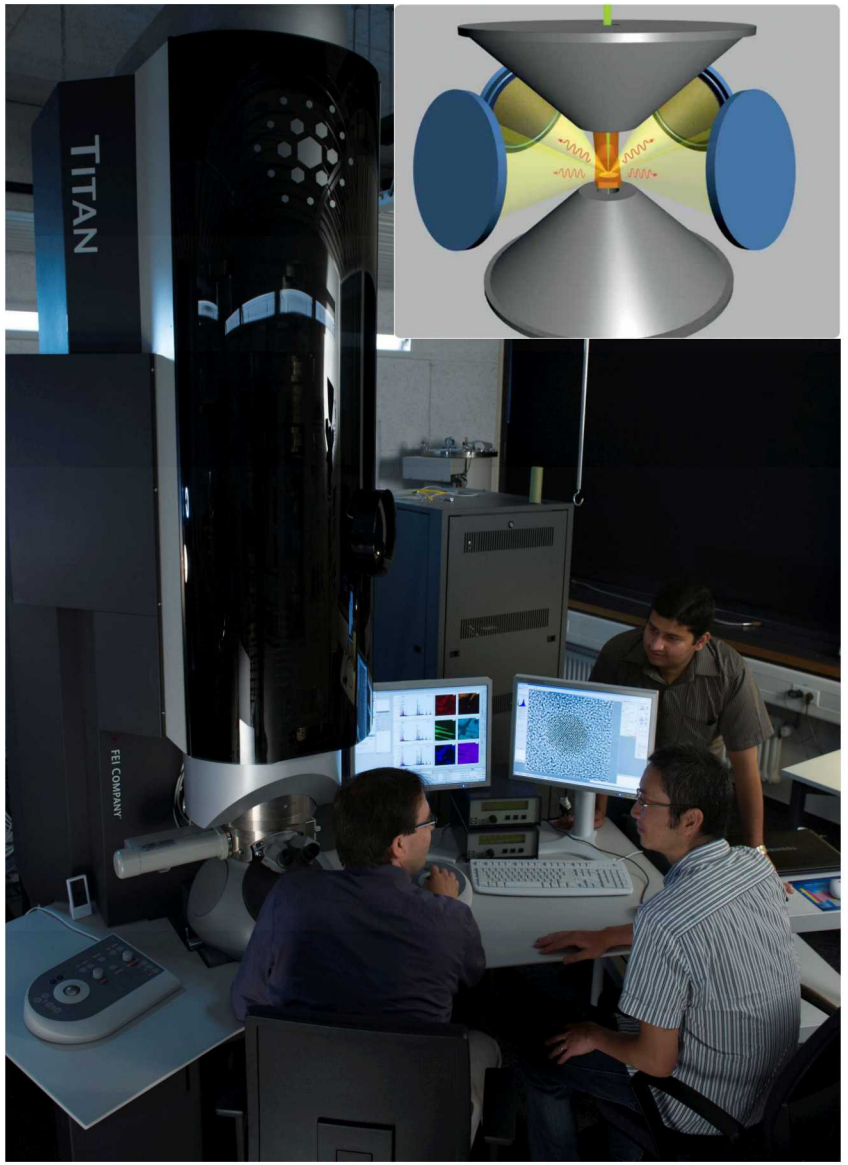

Characterization techniques for precipitates

Sandia National Laboratories

	Advantages	Disadvantages
Analytical TEM (STEM/EDS & EFTEM)	• Reveals microstructural heterogeneities • Quick/easy to perform • Direct microstructure observation	• Poor signal to noise ratio; can limit resolution • Moderate volume analyzed • Dependent on sample quality • Limited composition information
Small Angle Neutron Scattering (SANS)	• Large sampling volume; excellent counting statistics • Limited to no sample prep • Quick/easy to perform • Composition can be inferred (magnetic SANS only)	• Indirect microstructure observation • No microstructural relationships (i.e. assumes homogenous distributions) • Requires bulk sample; increased radioactivity
Atom Probe Tomography (APT)	• Composition information readily available • Excellent spatial resolution • Direct microstructure observation	• Small sample volume analyzed • Dependent on sample quality • Data interpretation can be convoluted; aberration effects • Time intensive

Characterization techniques for precipitates

Sandia National Laboratories

Complementary Techniques

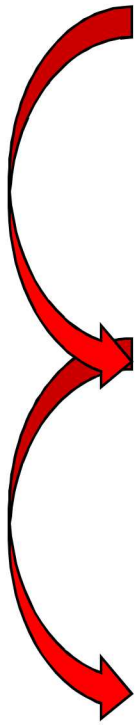

	Advantages	Disadvantages
Analytical TEM (STEM/EDS & EFTEM)	• Reveals microstructural heterogeneities • Quick/easy to perform • Direct microstructure observation	• Poor signal to noise ratio; can limit resolution • Moderate volume analyzed • Dependent on sample quality • Limited composition information
Small Angle Neutron Scattering (SANS)	• Large sampling volume; excellent counting statistics • Limited to no sample prep • Quick/easy to perform • Composition can be inferred (magnetic SANS only)	• Indirect microstructure observation • No microstructural relationships (i.e. assumes homogenous distributions) • Requires bulk sample; increased radioactivity
Atom Probe Tomography (APT)	• Composition information readily available • Excellent spatial resolution • Direct microstructure observation	• Small sample volume analyzed • Dependent on sample quality • Data interpretation can be convoluted; aberration effects • Time intensive

α’ Precipitation in Gen. I Fe-Cr-Al Model Alloys

Experimental Design

- Four Fe-(10-18)Cr-(5.8-9.3)Al+Y (at.%) model alloys have been selected for initial investigation
  - Y is added to enhance adhesion of Al_2O_3 scale

ID	Composition, at.%							
	Fe	**Cr**	**Al**	**Y**	C	S	O	N
Fe-10Cr-9.3Al	**80.46**	**10.15**	**9.34**	**0.023**	0.022	0.0016	0.0043	0.0011
Fe-12Cr-8.7Al	**79.13**	**12.16**	**8.66**	**0.016**	0.022	0.0021	0.0056	0.0034
Fe-15Cr-7.7Al	**76.92**	**15.33**	**7.70**	**0.021**	0.022	0.0007	0.0083	0.0026
Fe-18Cr-5.8Al	**76.15**	**18.00**	**5.81**	**0.010**	0.022	0.0010	0.0050	0.0042

- Model alloys were fabricated by arc-melting pure element feed stocks and pre-alloyed Al-Y specimens. After arc-melting the model alloys were hot forged/rolled and heat treated to control the grain size to 20-50 µm.[1]

- Warm rolling with a 10% thickness reduction was used to flatten the model alloy sheet samples prior to machining.

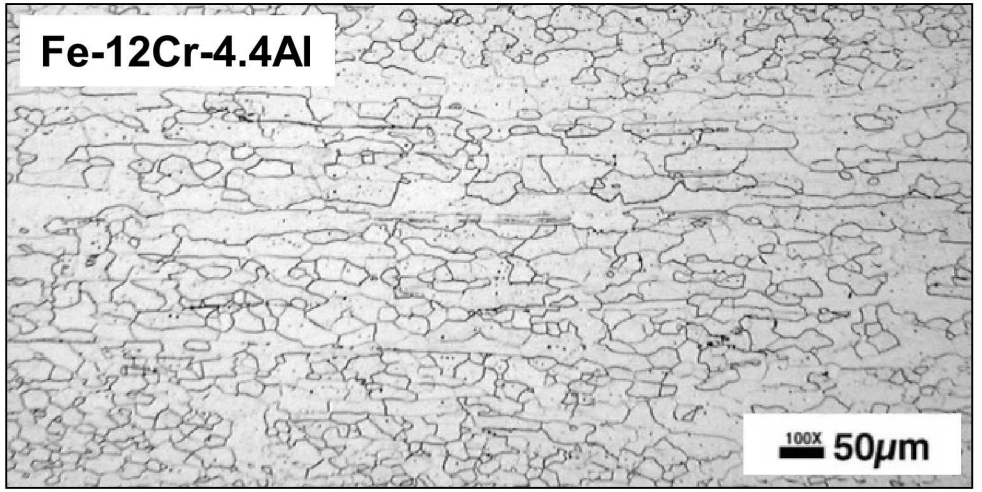

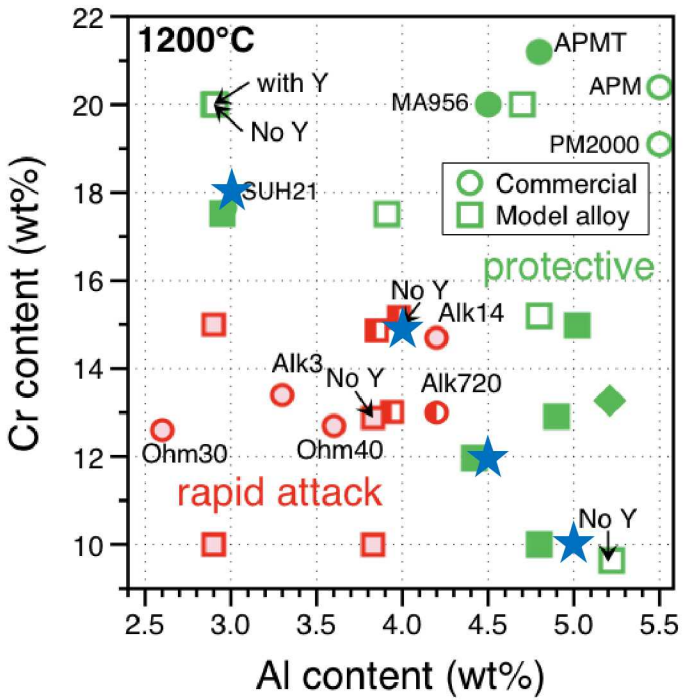

High temperature oxidation of model Fe-Cr-Al alloys exposed to steam at 1200 °C (source: B. Pint, ORNL)

[1] Yamamoto, Y., Pint, B. A., Terrani, K. A., Field, K. G., Yang, Y., & Snead, L. L. (2015). Development and property evaluation of nuclear grade wrought FeCrAl fuel cladding for light water reactors. *Journal of Nuclear Materials*, *467*, 703–716.

LEAP Data Collection

- Data collected on Cameca LEAP 4000X HR at the Center for Advanced Energy Studies (CAES) at INL and at the Center for Nanophase Materials Sciences (CNMS) at ORNL

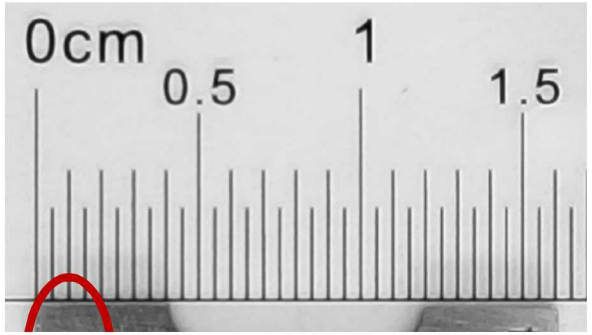

- APT samples prepared from broken half-tensile heads using FIB
  - Prepared from regions away from strained neck

- Operated in laser mode, specimen temp of 50K, pulse repetition rate of 200 kHz and laser energy of 50 pJ

- Clusters were indexed using the maximum separation method
  - d_{max} – max. separation distance between clustered atoms
  - N_{min} – minimum number of atoms required to define a cluster

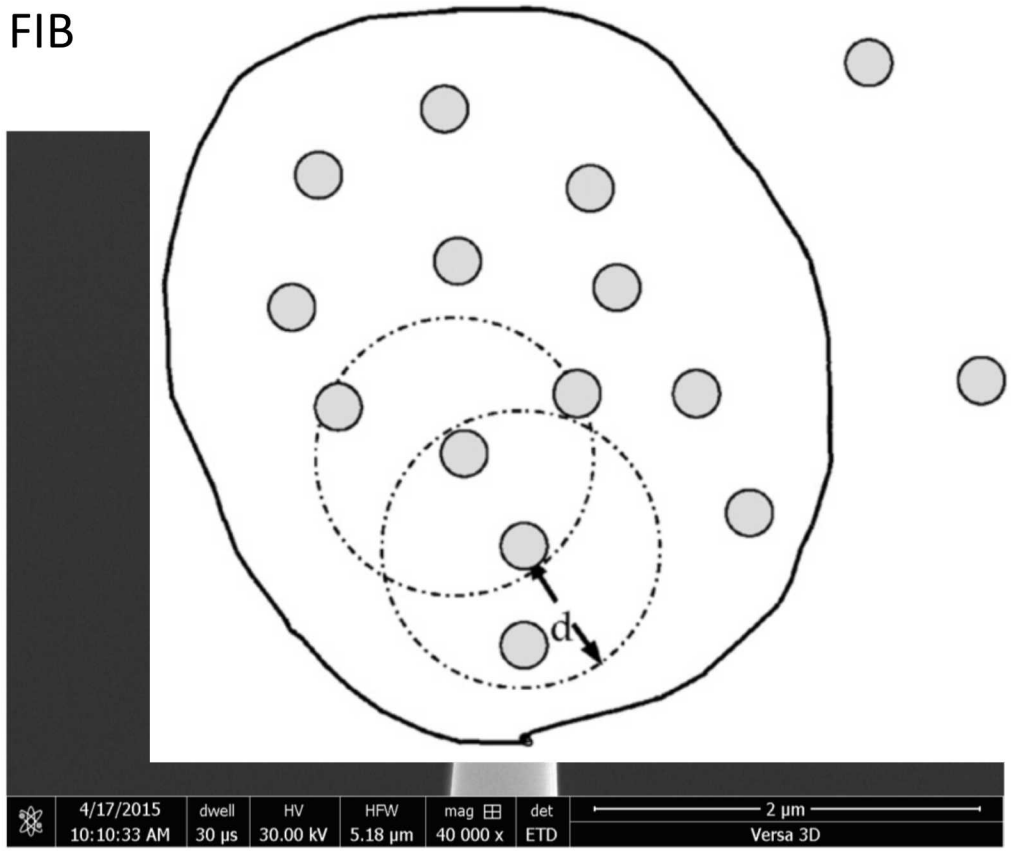

[1] Vaumousse, D., Cerezo, A., & Warren, P. J. (2003). A procedure for quantification of precipitate microstructures from three-dimensional atom probe data. Ultramicroscopy, 95(SUPPL.), 215–221.

Technique Development for APT Analysis

- Accurate deconvolution of peaks in the TOF spectrum required knowledge of isotopic composition following irradiation
  - Corrected via ORIGEN-2.2 burnup simulation
- Trajectory aberration artifacts are known to skew reported compositions due to the differences in which different phases evaporate
  - Compensated for by taking local density variation into account

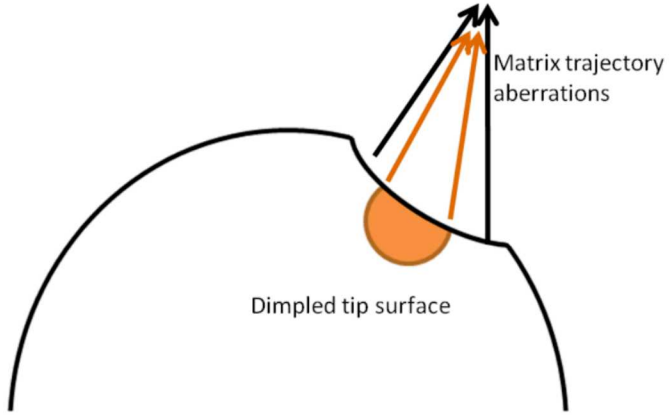

Low-Field Precipitate
High-Field Matrix

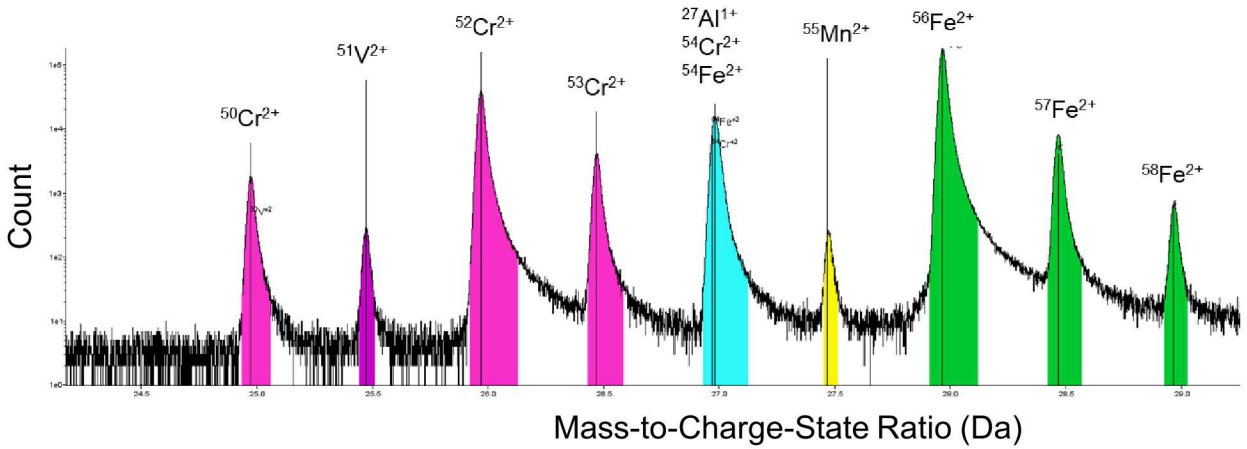

Isotope	Nat. Abun.	Mod. Abun.
^{50}Cr	4.34%	3.69%
^{52}Cr	83.79%	83.68%
^{53}Cr	9.50%	8.52%
^{54}Cr	2.37%	4.11%
^{54}Fe	5.85%	5.71%
^{56}Fe	91.75%	89.32%
^{57}Fe	2.12%	4.52%
^{58}Fe	0.28%	0.36%
^{27}Al	100%	100%

Adjusted isotopic abundances
Generated by ORIGEN-2.2

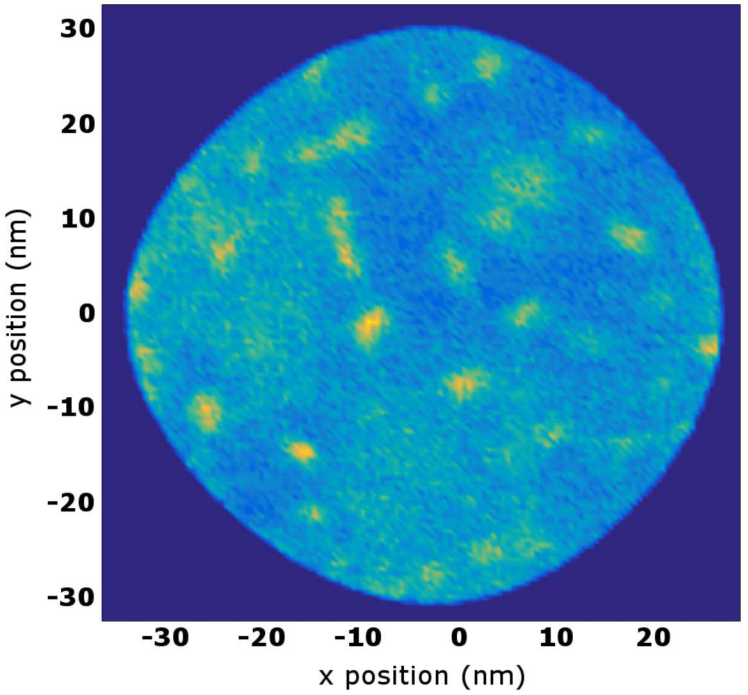

[1] A.G. Croff, (2002). ORIGEN-2.2 [Computer software]. Retrieved from https://www.oecd-nea.org/tools/abstract/detail/ccc-0371

Increasing Cr, Decreasing Al

7dpa Fe-10Cr-9.3Al

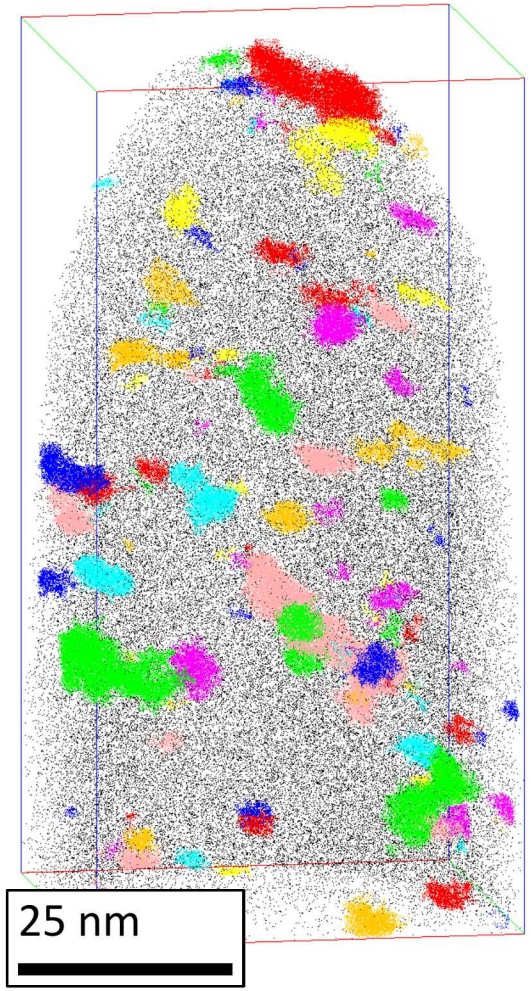

Total Volume Analyzed:
1.01×10^6 nm^3

7dpa Fe-12Cr-8.7Al

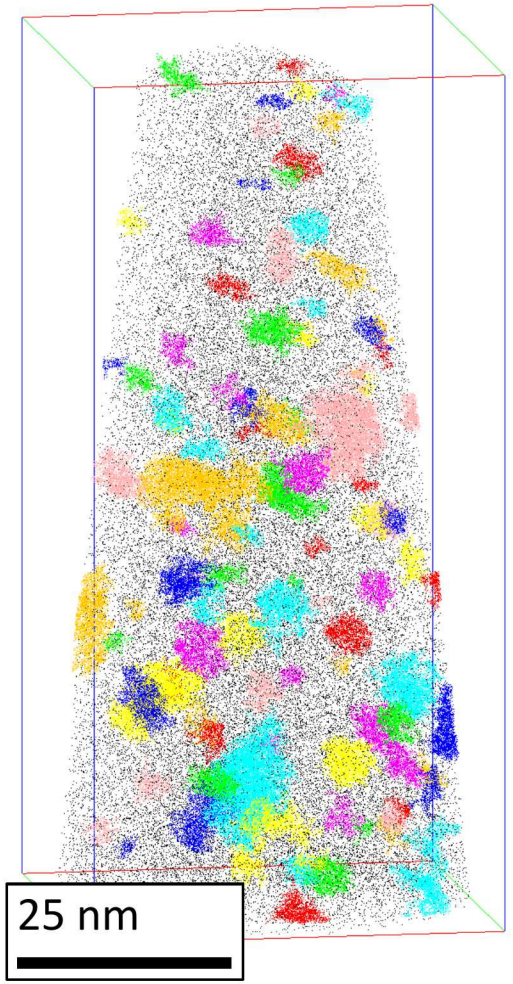

Total Volume Analyzed:
4.08×10^6 nm^3

7dpa Fe-15Cr-7.7Al

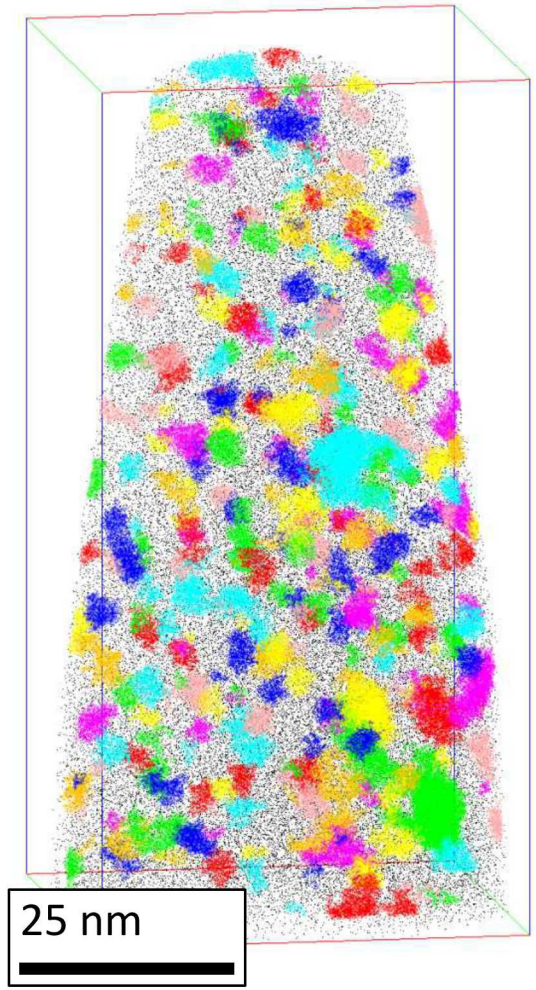

Total Volume Analyzed:
1.37×10^6 nm^3

7dpa Fe-18Cr-5.8Al

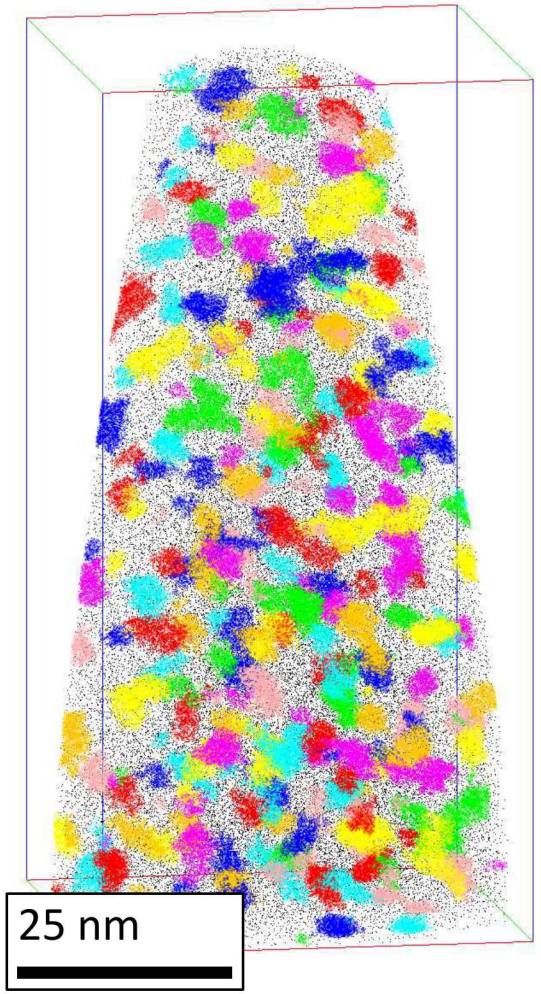

Total Volume Analyzed:
7.53×10^5 nm^3

Reconstructions cropped to 50x50x100 nm

Summarized APT Results for Fe-Cr-Al Alloys

Alloy	Irradiation Dose (dpa)	Irradiation Temp. (°C)	Matrix Composition (at. %) Fe	Cr	Al	Average Cluster Composition (at. %) Fe	Cr	Al	Number Density (×10^{24} m^{-3})	Volume Fraction (%)	Average Radius (nm)
Fe-10Cr-9.3Al	7.0	320 ± 12.7	80.99	9.26	9.54	30.59 ± 8.50	65.55 ± 9.67	3.73 ± 2.50	0.51	1.75	1.48 ± 0.89
Fe-12Cr-8.7Al	7.0	320 ± 12.7	80.69	10.61	8.57	32.85 ± 6.85	62.86 ± 7.30	4.13 ± 1.60	0.69	2.93	1.77 ± 0.81
Fe-15Cr-7.7Al	7.0	320 ± 12.7	80.30	11.91	7.60	20.64 ± 7.90	75.93 ± 8.36	3.30 ± 1.66	2.24	5.46	1.55 ± 0.61
Fe-18Cr-5.8Al	0.8	355 ± 3.4	79.11	14.90	5.90	25.02 ± 6.38	72.62 ± 6.65	2.29 ± 1.06	3.14	5.29	1.47 ± 0.40
	1.8	382 ± 5.4	80.61	13.21	6.07	16.51 ± 7.00	81.37 ± 7.37	2.06 ± 1.08	2.93	6.99	1.62 ± 0.52
	7.0	320 ± 12.7	80.61	13.13	6.02	9.46 ± 6.93	88.20 ± 7.31	2.23 ± 1.28	1.92	6.56	1.79 ± 0.67

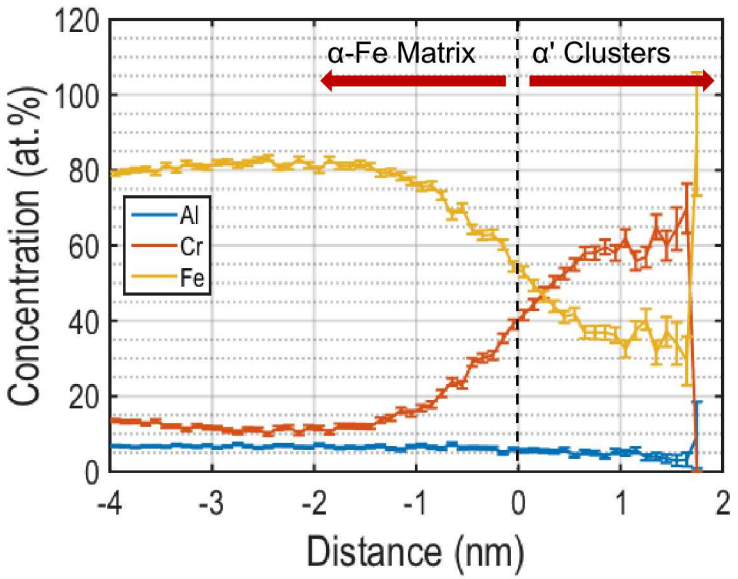

- ↑ dpa leads to ↑ avg. cluster size, ↓ cluster number density
  - Volume fraction saturates early, clusters continue to coarsen
- ↑ Cr generally leads to ↑ cluster number density, ↑ volume fraction
- α′ precipitate Cr content decreases with increasing alloy Al content
  - Al is also seen to be rejected from the precipitates volume

P.D. Edmondson, *et al.*, (2016). Irradiation-Enhanced α' Precipitation in Model FeCrAl Alloys. *Scripta Materialia* **116** (2016) 112-116.
S.A. Briggs, *et al.*, (2017). A combined APT and SANS investigation of α' phase precipitation in neutron-irradiated model FeCrAl alloys. *Acta Materialia* **129** (2017) 217-228.

Standard SANS Analysis Methodology

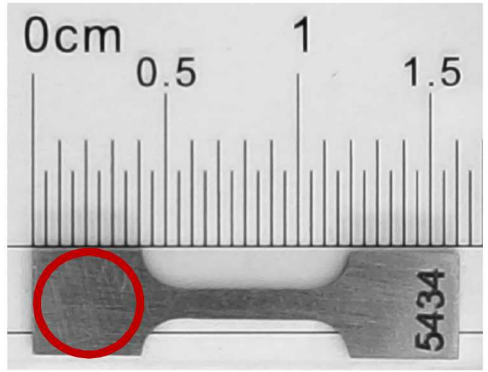

- All measurements performed at room temperature on broken half-tensile specimens at CG-2 general purpose SANS beamline at HFIR
- Final curves combine data from three detector configurations
  - Spans a greater momentum transfer (Q) range: $0.01 < Q < 10\ nm^{-1}$
- Fits assume monodisperse distribution of spherical precipitates interacting with an exclusion volume – not physical but should provide an adequate description of the precipitate microstructure

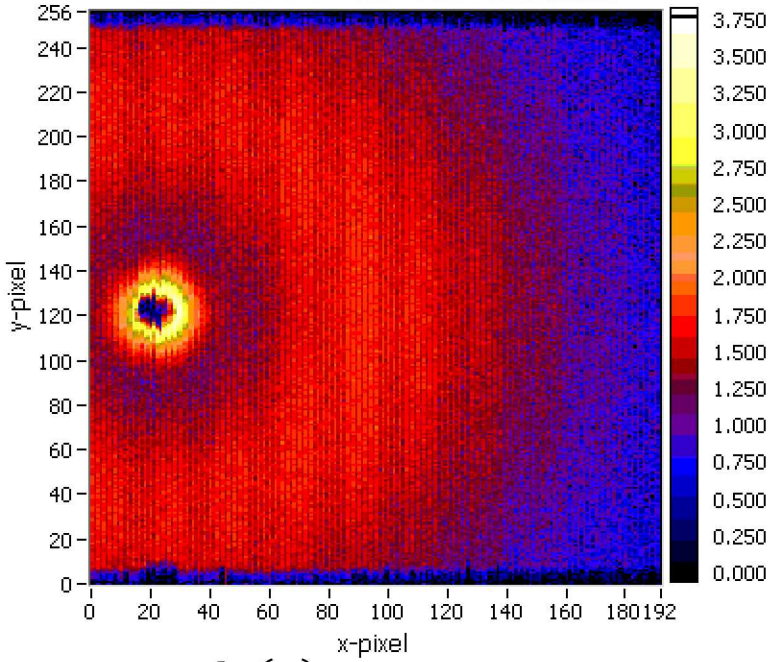

Convert 2D to 1D

Fit Model to Data

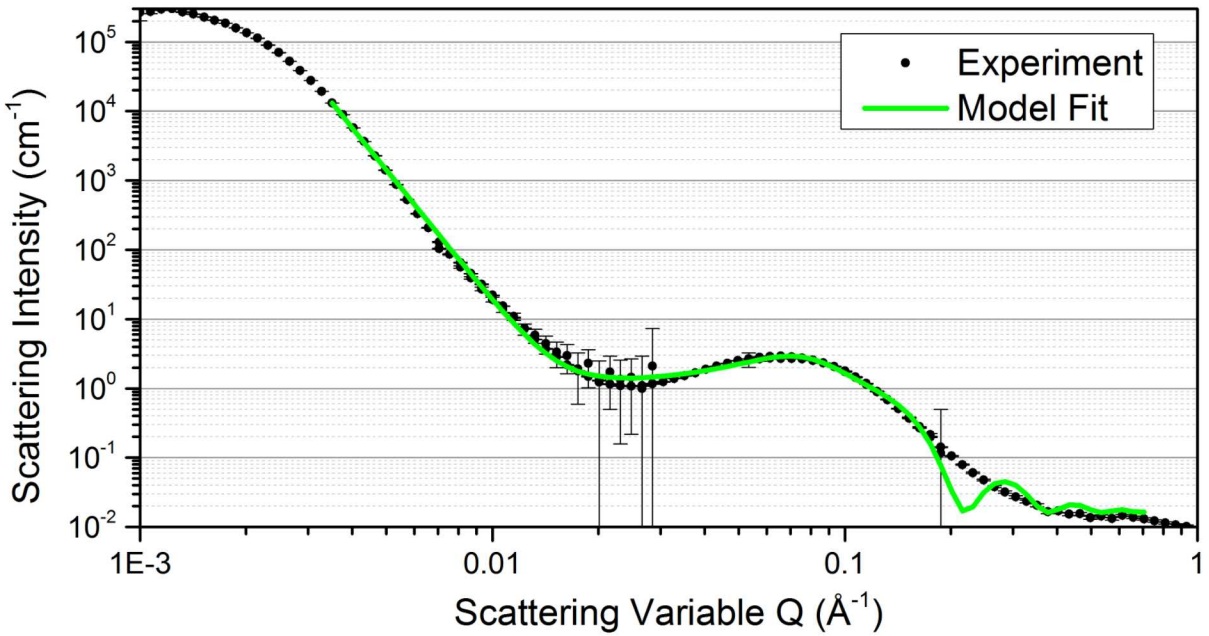

$$\frac{d\sigma(q)}{d\Omega} = n\Delta\rho^2 V^2 P(q,r)S(q) = I_0 P(q,r)S(q)$$

Discussion – LSW/UOKV Models for Precipitate Evolution

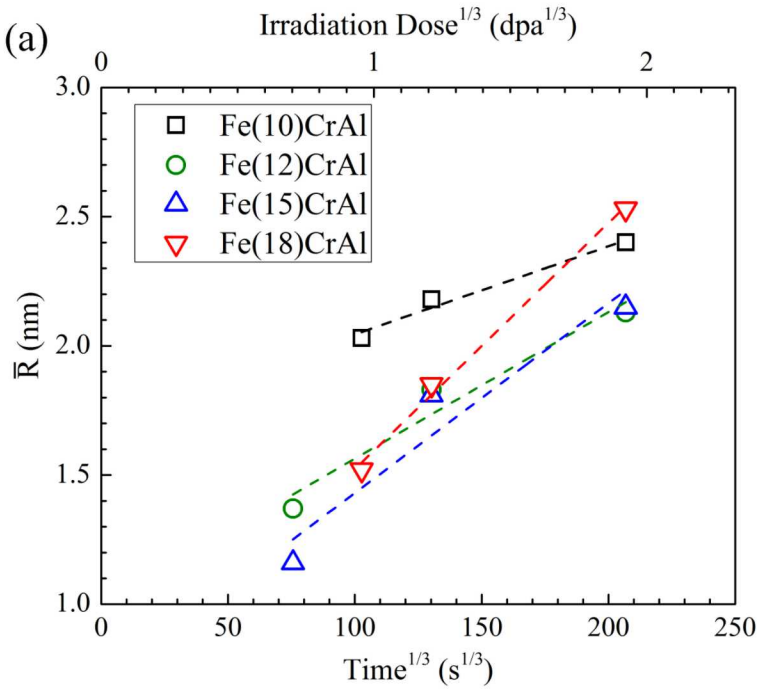

$$\overline{R}_{\alpha'}(t) = K_R t^{1/3}$$

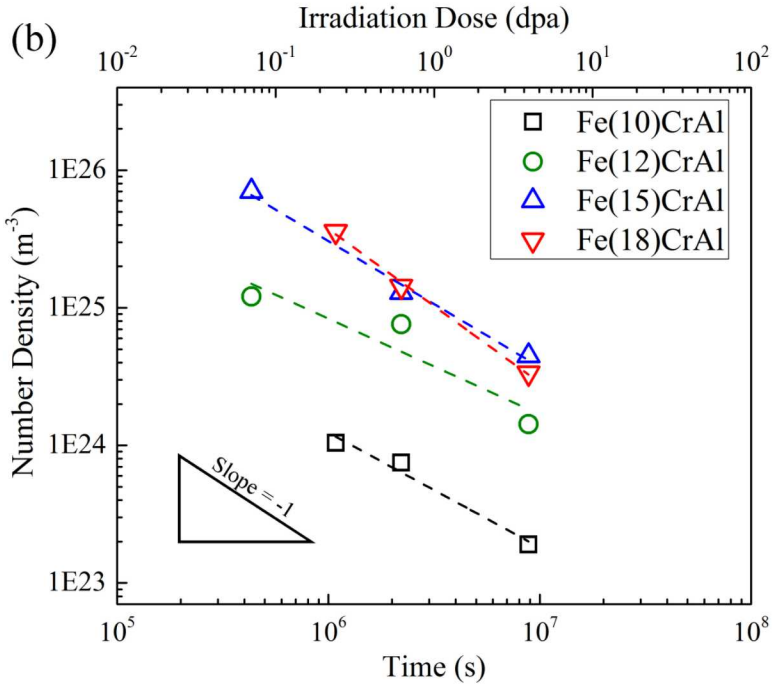

$$N_{\alpha'}(t) = K_N t^{-1}$$

- Suggests a similar mechanism for precipitation in irradiated Fe-Cr-Al as in thermally aged systems and that α′ precipitation is a diffusion-limited phenomenon
- Susceptibility for α′ precipitation in irradiated materials can likely be screened using thermal aging experiments

TEM/STEM Investigation

- Precipitates characterized using STEM/EDS on FEI Talos 200X at ORNL Low-Activation Materials Development & Analysis (LAMDA) Laboratory
- Samples prepared using FIB lift-out method
- Data collection with 2 nA beam on [110] zone axis allows for simultaneous imaging of precipitates (STEM/EDS) and dislocation loops (BF STEM)

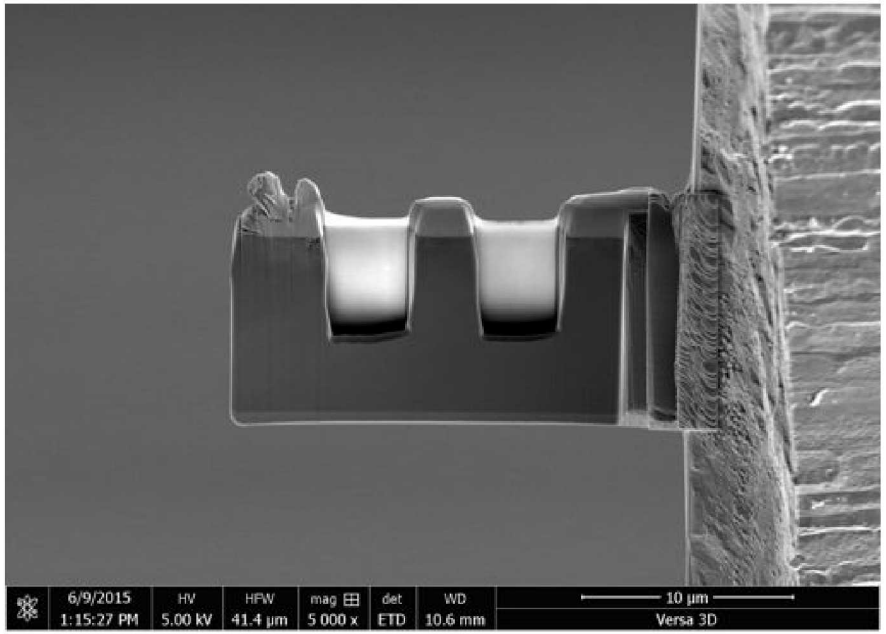

STEM/EDS Results

Fe-18Cr-5.8Al, 7.0 dpa, 320 °C

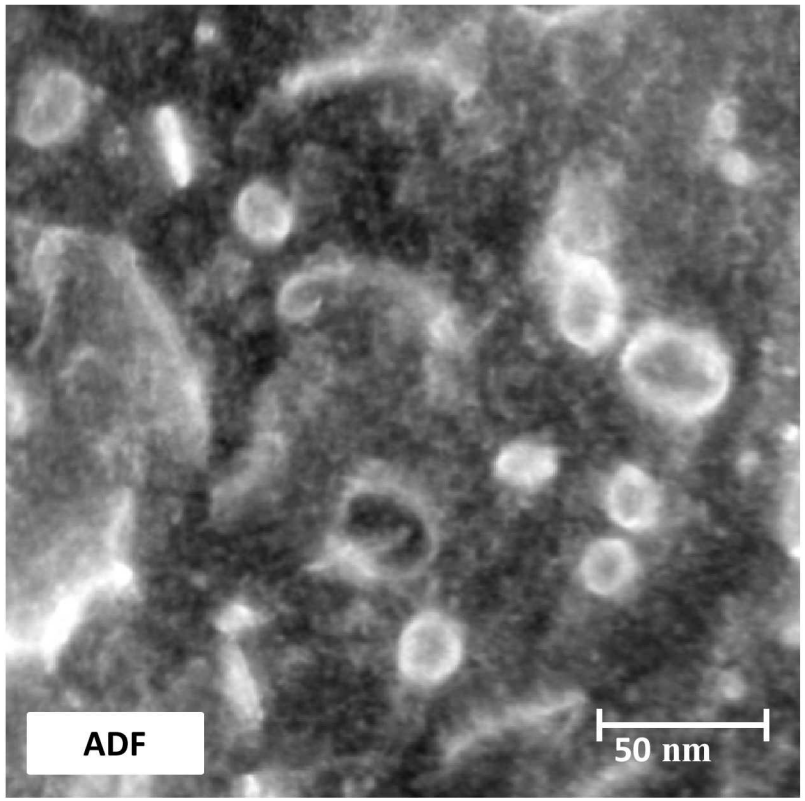

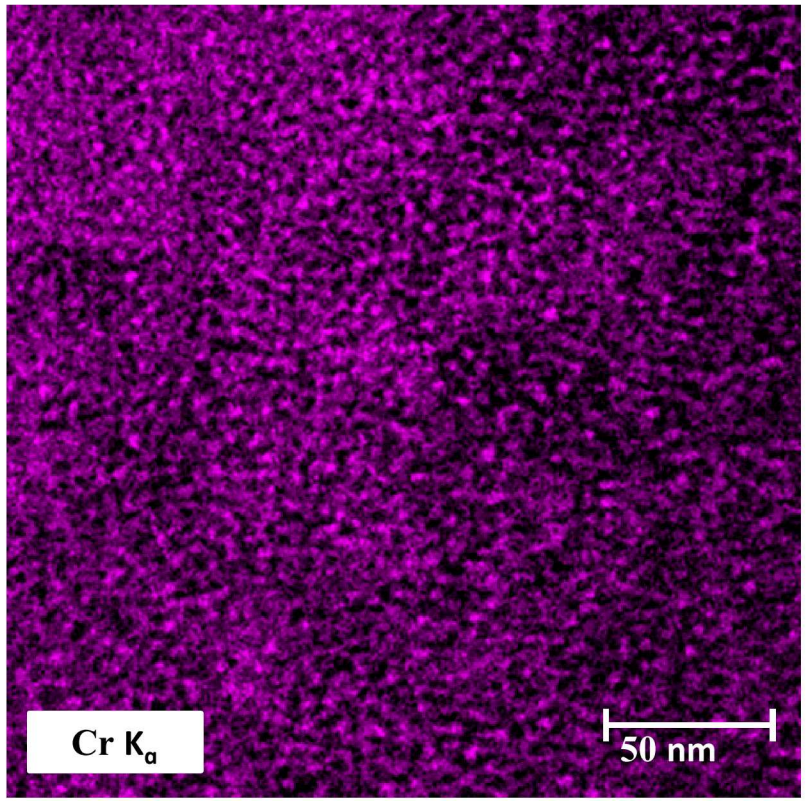

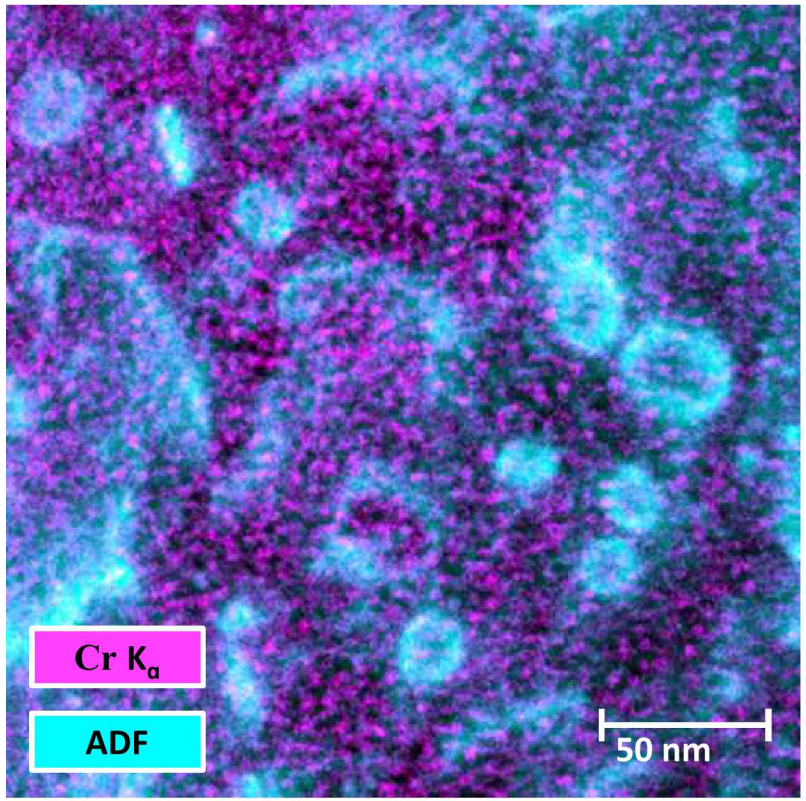

- Correlation of precipitates with dislocation loops can be studied by overlaying a [100] on-zone STEM image with STEM/EDS map for Cr-K_α x-rays
- α′ precipitates appears to nucleate homogeneously in the Fe-Cr-Al matrix and is not preferentially co-located with loops (supported by APT data)

STEM/EDS Results

Fe-12Cr-8.7Al, 7.0 dpa, 320 °C

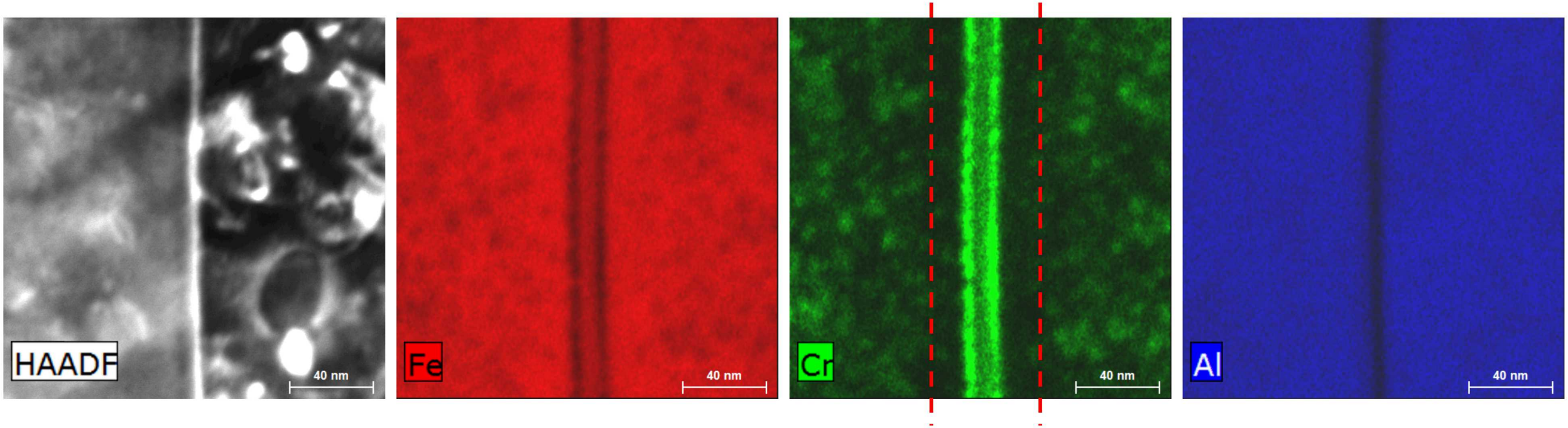

- Exception is observed at grain boundaries where precipitate denudation is observed
- Suggests that α′ precipitation might be mitigated using either a nanocrystalline material or by engineering a high density of defect sinks (i.e., ODS variants)

Observed Trends and Their Significance

- A high density of small precipitates form at low doses, coarsening over time with increasing dose
- Increasing Cr results in higher number densities and volume fractions of precipitates
- These general trends agree with past studies on aged and irradiated binary Fe-Cr and high-Cr ferritic alloys
- Large spread in reported data reinforces the importance of systematic studies of α' precipitates

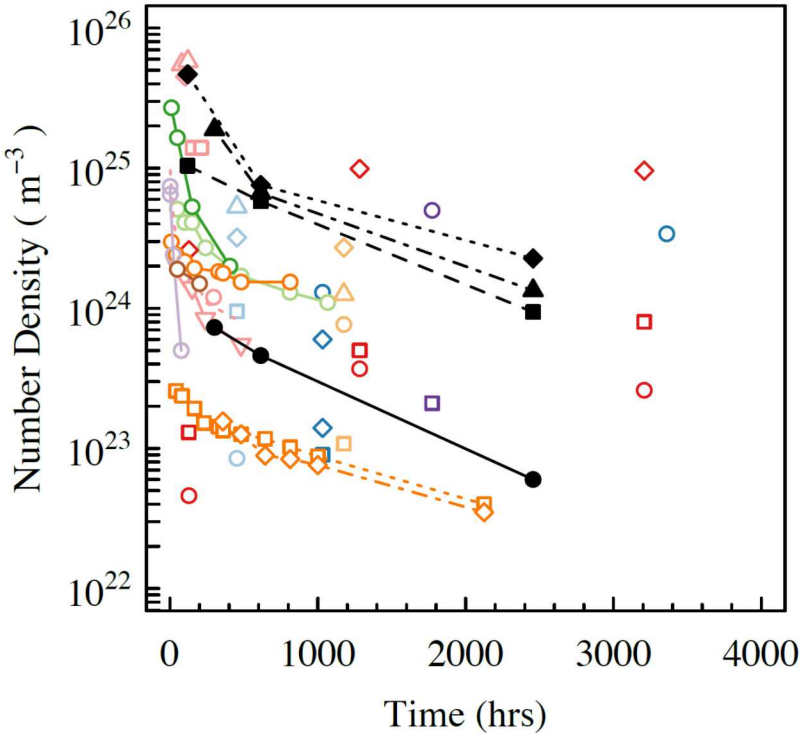

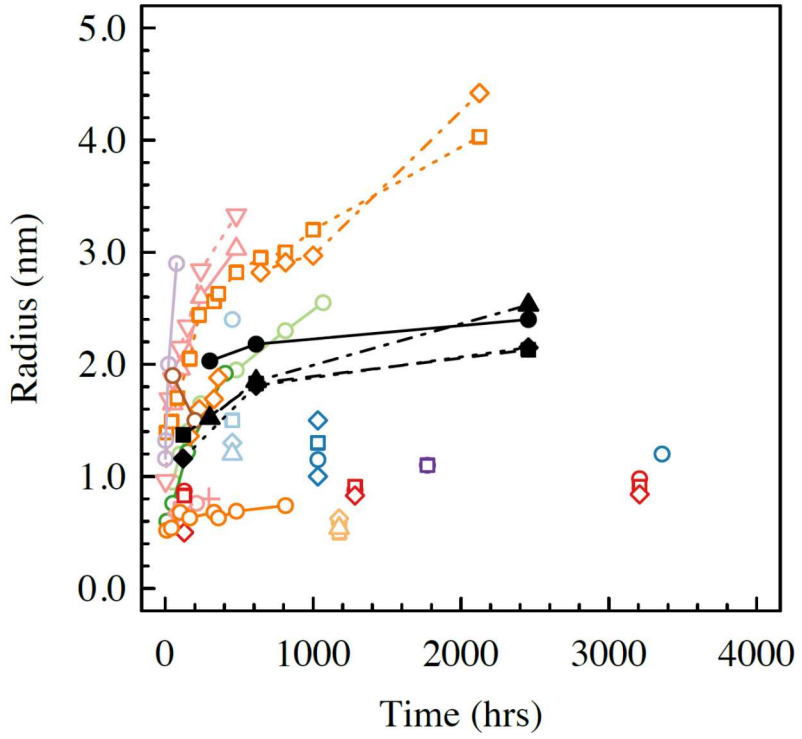

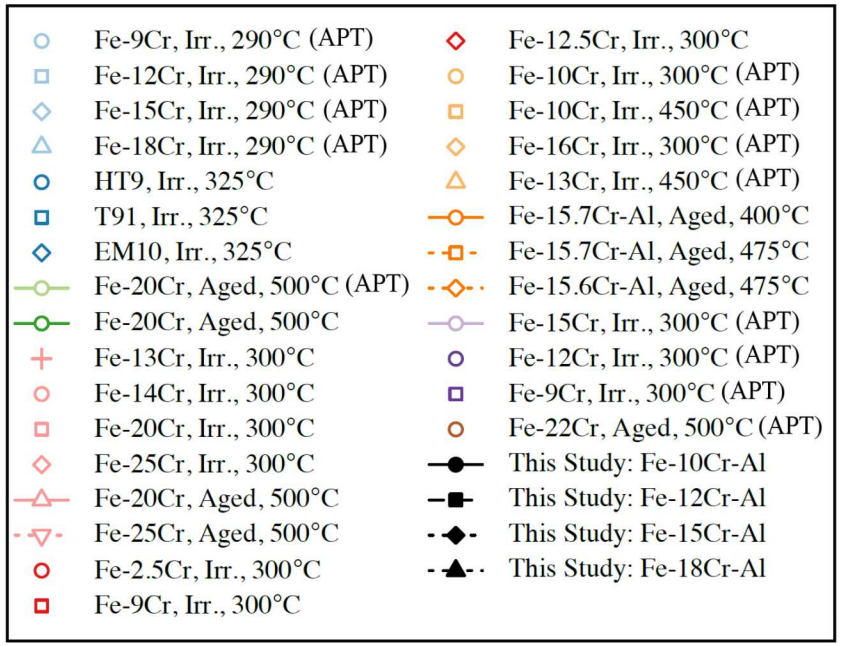

Observed Trends and Their Significance

- Precipitation observed in all compositions, contrary to expectations based on phase boundary proposed by Kobayashi et al.
- This boundary is based on hardness measurements – suggests that not all precipitation is application limiting
- Phase boundary is for 475 °C, irradiations performed at ~320 °C – less Cr solubility expected at lower temperatures

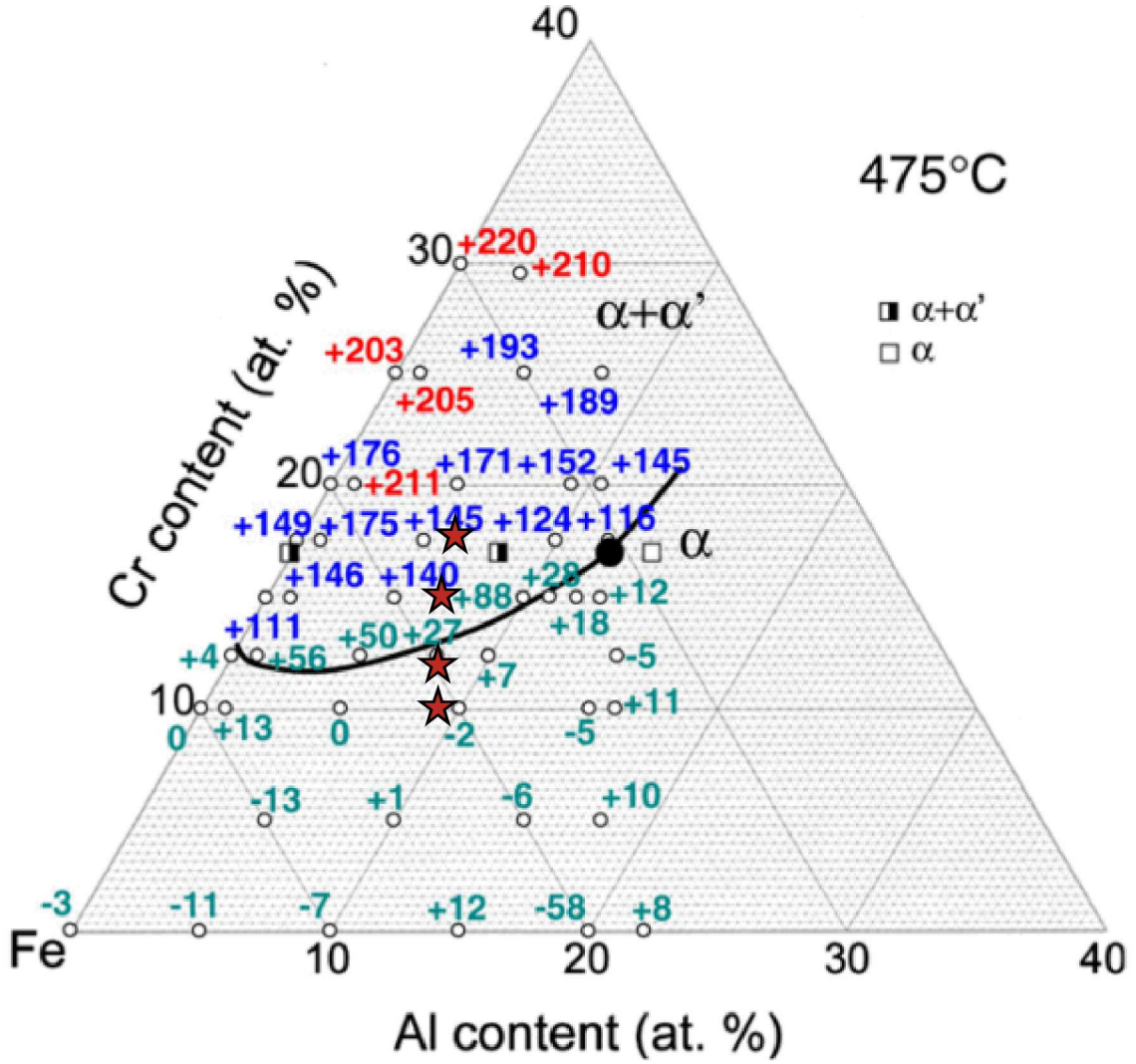

Observed Trends and Their Significance

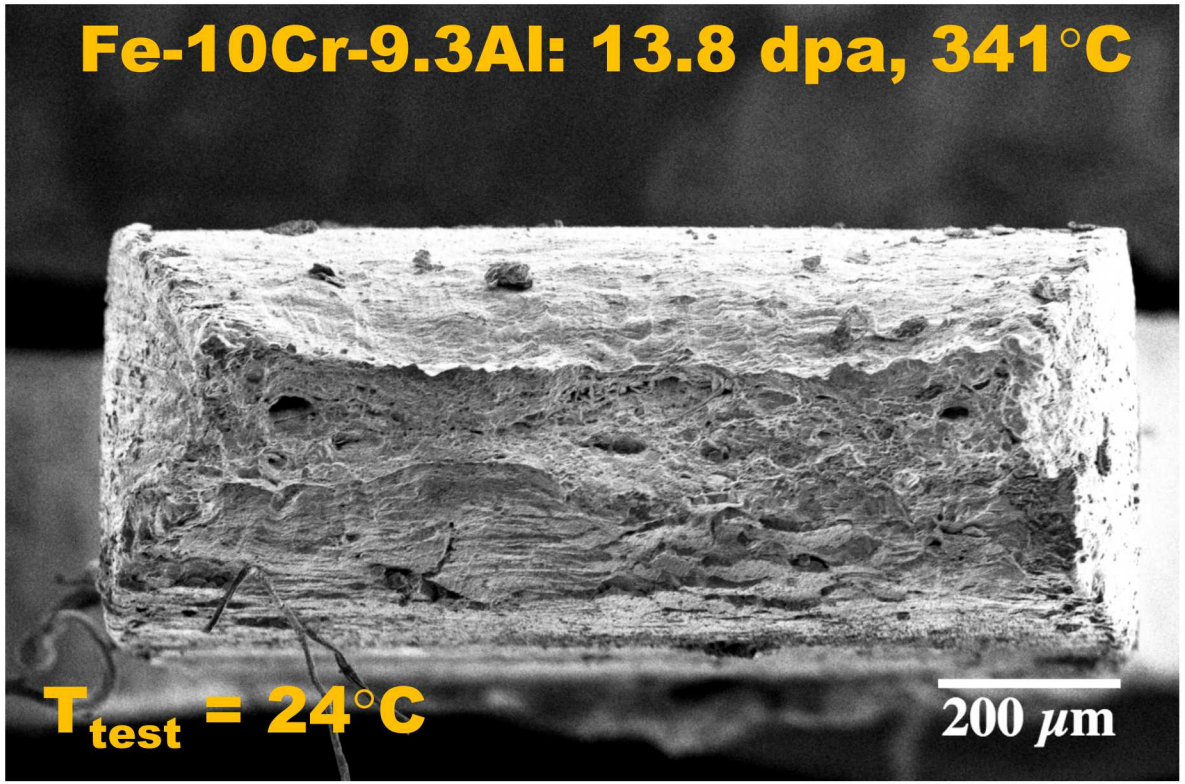

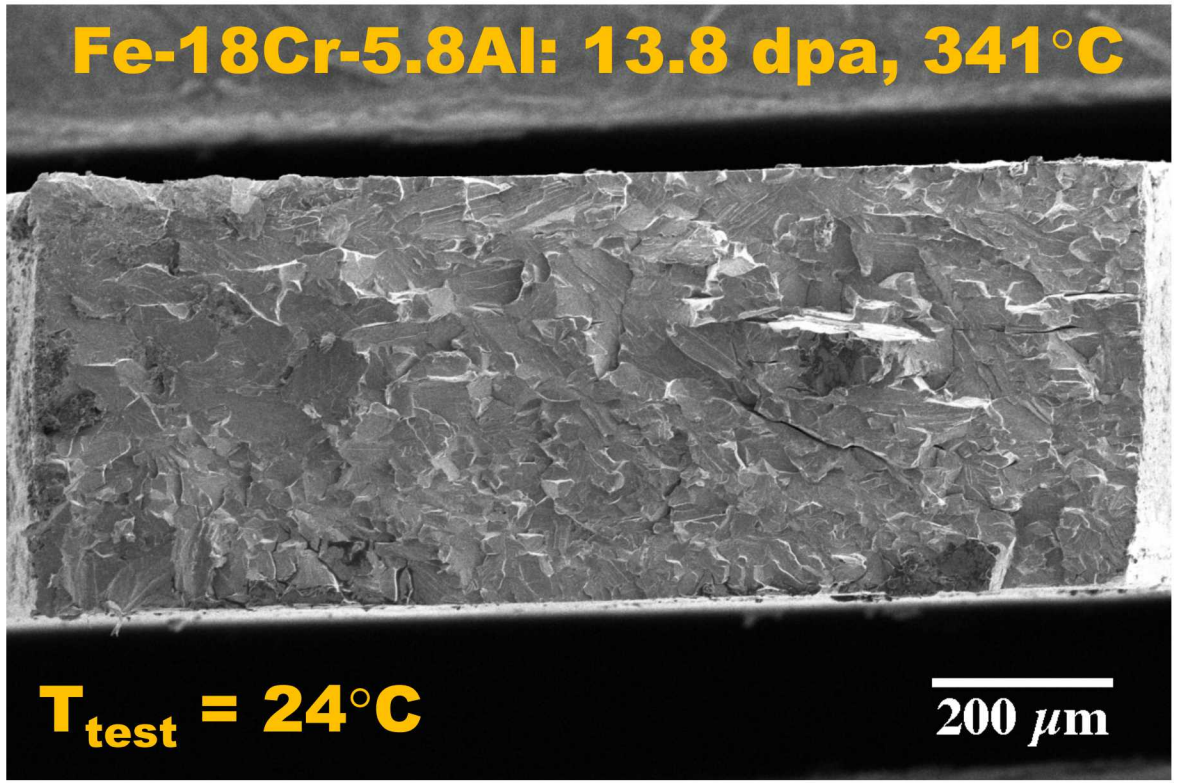

- α′ precipitation needs to be mitigated in these materials for nuclear applications
  - Minimize Cr content, maximize Al content while maintaining adequate mechanical/oxidation performance
  - Microstructural engineering may have some effect at reducing or retarding precipitation response

In-Situ SANS Overview

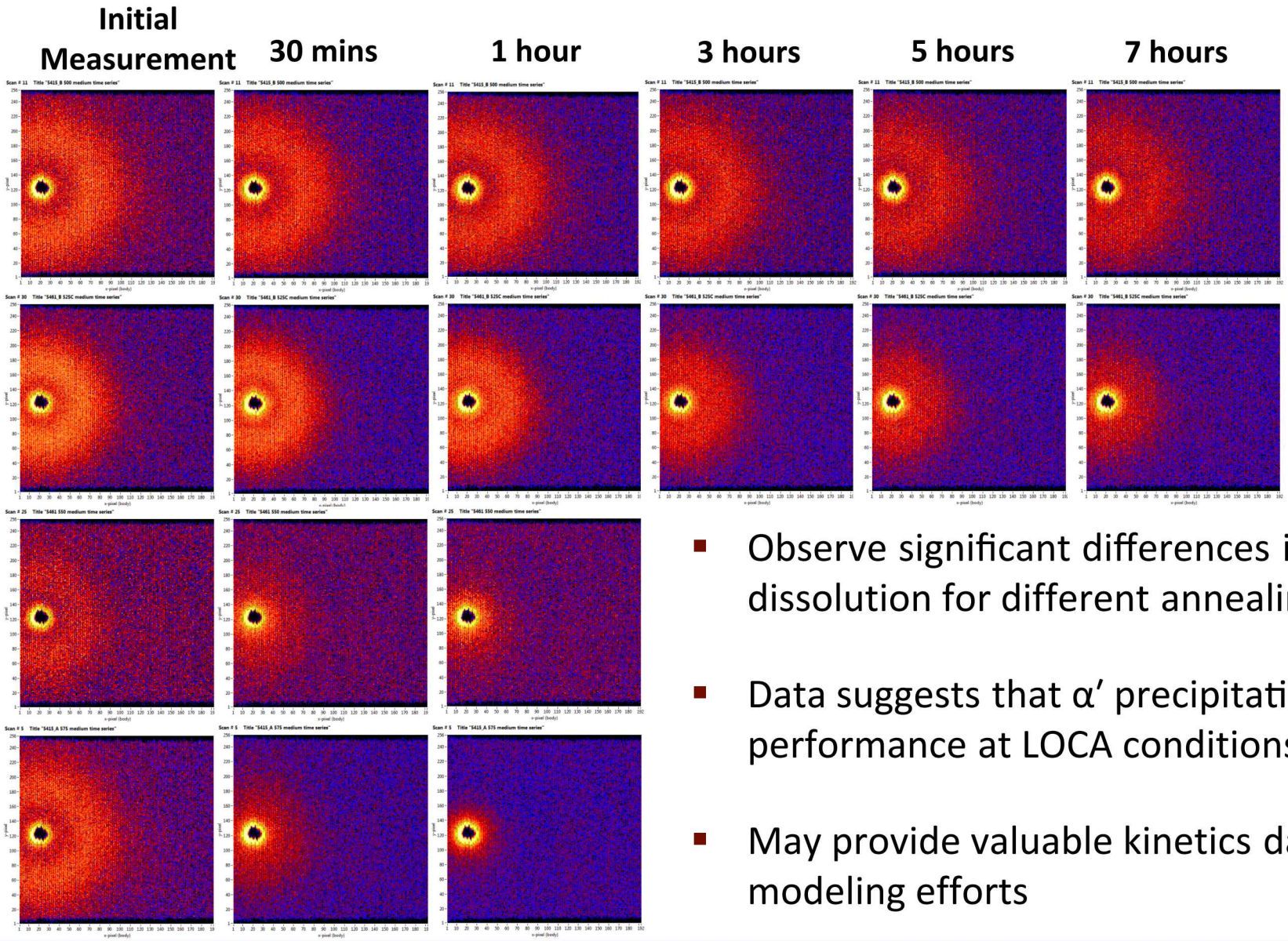

- Observe significant differences in rate of α' dissolution for different annealing temperatures
- Data suggests that α' precipitation will not influence performance at LOCA conditions (as expected)
- May provide valuable kinetics data for predictive modeling efforts

In-Situ TEM Experiments

Fe-15Cr-3.9Al, Speed 25x

$Near\ [001]\ zone\ axis, g = 011$

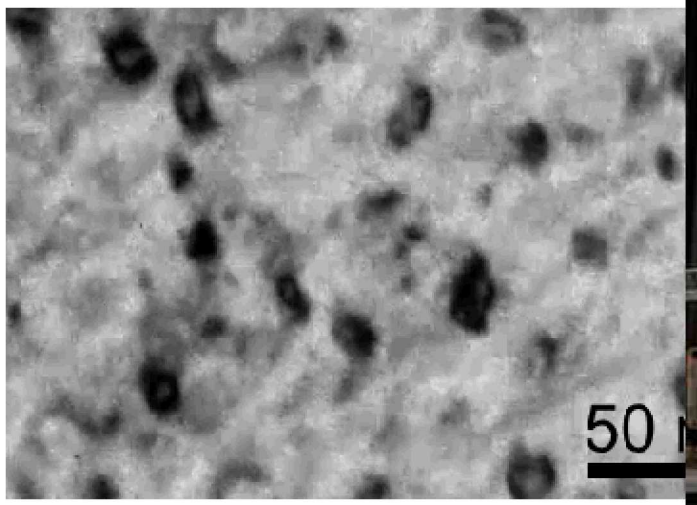

Defect Hopping:

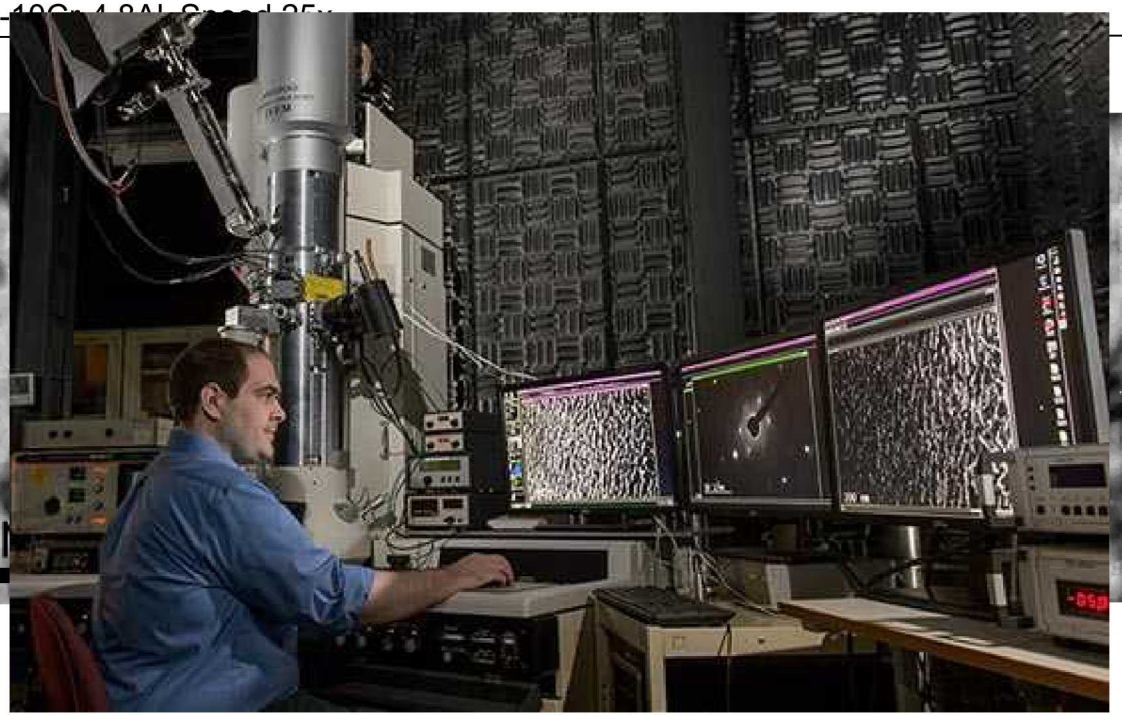

Fe-15Cr-3.9Al, Speed 25x

$Near\ [001]\ zone\ axis, g = 011$

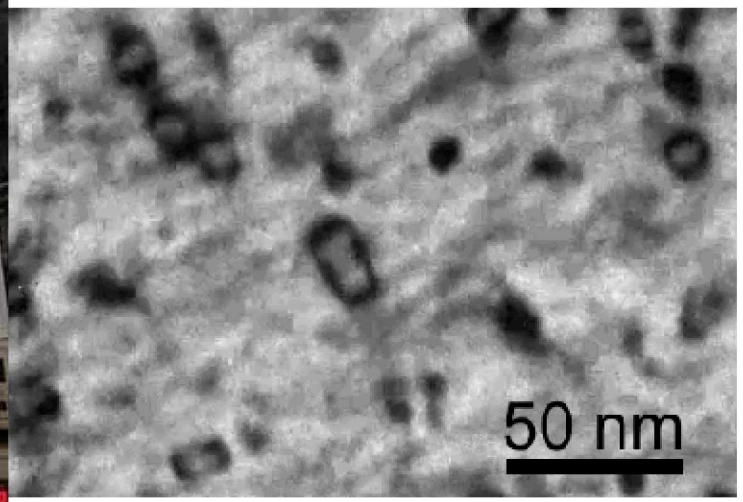

Defect-Defect Interaction/Defect growth:

- Dislocation loops also contribute to hardening & embrittlement in irradiated Fe-Cr-based alloys and are of interest for determining alloy viability and radiation tolerance
- Ion-irradiation in-situ with TEM imaging allows for dynamic observation of loop microstructural evolution and defect interactions

J.C. Haley, et al. Dislocation loop evolution during in-situ irradiation of model FeCrAl alloys. *Acta Materialia* **136** (2017) 390-401.

In-Situ TEM Experiments

Fe-10Cr-4.8Al, Speed 25x

Fe-15Cr-3.9Al, Speed 25x

$Near\ [001]\ zone\ axis, g = 011$

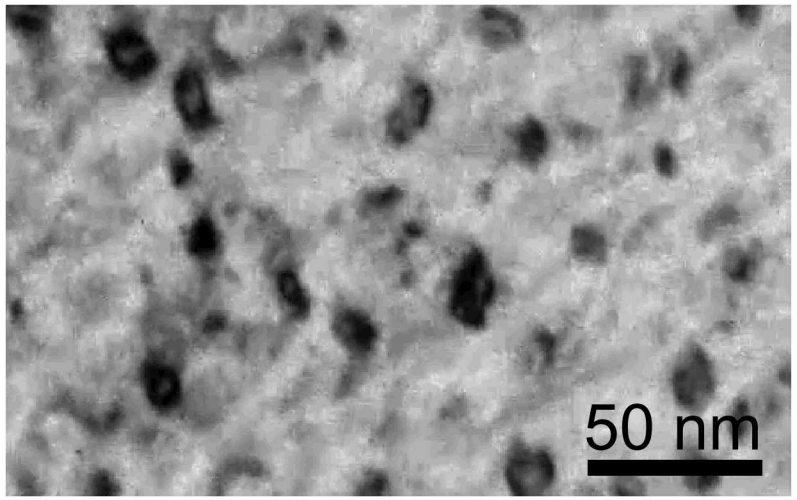

Defect Hopping:
Infrequent Observation

$Near\ [001]\ zone\ axis, g = 011$

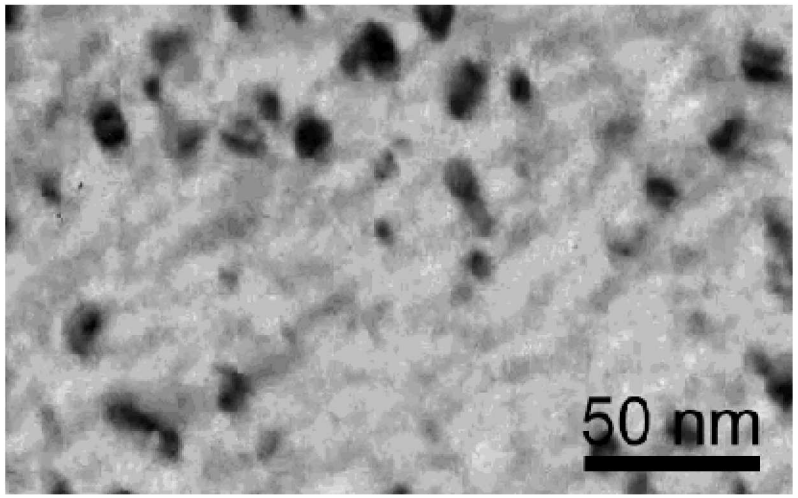

Defect loss/Defect shrinking:

$Near\ [001]\ zone\ axis, g = 011$

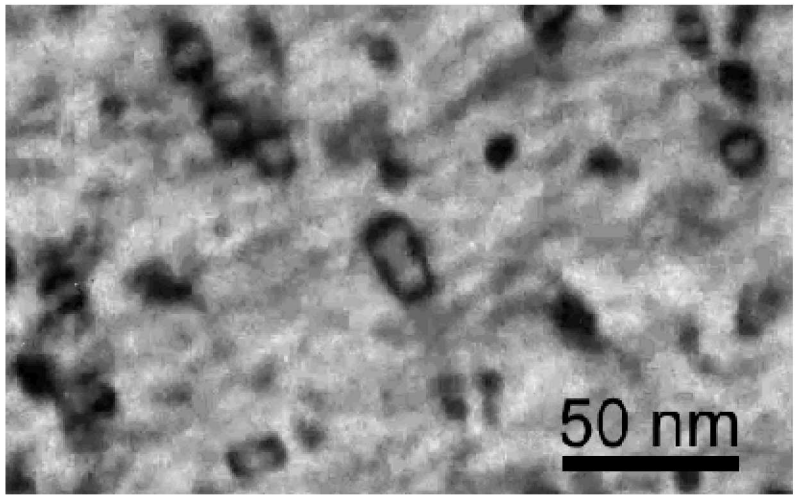

Defect-Defect Interaction/Defect growth:

- Dislocation loops also contribute to hardening & embrittlement in irradiated Fe-Cr-based alloys and are of interest for determining alloy viability and radiation tolerance
- Ion-irradiation in-situ with TEM imaging allows for dynamic observation of loop microstructural evolution and defect interactions

J.C. Haley, et al. Dislocation loop evolution during in-situ irradiation of model FeCrAl alloys. *Acta Materialia* **136** (2017) 390-401.

In-Situ TEM Experiments

Fe-10Cr-4.8Al, Speed 25x

$Near\ [001]\ zone\ axis, g = 011$

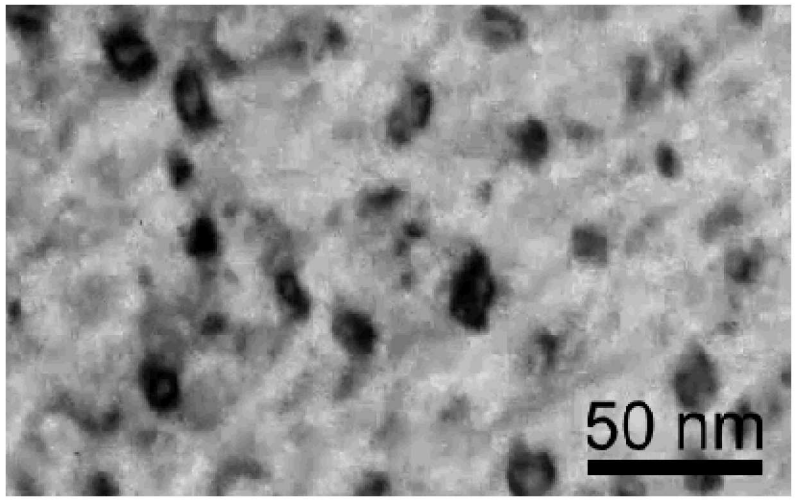

Defect Hopping:
Infrequent Observation

$Near\ [001]\ zone\ axis, g = 011$

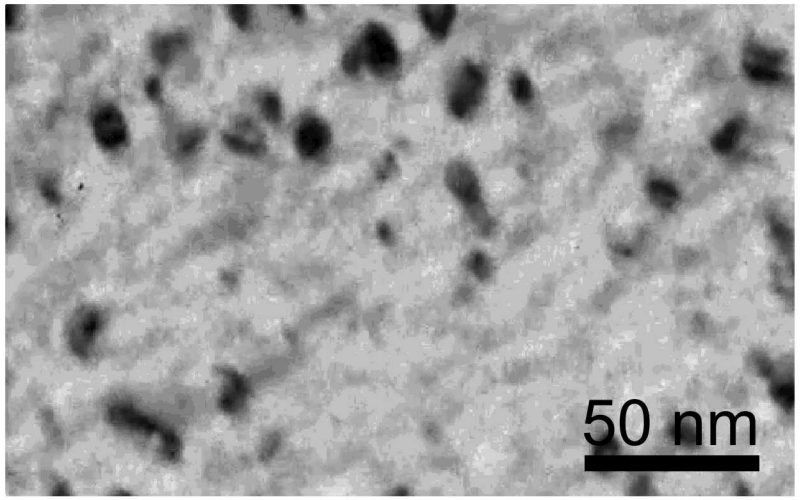

Defect loss/Defect shrinking:
Frequent Observation

Fe-15Cr-3.9Al, Speed 25x

$Near\ [001]\ zone\ axis, g = 011$

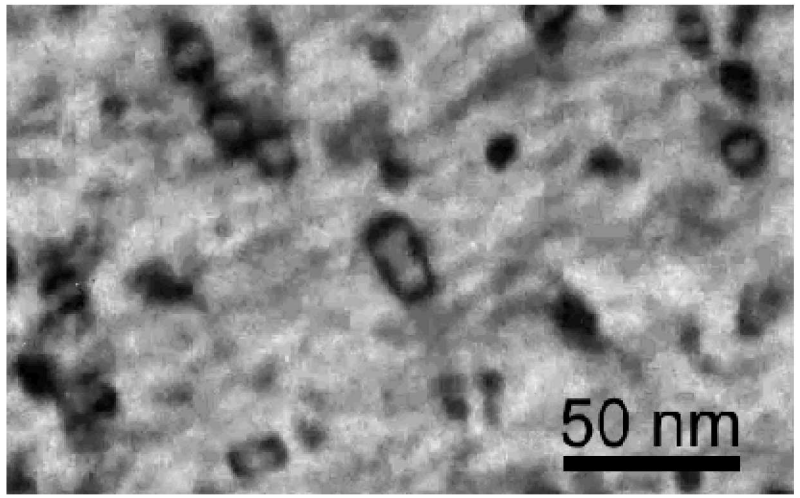

Defect-Defect Interaction/Defect growth:

- Dislocation loops also contribute to hardening & embrittlement in irradiated Fe-Cr-based alloys and are of interest for determining alloy viability and radiation tolerance
- Ion-irradiation in-situ with TEM imaging allows for dynamic observation of loop microstructural evolution and defect interactions

J.C. Haley, et al. Dislocation loop evolution during in-situ irradiation of model FeCrAl alloys. *Acta Materialia* **136** (2017) 390-401.

In-Situ TEM Experiments

Fe-10Cr-4.8Al, Speed 25x

Fe-15Cr-3.9Al, Speed 25x

$Near\ [001]\ zone\ axis, g = 011$

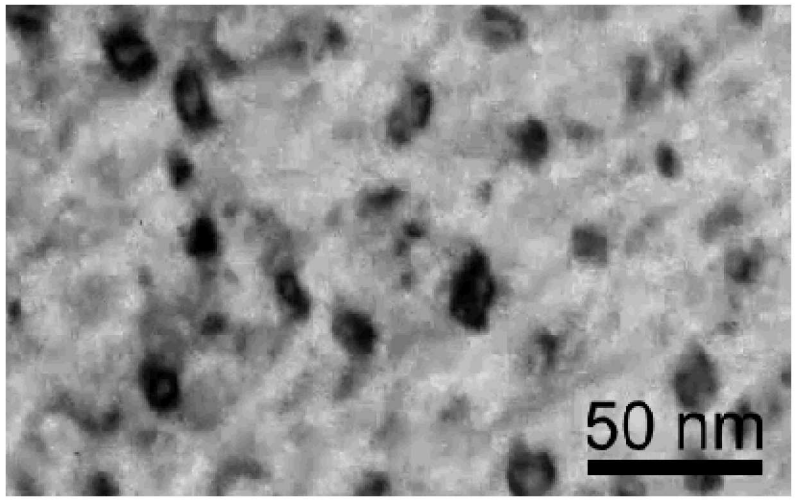

Defect Hopping:
Infrequent Observation

$Near\ [001]\ zone\ axis, g = 011$

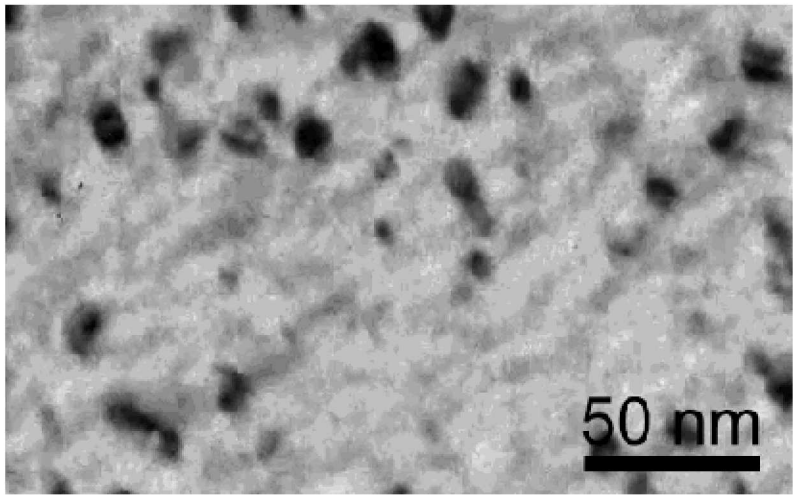

Defect loss/Defect shrinking:
Frequent Observation

$Near\ [001]\ zone\ axis, g = 011$

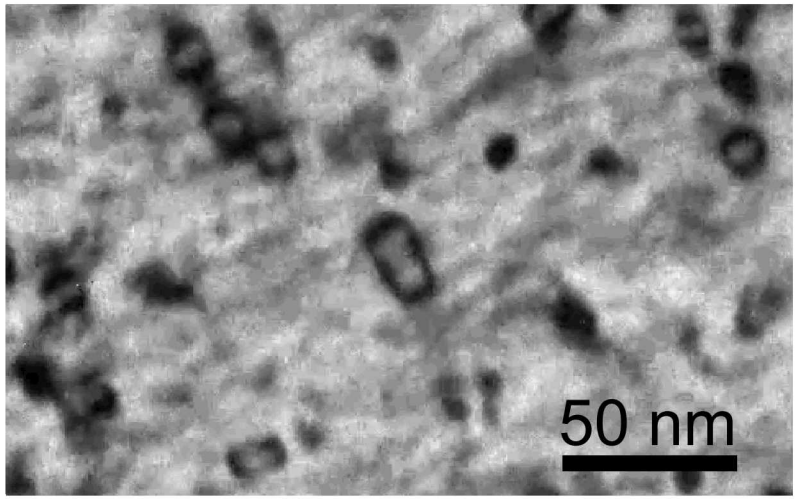

Defect-Defect Interaction/Defect growth:
Moderately Frequent Observation

- Dislocation loops also contribute to hardening & embrittlement in irradiated Fe-Cr-based alloys and are of interest for determining alloy viability and radiation tolerance
- Ion-irradiation in-situ with TEM imaging allows for dynamic observation of loop microstructural evolution and defect interactions

J.C. Haley, et al. Dislocation loop evolution during in-situ irradiation of model FeCrAl alloys. *Acta Materialia* **136** (2017) 390-401.

Particle Stability in Gen. II ODS Fe-Cr-Al Variants

Oxide dispersion-strengthened materials

- ODS alloys employ advanced powder metallurgy techniques to force a fine dispersion of nano-sized oxide precipitates into the material microstructure
- These become obstacles to dislocation motion, increasing strength and creep resistance, and also provide a higher density of interfaces to serve as sinks for irradiation-induced defects

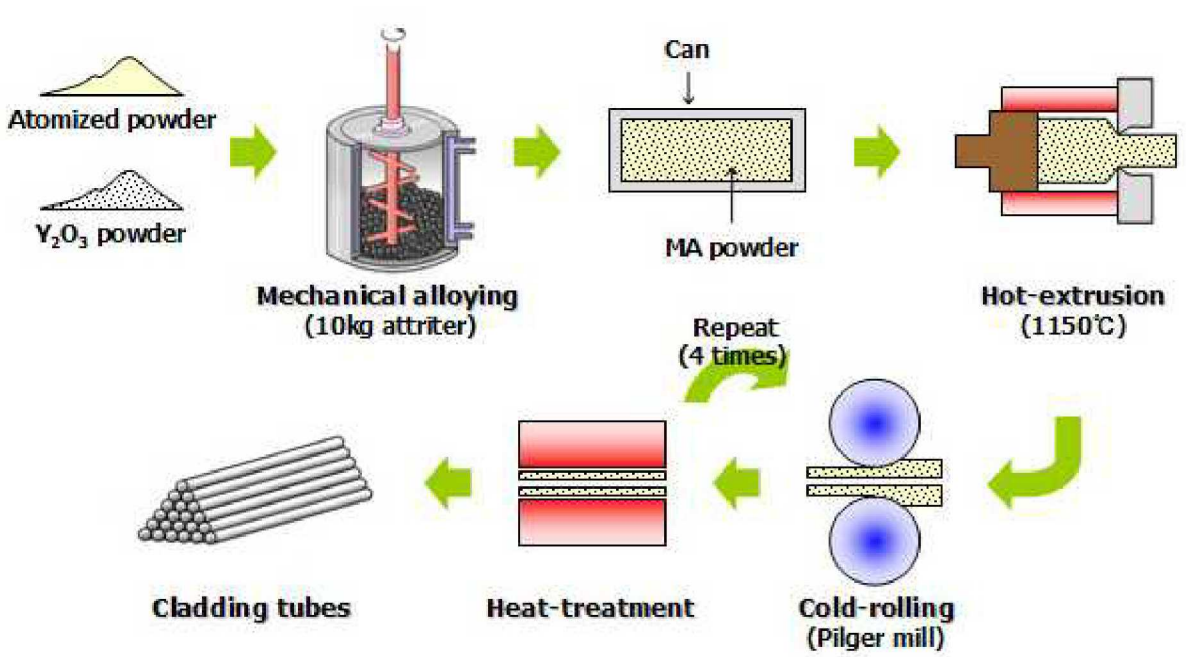

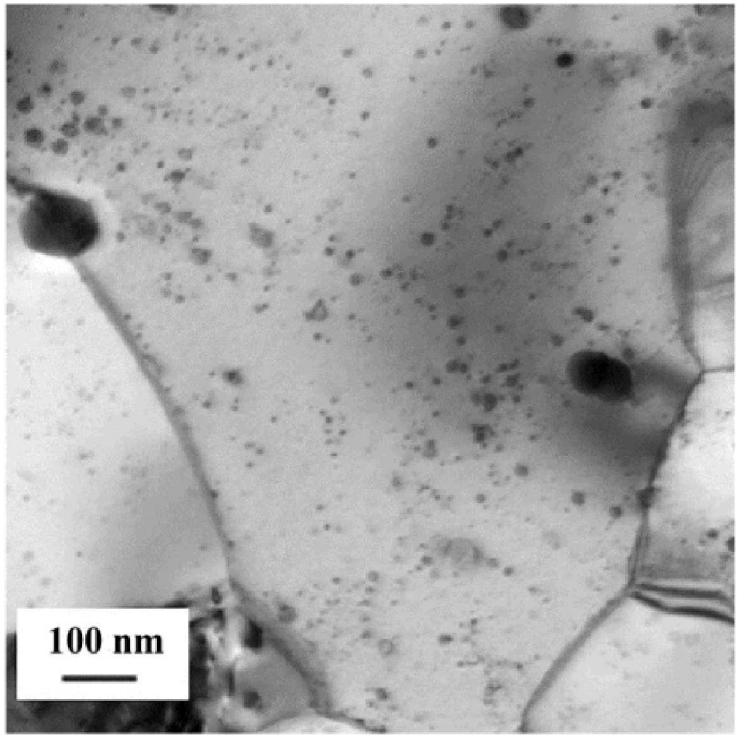

[1] Japan Atomic Energy Agency. https://www.jaea.go.jp/english/news/p06101302/index.shtml
[2] Sanctis, M.D., *et al.* (2017). Mechanical characterization of a nano-ODS steel prepared by low-energy mechanical alloying. *Metals,* 7(8), pp. 283.

Experimental Design

- One Fe-12Cr-5Al+Y_2O_3 (wt.%) powder metallurgy FeCrAl variant selected for study

- Gas atomized Fe-12Cr-5Al power was ball milled with Y_2O_3 powder in Ar for 40 hrs, degassed for 24 hrs at 300 °C, and extruded at 950 °C.[1]

- 100-300 nm grain sizes, with some alumina stringers apparent

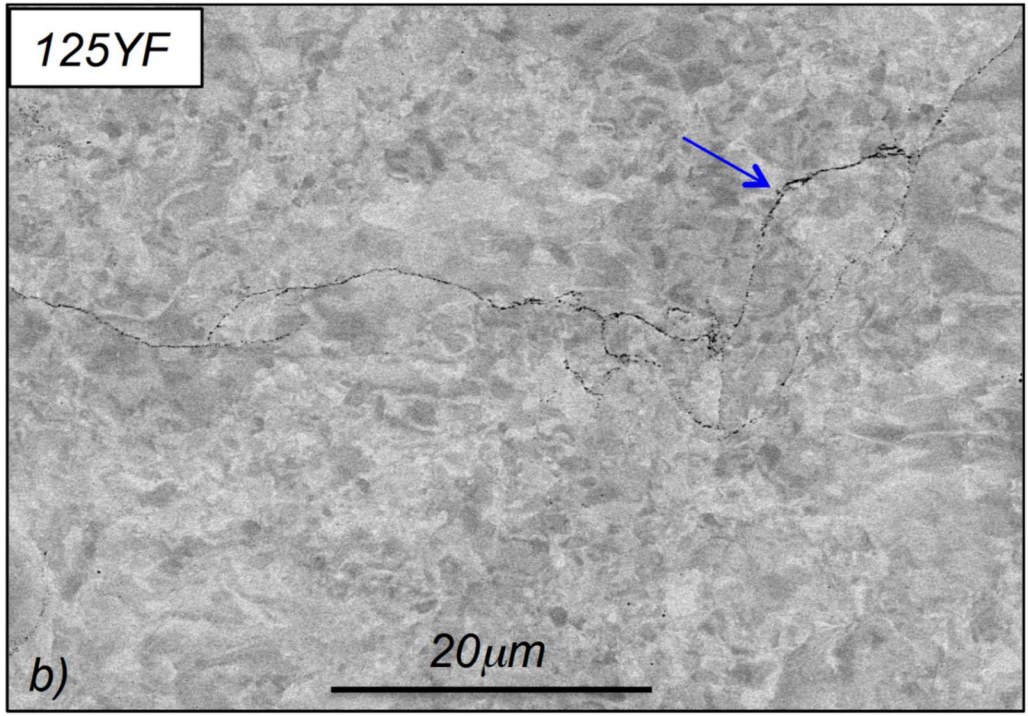

ID	Composition, wt.%								
	Fe	**Cr**	**Al**	**Y**	Si	C	S	O	N
125YF	**82.99**	**11.67**	**4.73**	**0.19**	0.010	0.020	0.0030	0.192	0.0202

Capsule ID	Exposure Time (hrs)	Neutron Flux (n/cm²s) E > 0.1 MeV	Neutron Fluence (n/cm²) E > 0.1 MeV	Dose Rate (dpa/s)	Dose (dpa)	Irradiation Temperature (°C)
FCAT-01	590	1.10×10^{15}	2.17×10^{21}	9.8×10^{-7}	1.9	194.5 ± 37.9
FCAT-02	590	1.04×10^{15}	2.17×10^{21}	9.3×10^{-7}	1.8	363.6 ± 23.1
FCAT-03	590	1.10×10^{15}	2.17×10^{21}	9.8×10^{-7}	1.9	559.4 ± 28.1

[1] Dryepondt, S., *et al.* (2015). Oak Ridge National Laboratory Development of ODS FeCrAl Alloys for Accident-Tolerant Fuel Cladding. ORNL/TM-2015/539.

ODS FeCrAl Mechanical Properties at ~2 dpa

- Tensile tests performed in ambient air
- Medium to elevated temperature irradiations show little change in mechanical properties

Specimen	Irradaition Temperature (°C)	Yield Strength (MPa)	Ultimate Tensile Strength (MPa)	Uniform Elongation (%)	Tensile Elongation (%)
OD34	-	1085	1137	4.8	5.8
OD01	**195**	**1108**	**1130**	**0.8**	**5.0**
OD03	363	1037	1074	5.0	9.7
OD06	559	1104	1160	6.2	11.2

- Low temperature irradiation showed embrittlement
  - *Due to cluster stability even at low dose?*

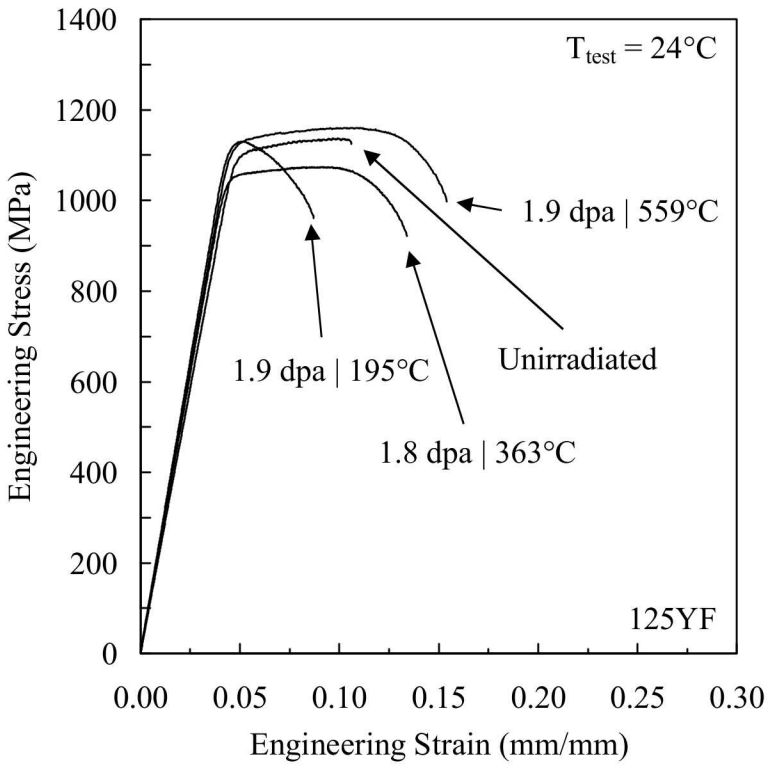

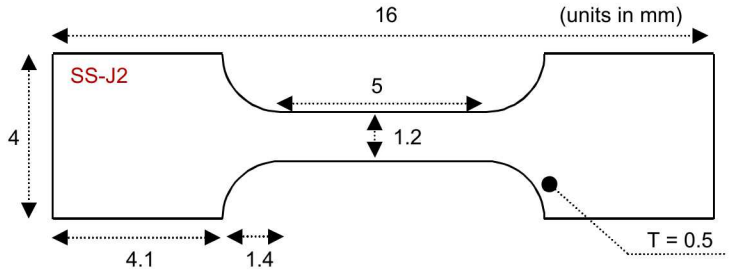

EFTEM Data Configuration and Analysis

- EFTEM Configuration:
  - JEOL 2100F in LAMDA at ORNL
  - Fe_M jump-ratio map & thickness map per RO
    - 10 eV slits
    - Manual drift correction

- EFTEM analysis:
  - Subdivided into 25 area bins
  - B/C Correction + Mean Image Filter
  - Manually counted precipitates using ImageJ
  - Volume calculated using avg. thickness in each bin

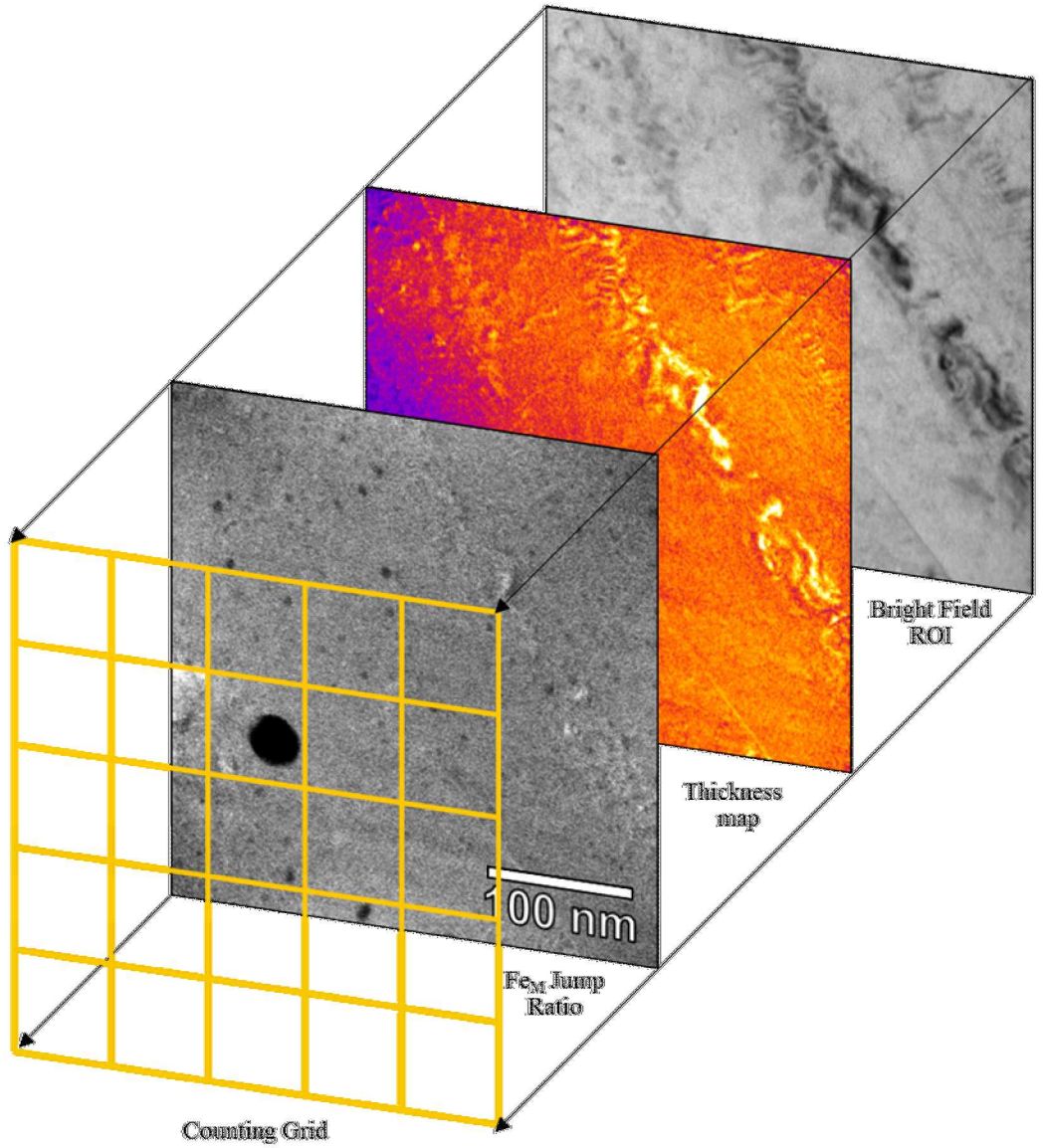

EFTEM Qualitative Observations

- Bimodal size distribution apparent
  - Larger precipitates decorate grain boundaries (likely $Y_3Al_5O_{12}$ (YAG) and alumina phases)
  - Finer precipitate dispersion throughout bulk material
- Heterogeneous distributions – large grain-to-grain variation

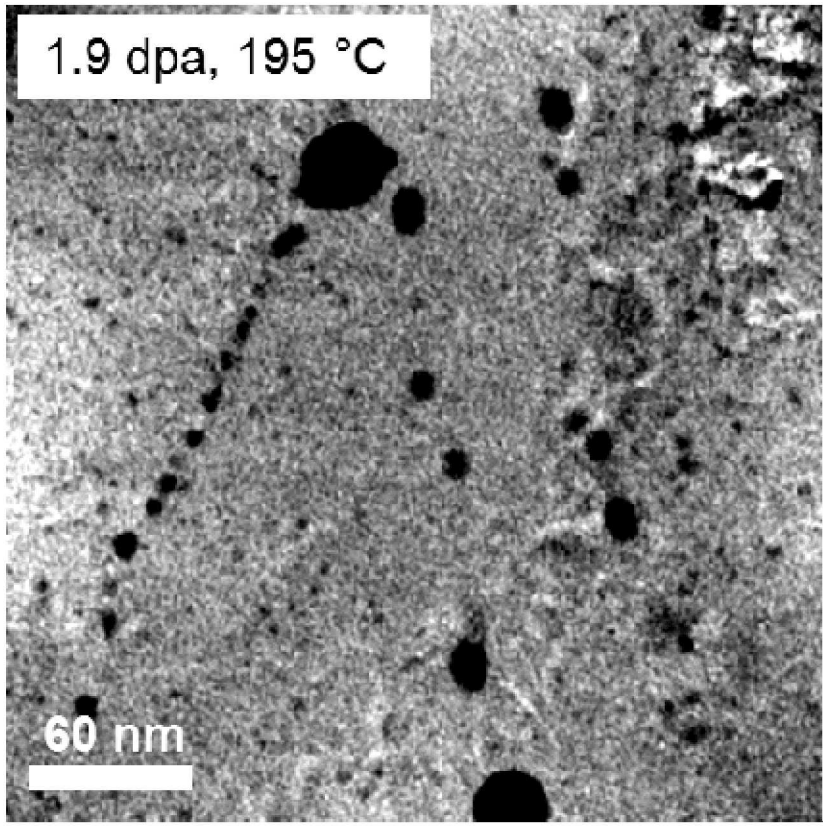

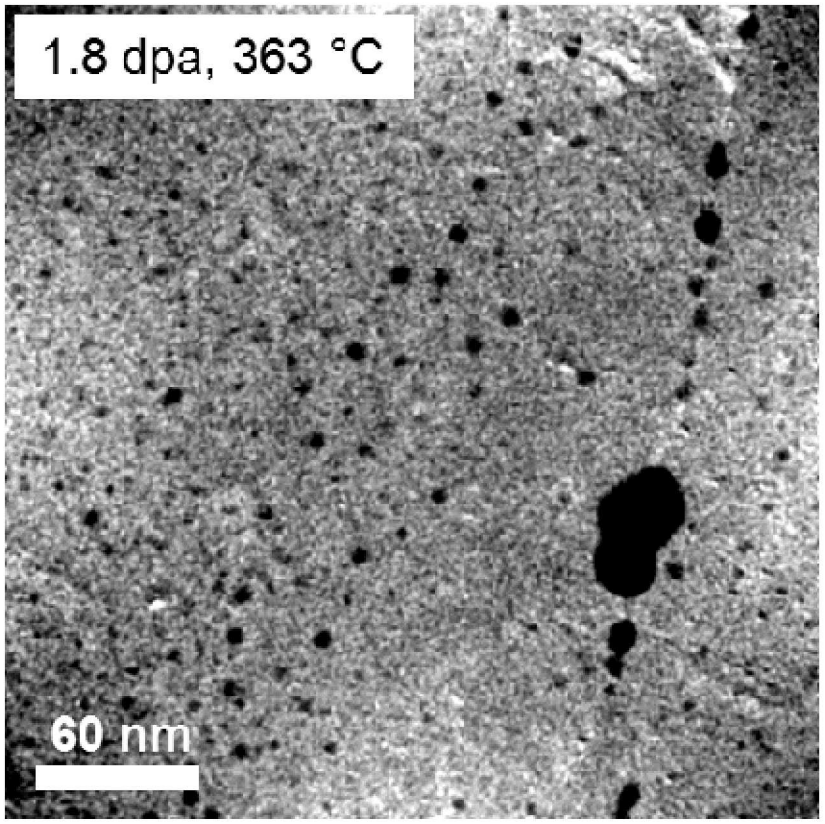

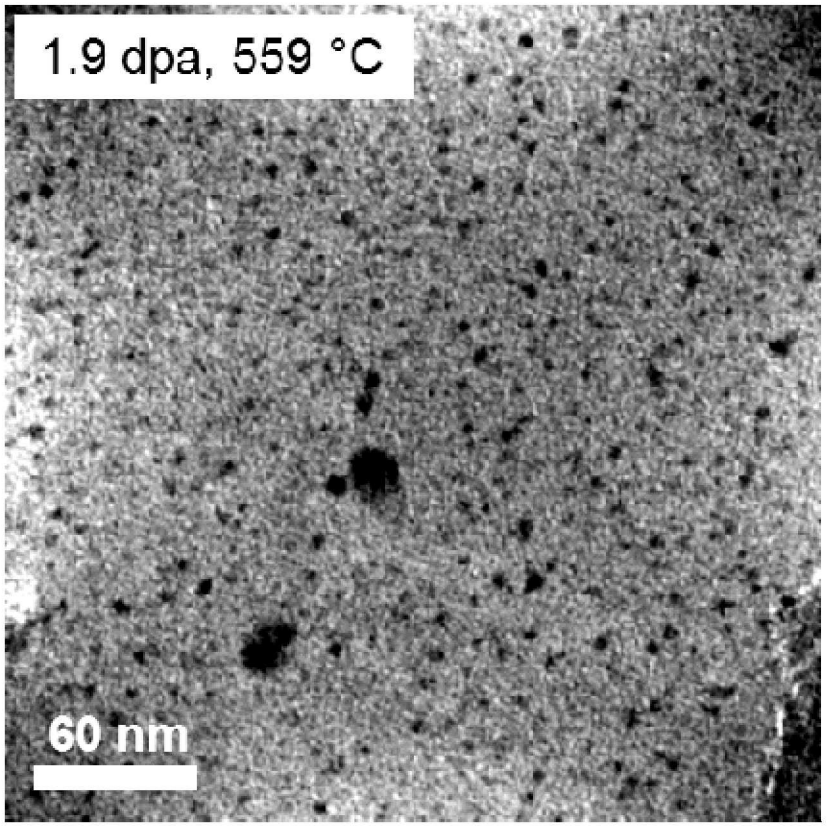

Size Distributions

- Peak shifts and distribution broadening/tailing towards larger sizes suggest:
  - 1.9 dpa | 195° C: NP instability
  - 1.8 dpa | 363° C: NP stability
  - 1.9 dpa | 559° C: NP coarsening
- Difference in size distributions between SANS and EFTEM due to varying resolution limits
- Large error in EFTEM results are indicative of technique errors and grain-to-grain heterogeneity
- Reasonable agreement between the monodispersed (MD) approximation and ”brute-force” Monte Carlo (MC) model mean size suggests monodispersed model is a reasonable first-order analysis

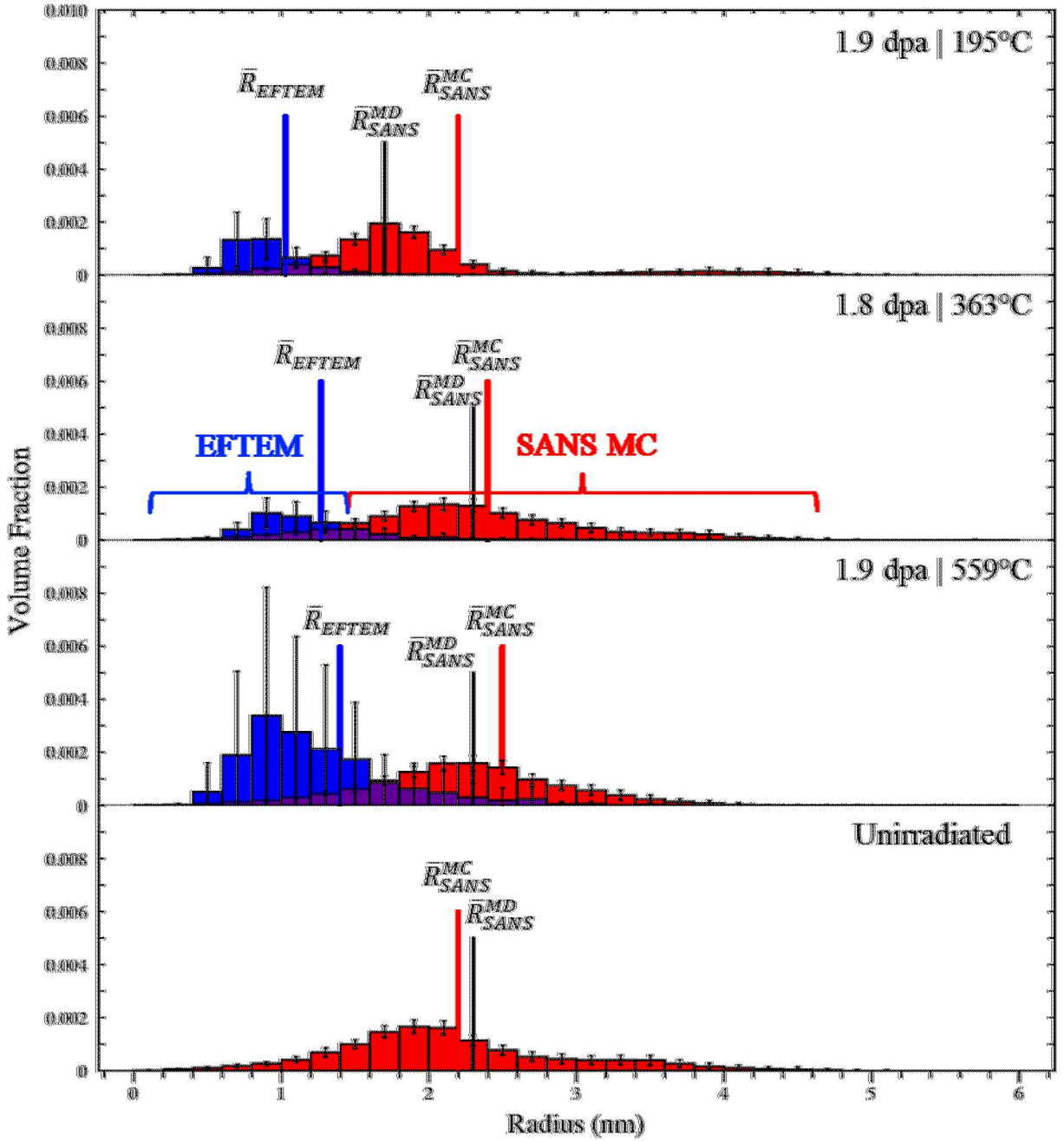

A-ratio determination (composition + structure)

Particle	ρ (g/cm^3)	$\Delta\rho^2_{nuclear}$ ($\times 10^{-12}$ Å)	$\Delta\rho^2_{magnetic}$ ($\times 10^{-12}$ Å)	Calculated A-ratio
YAG - $Y_3Al_5O_{12}$	4.56	2.73	0.16	6.68
YAP – $YAlO_3$	5.35	1.26	0.16	13.30
YAM – $Y_4Al_2O_9$	4.56	5.18	0.16	3.99
Al_2O_3	3.95	1.16	0.16	14.40
AlN	3.26	37.5	0.16	42.34
Y_2O_3	5.01	5.52	0.16	3.81
α'	7.20	0.11	0.16	2.44

Specimen ID	Irradiation Temp. (°C)	A-ratio (unitless)	
		SANS MD	SANS Monte Carlo
OD34	-	1.75±0.05	2.75±0.54
OD01	195	1.31±0.08	2.06±0.37
OD03	363	1.63±0.05	2.51±0.48
OD06	559	1.96±0.11	2.32±0.40

Contrast (ρ^2) independant

Contrast (ρ^2) used as a fitting parameter

Reduction after low temperature irradiation -> instability?

- Highly dependent on stoichiometry, chemical composition, and structure (density)
- A-ratio of 1.75-2.75 in the as-received condition suggests far-from perfect particle phases (amorphization, Fe/Cr substitution, etc.)
- Reduction after irradiation could be due to particles changing over the course of irradiation or the addition of the Cr-rich α’ phase in OD01 and OD03

Studies at Sandia's I^3TEM Facility

Sandia's I³TEM Facility

- Direct real time observation
  tion, ion
  , or both with
  esolution
  th several in-
  ges

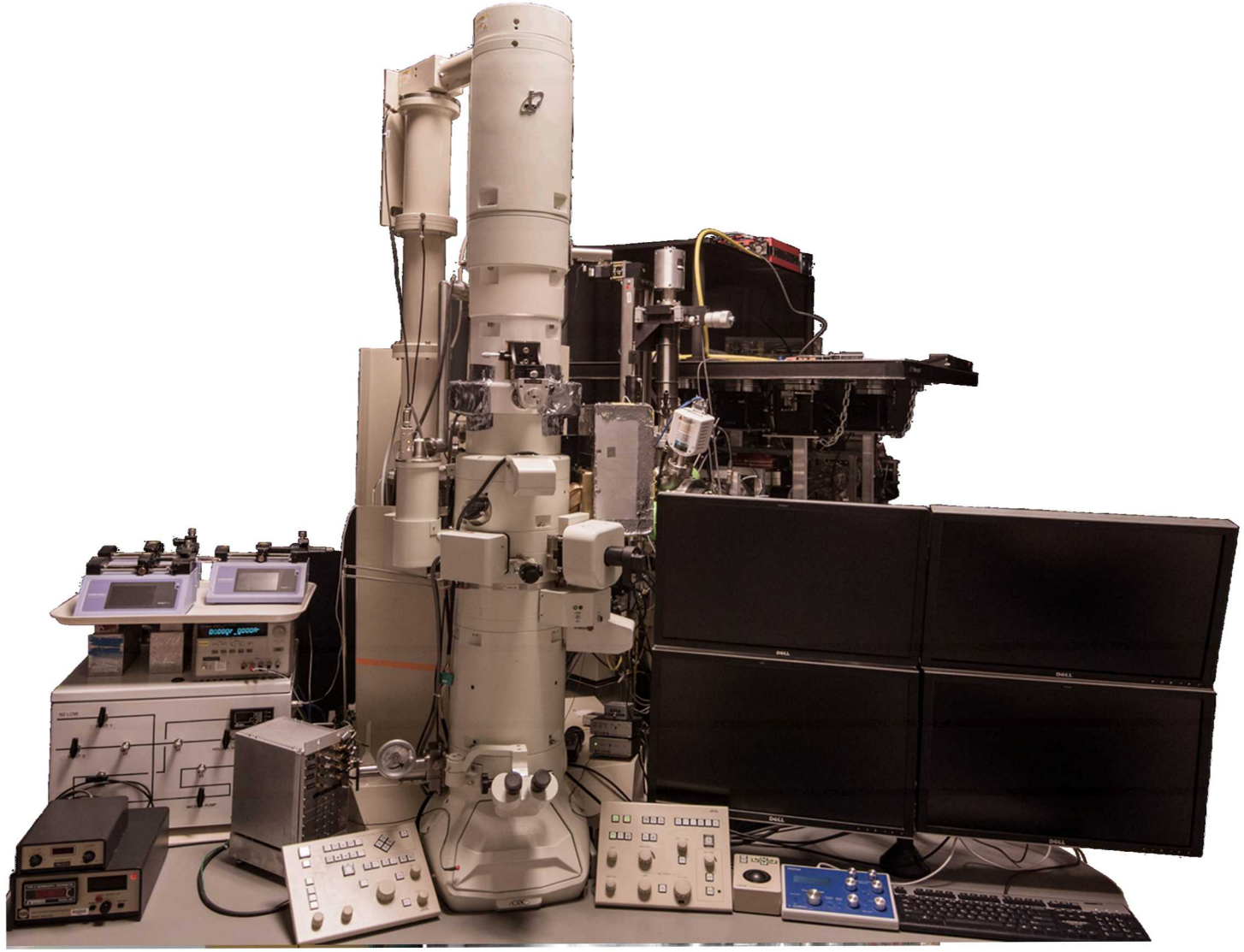

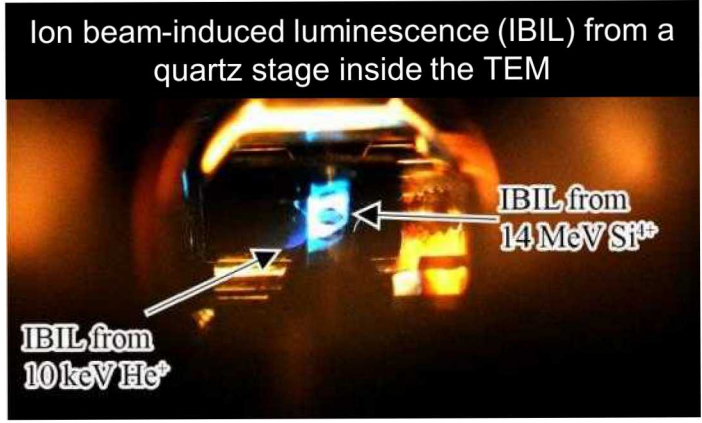

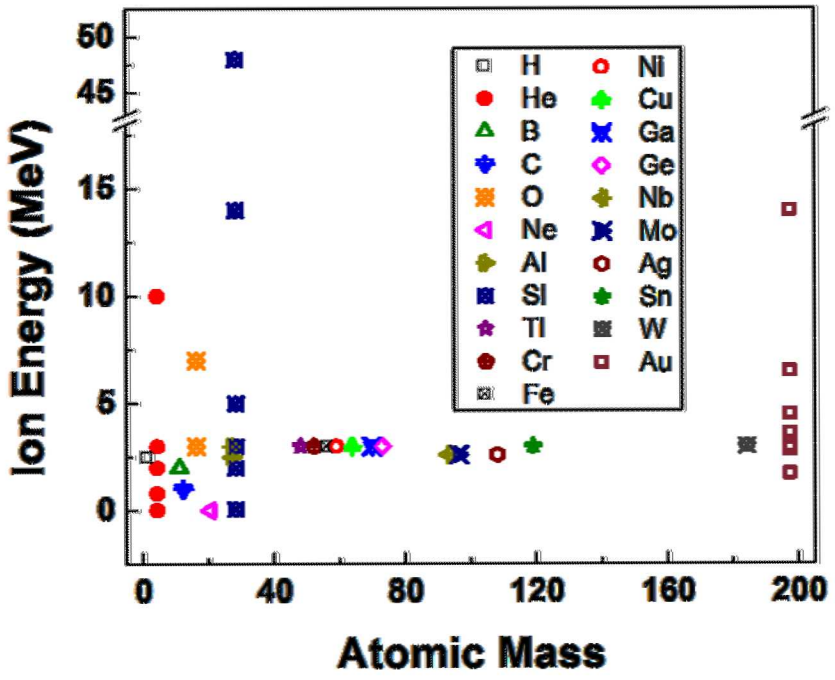

Nanodispersed CuNb for Enhanced Radiation Tolerance

- Lots of previous work on nanolaminates
- Working on developing nanodispersed CuNb thin films as model systems for nanofeatured alloys

- 50/50 Cu/Nb on Si_3N_4 grid
- Held at 700 °C for 20 mins
- Ramped to and held at 750, 800 °C for 5 to 10 mins

- Cu phase precipitates start to grow at ~120 °C, coarsening at ~200 °C
- Recrystallization of smaller Nb grains after holding at 700 °C
- Faster kinetics at higher temperatures

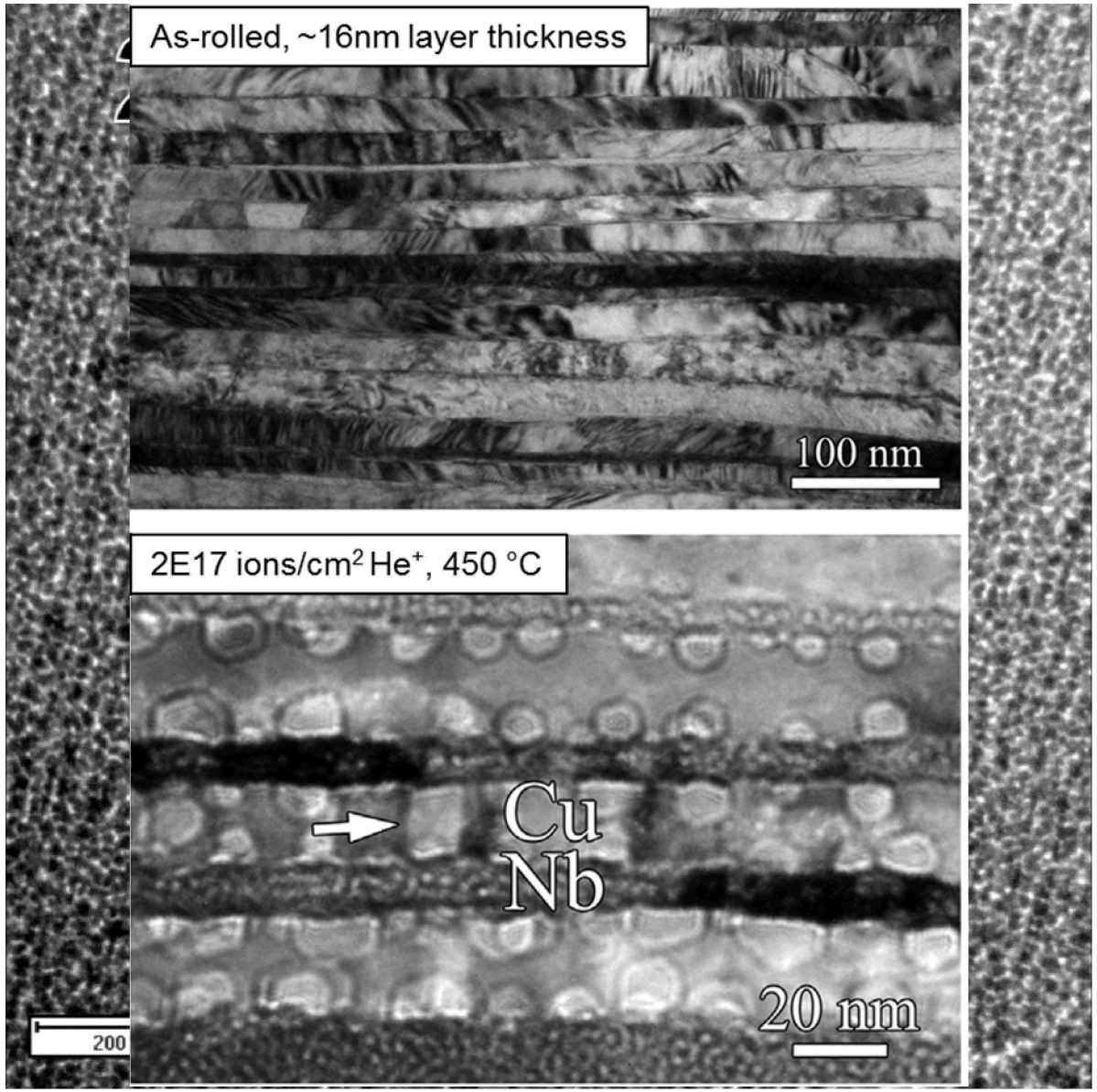

Synthesis and Characterization of d-UO_2 Nanoparticles

- Nanoparticles prepared by PAD ($UO_2(NO_3)_2 \cdot 6H_2O$, EDTA, PEI) followed by sintering at 1000 °C under varied atmospheric conditions
- Air-sintered show some crystalline phase, but mostly amorphous
- Ar-sintered show smaller nanoparticles that appear to be $UO_{2\pm x}$ phase

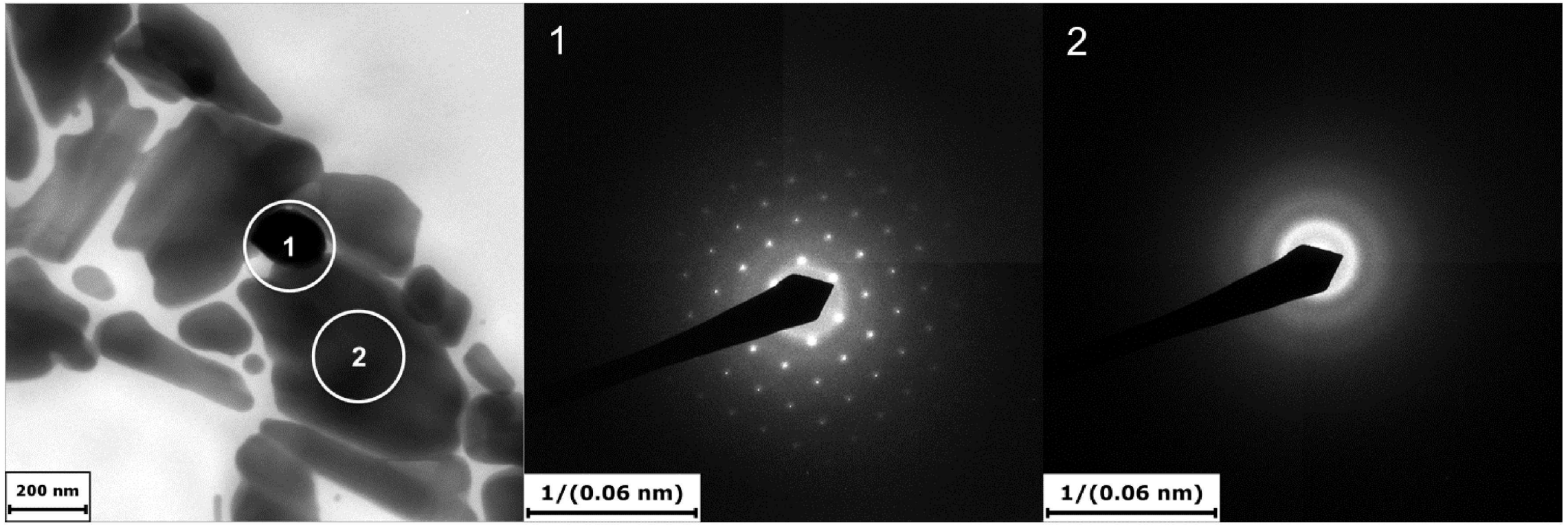

Synthesis and Characterization of d-UO_2 Nanoparticles

- Nanoparticles prepared by PAD ($UO_2(NO_3)_2 \cdot 6H_2O$, EDTA, PEI) followed by sintering at 1000 °C under varied atmospheric conditions
- Air-sintered show some crystalline phase, but mostly amorphous
- Ar-sintered show smaller nanoparticles that appear to be $UO_{2\pm x}$ phase

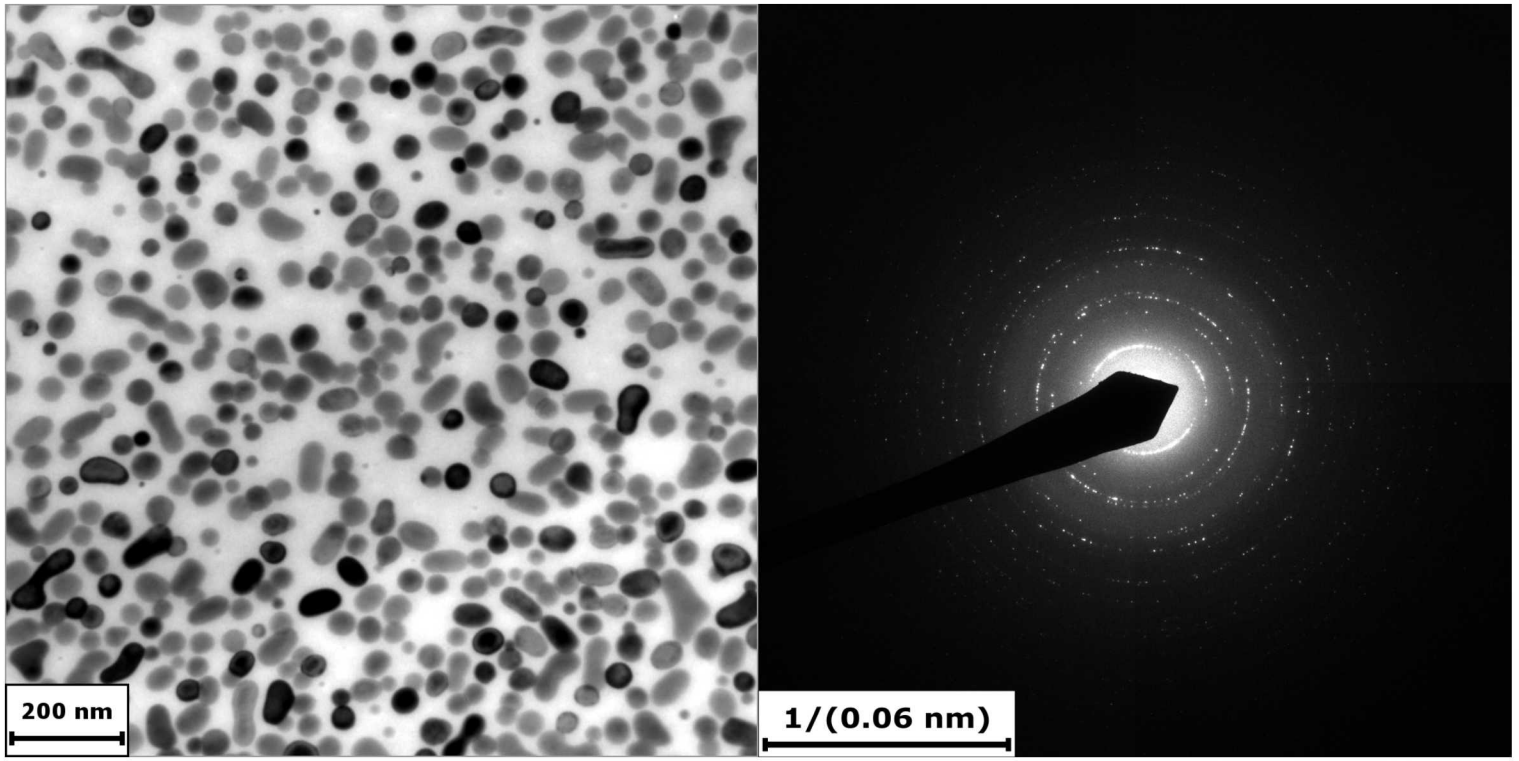

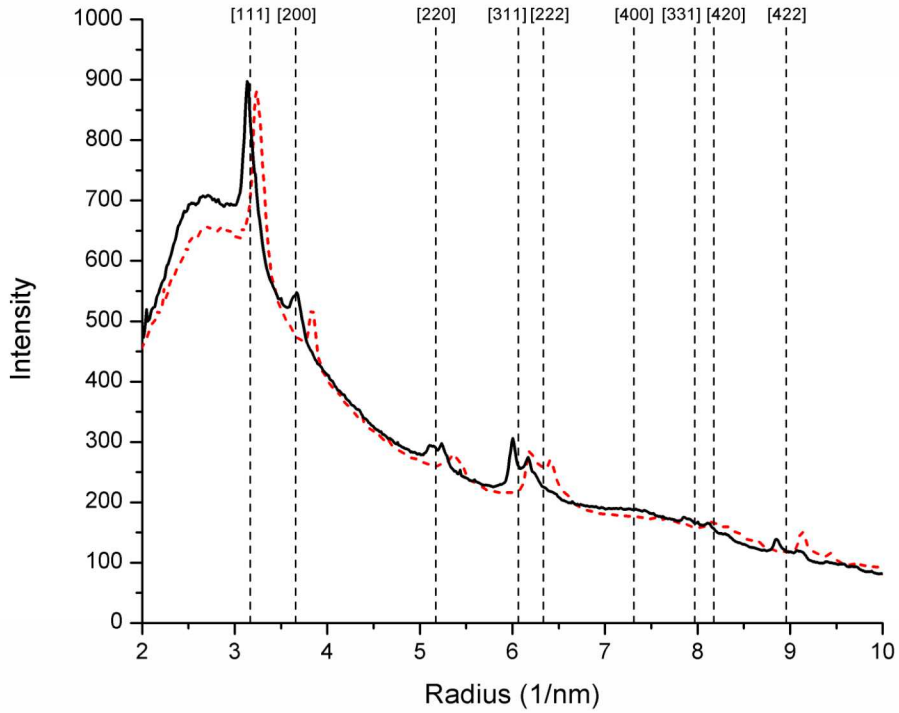

Synthesis and Characterization of d-UO_2 Nanoparticles

- Nanoparticles prepared by PAD ($UO_2(NO_3)_2 \cdot 6H_2O$, EDTA, PEI) followed by sintering at 1000 °C under varied atmospheric conditions
- Air-sintered show some crystalline phase, but mostly amorphous
- Ar-sintered show smaller nanoparticles that appear to be $UO_{2\pm x}$ phase

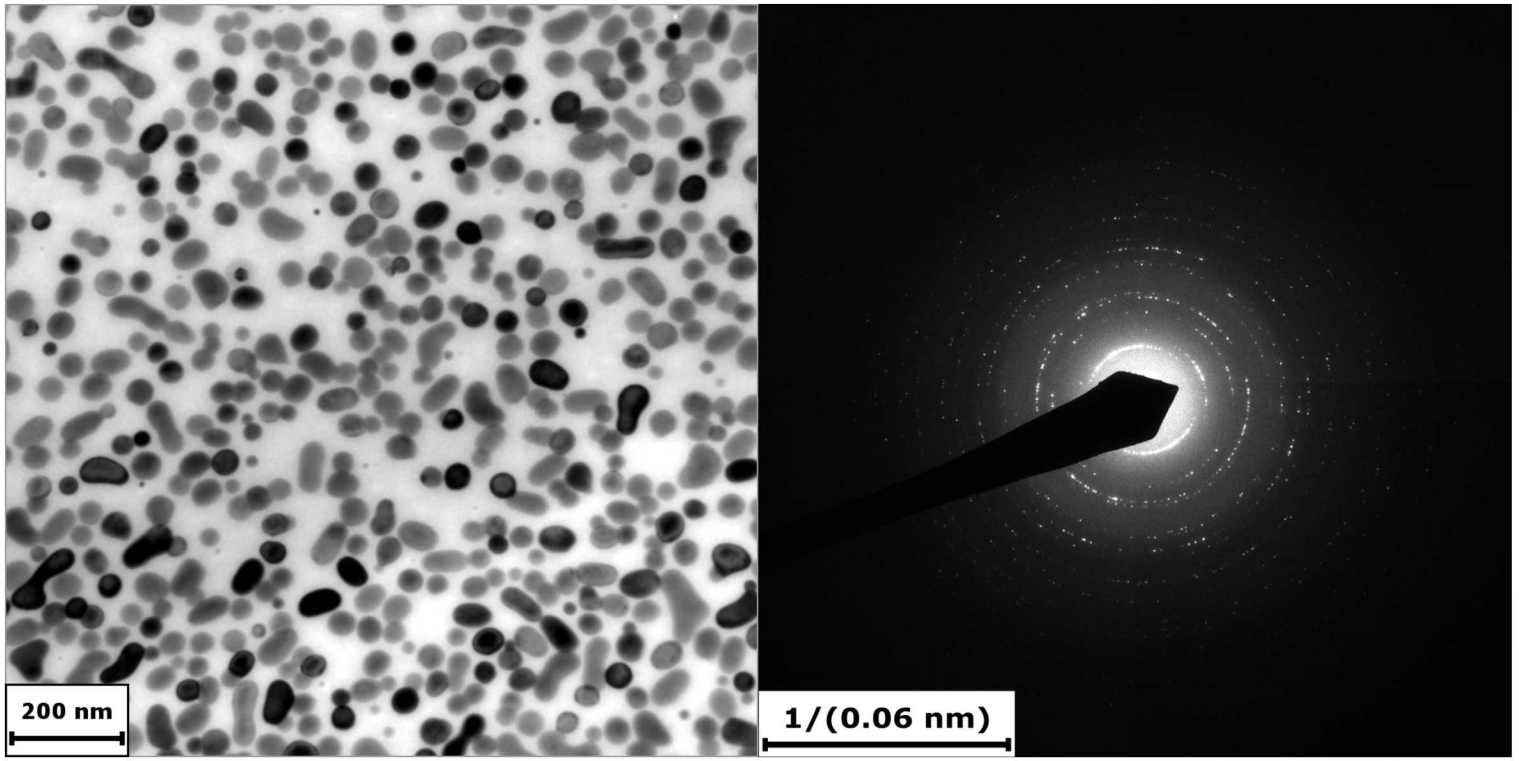

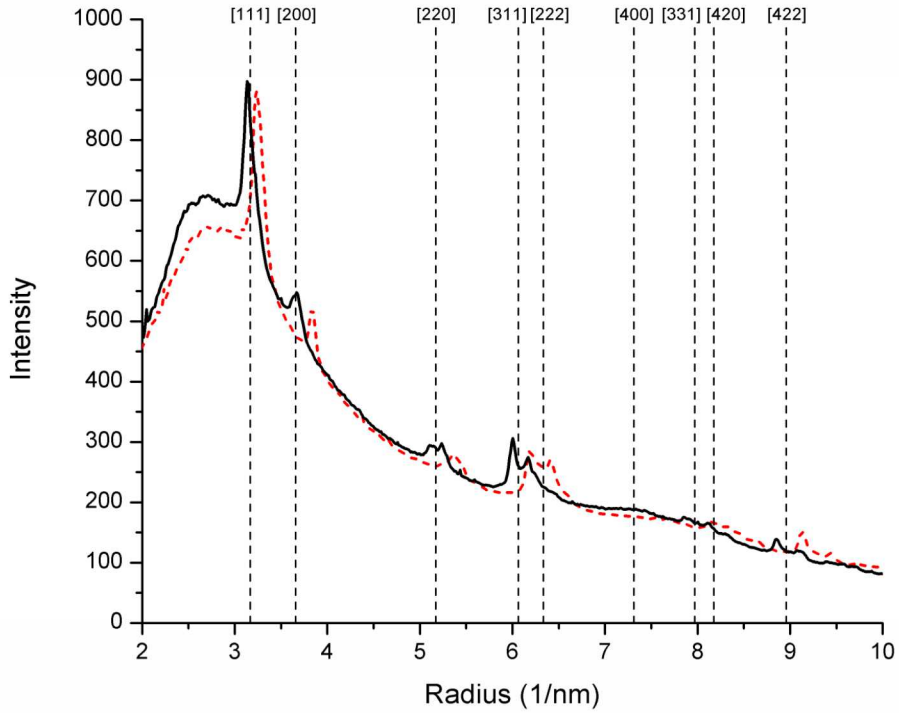

Characterization of High Burnup Spent Fuel

- Preliminary investigation of spent fuel from HB Robinson Nuclear Generating Station shows extremely complex high-burnup structure
- Proposal submitted to investigate chemistry of pellet-cladding chemical interaction (PCCI) layer

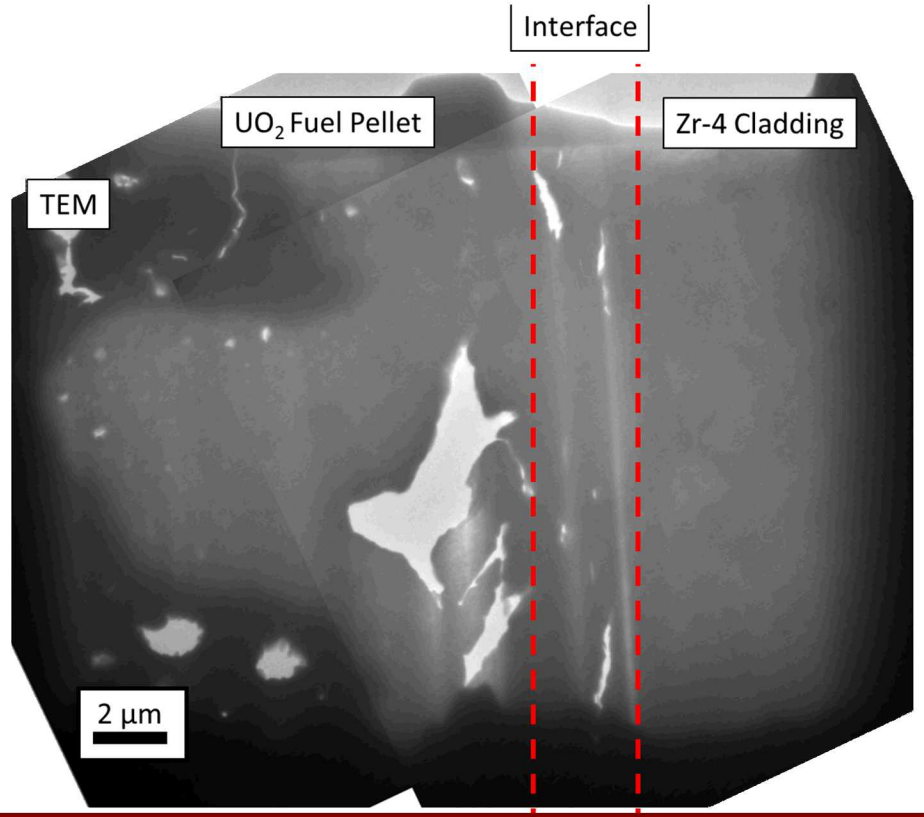

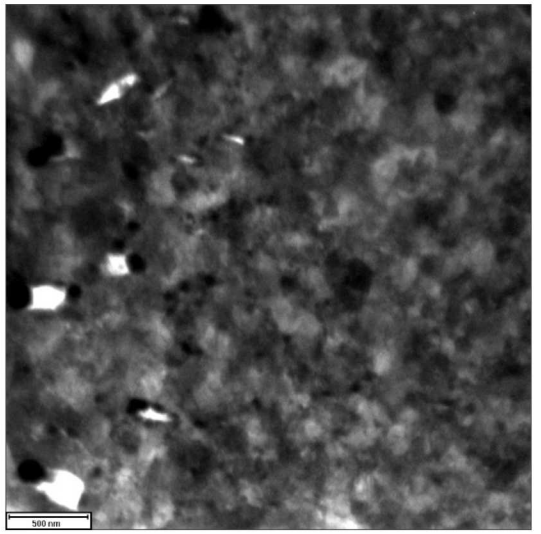

UO_2 Fuel Pellet

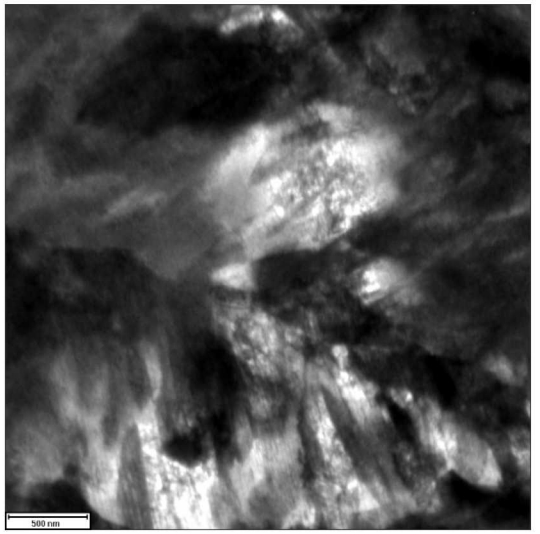

Zr-4 Cladding

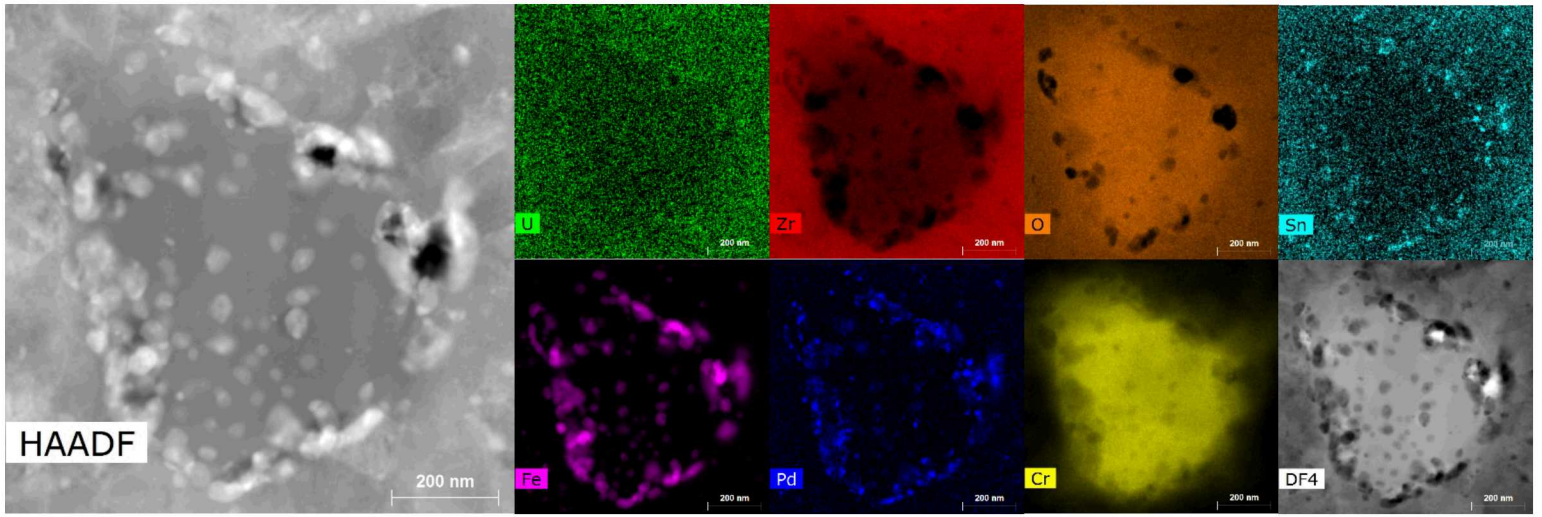

In-Situ SEM Development

- Led efforts for beamline and instrument development of an SEM capable of performing complex ion irradiation + straining experiments in-situ
- Currently includes three straining stages and connections to 6 MV and 1 MV tandem accelerators, with 1.2 kV ion source arriving next month

Kaufman & Robinson
KDC10 1.2 kV Ion Source

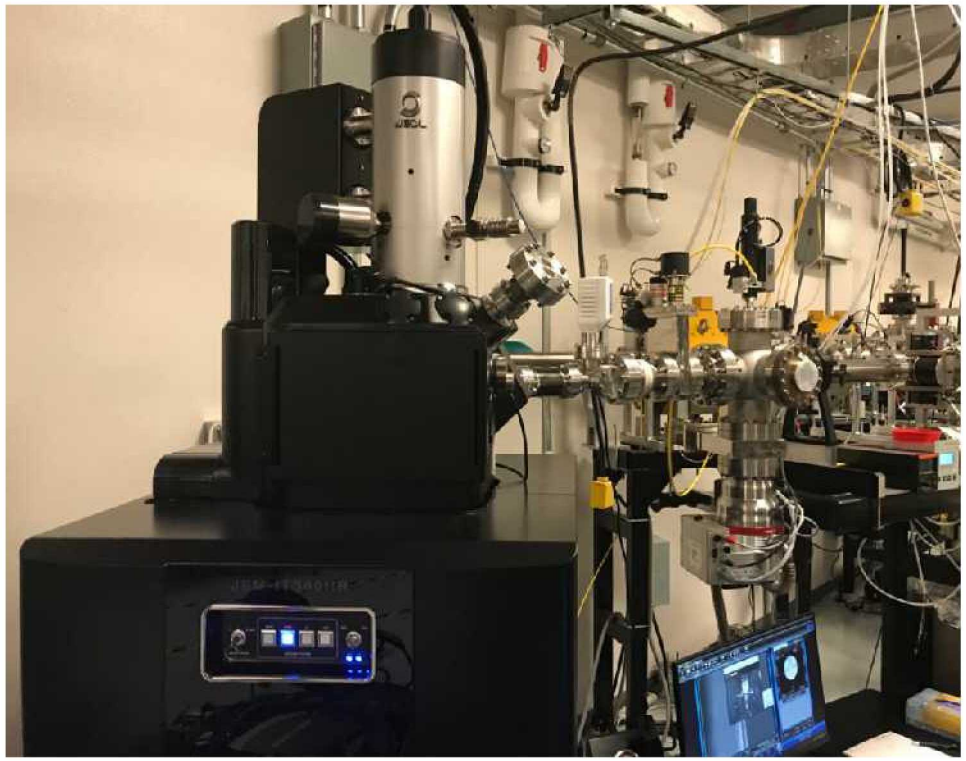

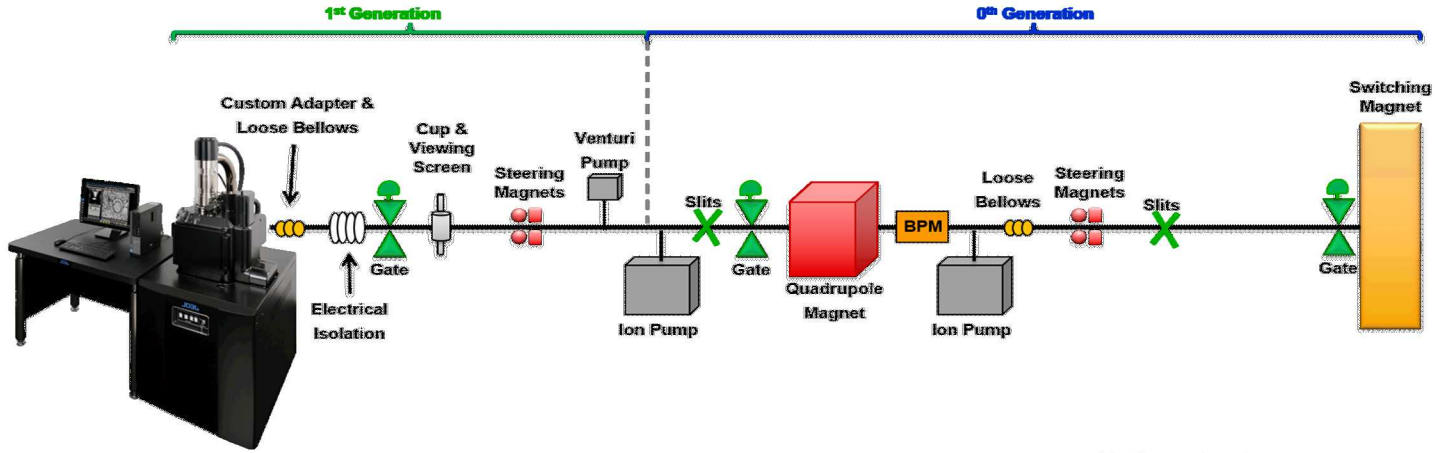

MTI Fullam
Straining Heating

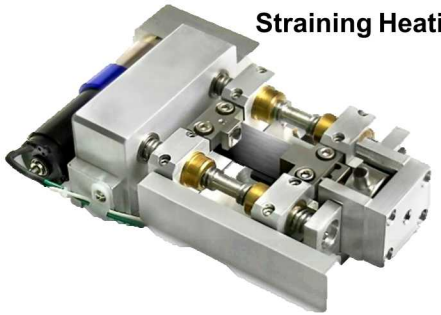

Hysitron PI85
Nanoindenter

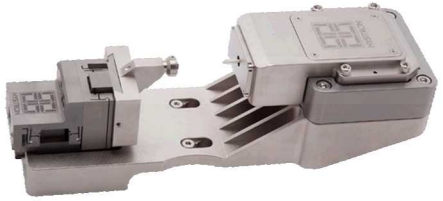

Fatigue tester

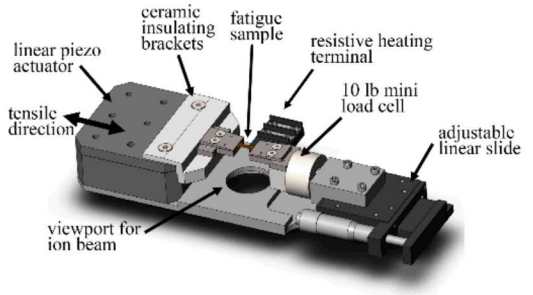

Summary & Conclusions

- **Gen. I Fe-Cr-Al Model Alloys**
  - Al additions result in a lower α′ phase Cr content than in binary Fe-Cr systems
  - Precipitate coarsening behavior has a similar mechanism to the thermally-aged system
  - Precipitates appear to nucleate homogeneously except for at grain boundaries where segregation and local denudation is observed
  - Precipitates dissolve rapidly at temperatures above the phase boundary
  - Dislocation loop density decreases with Cr content and <100> loops appear to grow faster than ½<111> loops

Summary & Conclusions

- **Gen. II Fe-Cr-Al ODS Variants Alloys**
  - Nanoclusters appear stable during medium- and high-temperature irradiation
  - Some signs of cluster instability during low temperature irradiation – additional work require to determine exact mechanism
  - Dislocation loop microstructure has strong temperature dependence and is greatly affected by ODS inclusions and/or small grain sizes and internal stresses

Colleagues & Collaborators

Special thanks to:

- Kevin Field (ORNL)
- Kumar Sridharan (UW)
- Khalid Hattar (SNL)
- Phil Edmondson (ORNL)
- Chad Parish (ORNL)
- Yukinori Yamamoto (ORNL)
- Ken Littrell (ORNL)
- Richard Howard (ORNL)
- Jack Haley (Oxford)
- Sebastien Dryepondt (ORNL)
- Caleb Massey (ORNL)
- David Hoelzer (ORNL)
- Remi Dingreville (SNL)
- Ryan Hess (SNL)

Miscellaneous Other Projects

Radiation-induced segregation in Ni-Cr Alloys

Collaborators: U. Wisc., Drexel University

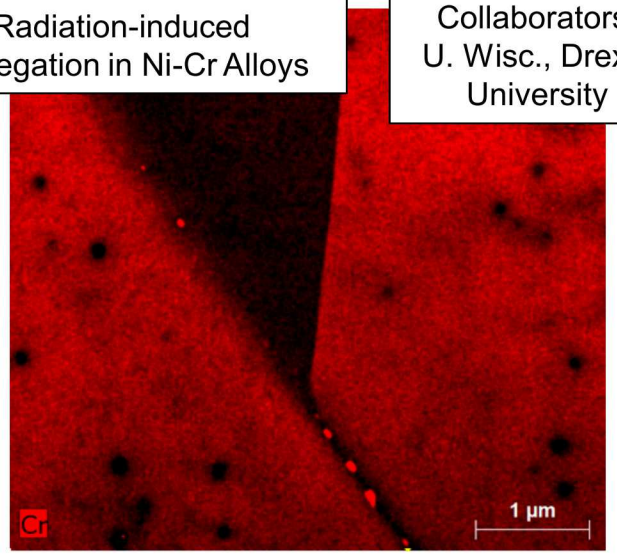

He bubble formation in hydrided Pd

Collaborators: PNNL, U. of Huddersfield

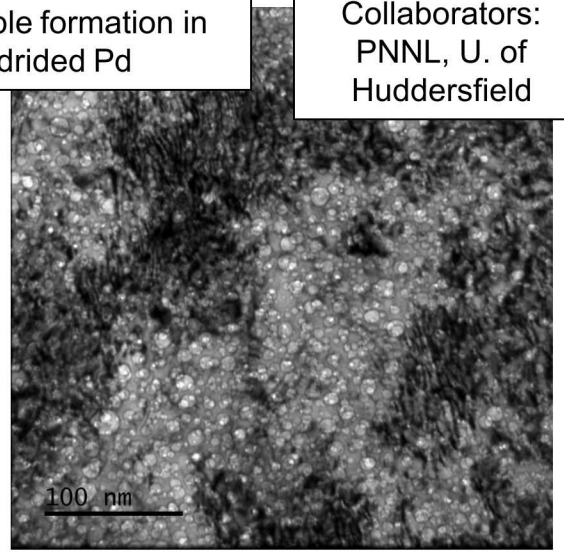

Coupling MD and Experiments in Oxide Nanoparticles

Collaborators: Ben Cowen (UNM)

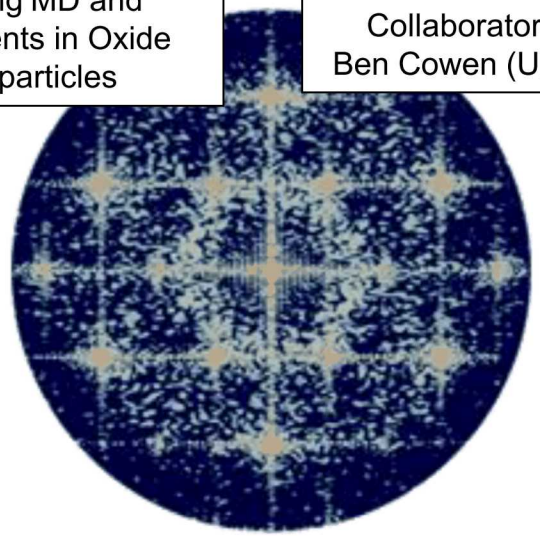

DTEM & Temporal Compression Development

Collaborators: LLNL, IDES

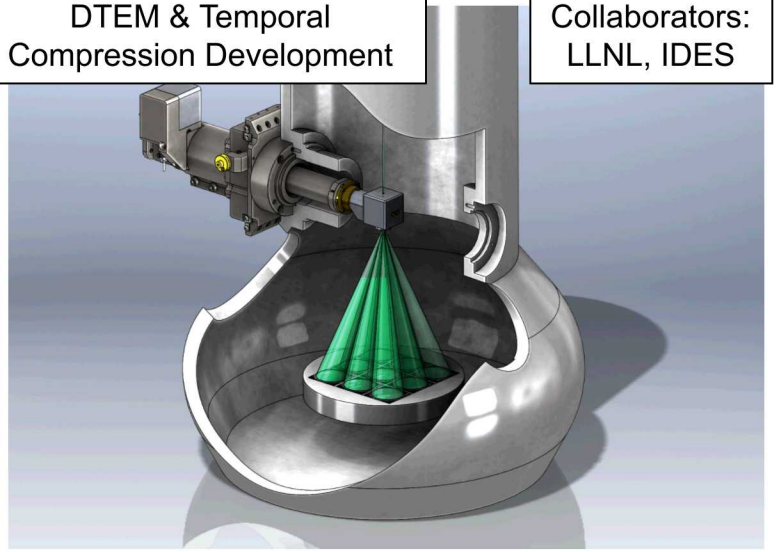

In-situ laser sintering of metallic nanoparticles

Collaborators: Patrick Price (SNL), IDES

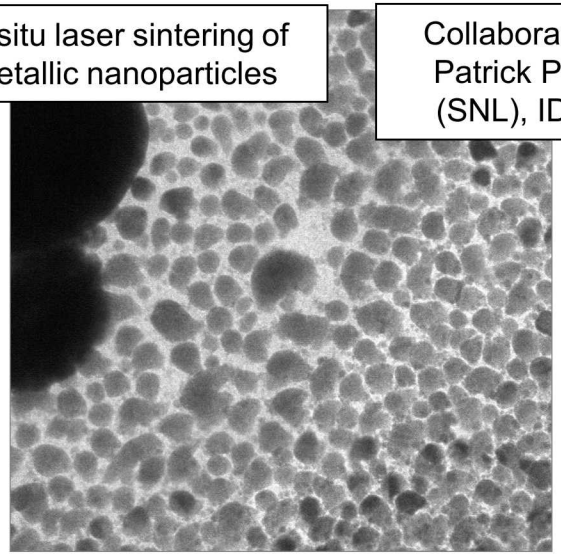

Rad. Damage in MA956

Collaborators: Liz Getto (USNA)

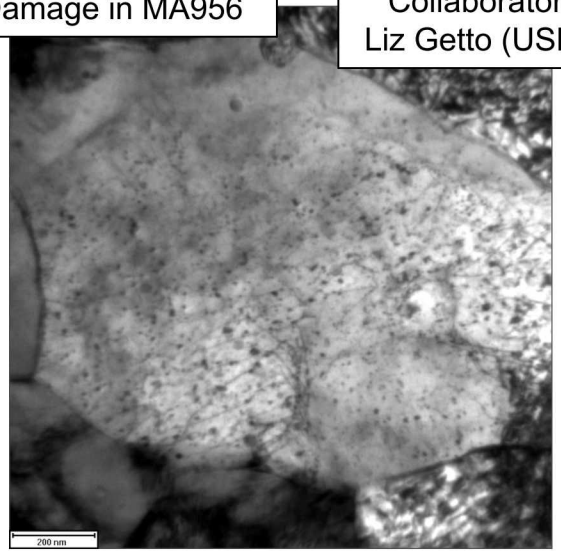

Acknowledgements

Primary funding provided by the U.S. Department of Energy (DOE), Office of Nuclear Energy, Advanced Fuel Campaign of the Fuel Cycle R&D Program and the U.S. DOE's Office of Science, Fusion Energy Sciences.

Use of CG-2 General Purpose SANS beamline at ORNL's HFIR facility sponsored by the U.S. DOE, Scientific User Facilities Division, Office of Basic Energy Sciences.

Use of Cameca LEAP 4000X HR at the Center for Advanced Energy Studies and at ORNL sponsored by the Nuclear Science User Facilities (NSUF) and the Center for Nanomaterials Science (CNMS), respectively.

This research was performed, in part, using instrumentation (FEI Talos F200X TEM) provided by the Department of Energy, Office of Nuclear Energy, Fuel Cycle R&D Program, and the Nuclear Science User Facilities.

Extra Slides

Radiation-enhanced precipitation (α’)

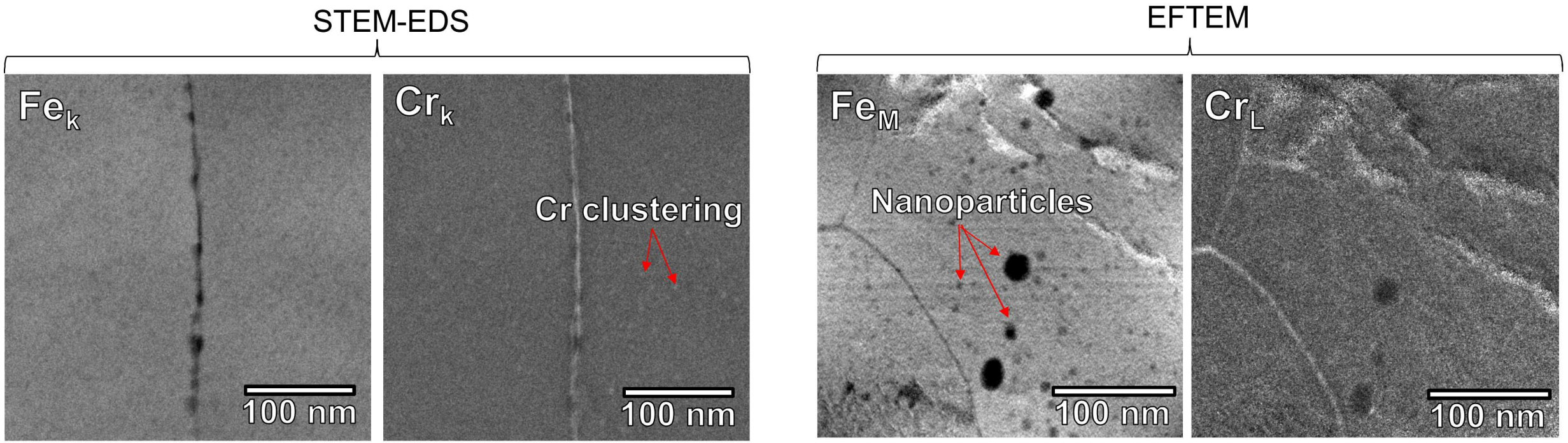

- FeCrAl alloys have been shown to be susceptible to Cr-rich α’ precipitation under neutron irradiation[1]
- STEM-EDS reveals possible Cr-clustering but most likely weak composition variance to matrix
- EFTEM insensitive to detection of Cr-cluster found in STEM-EDS

[1]Briggs et al. Acta Mat. 129, 2017, 217-228

SiC Thermometry

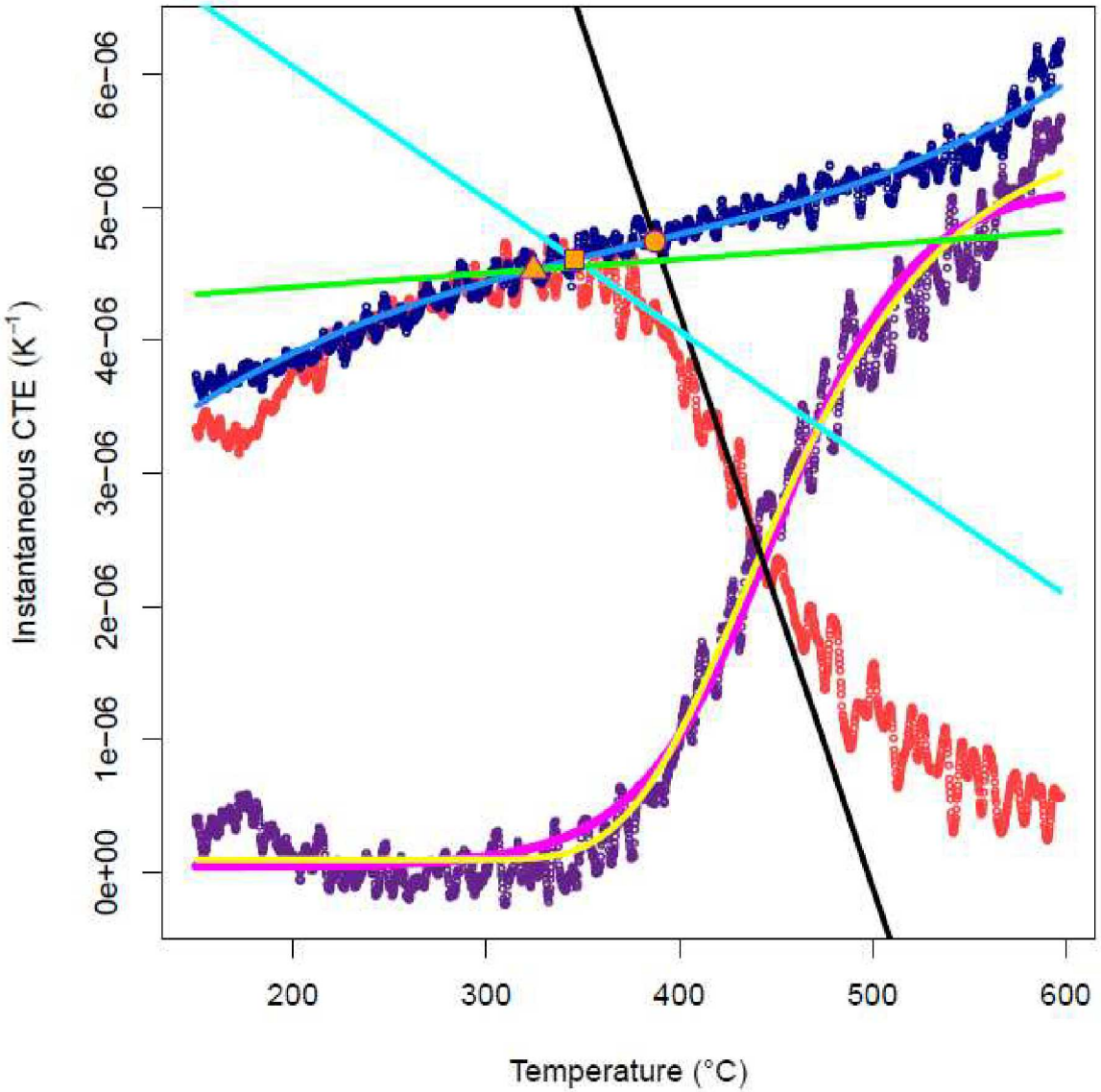

- Measure length change of specimens as you heat and cool the material (dilatometry)
- At the irradiation temperature, radiation-induced defects begin to anneal out
- Fitting to the heating and cooling curves yields the irradiation temp

Comparison of SANS Scattering Intensities

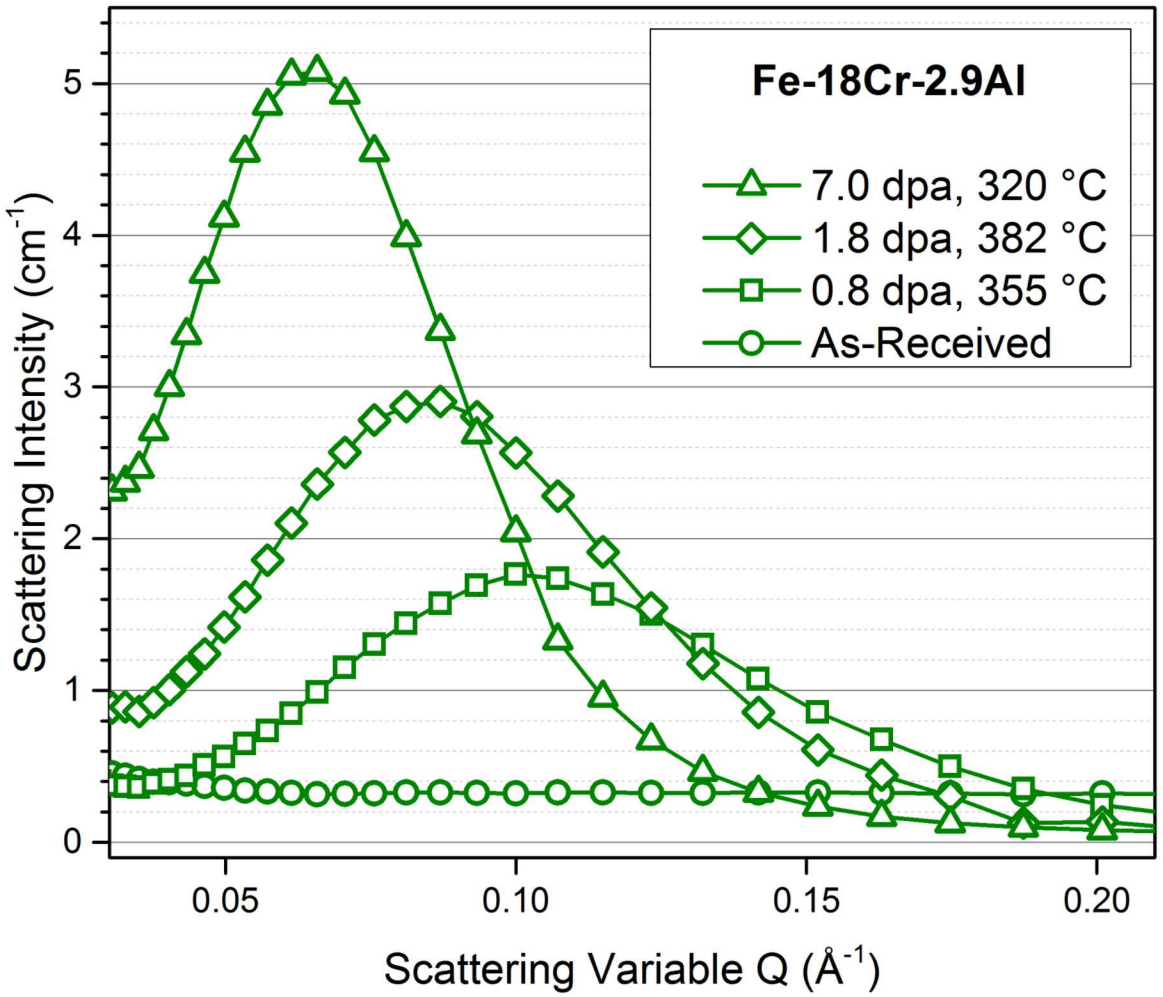

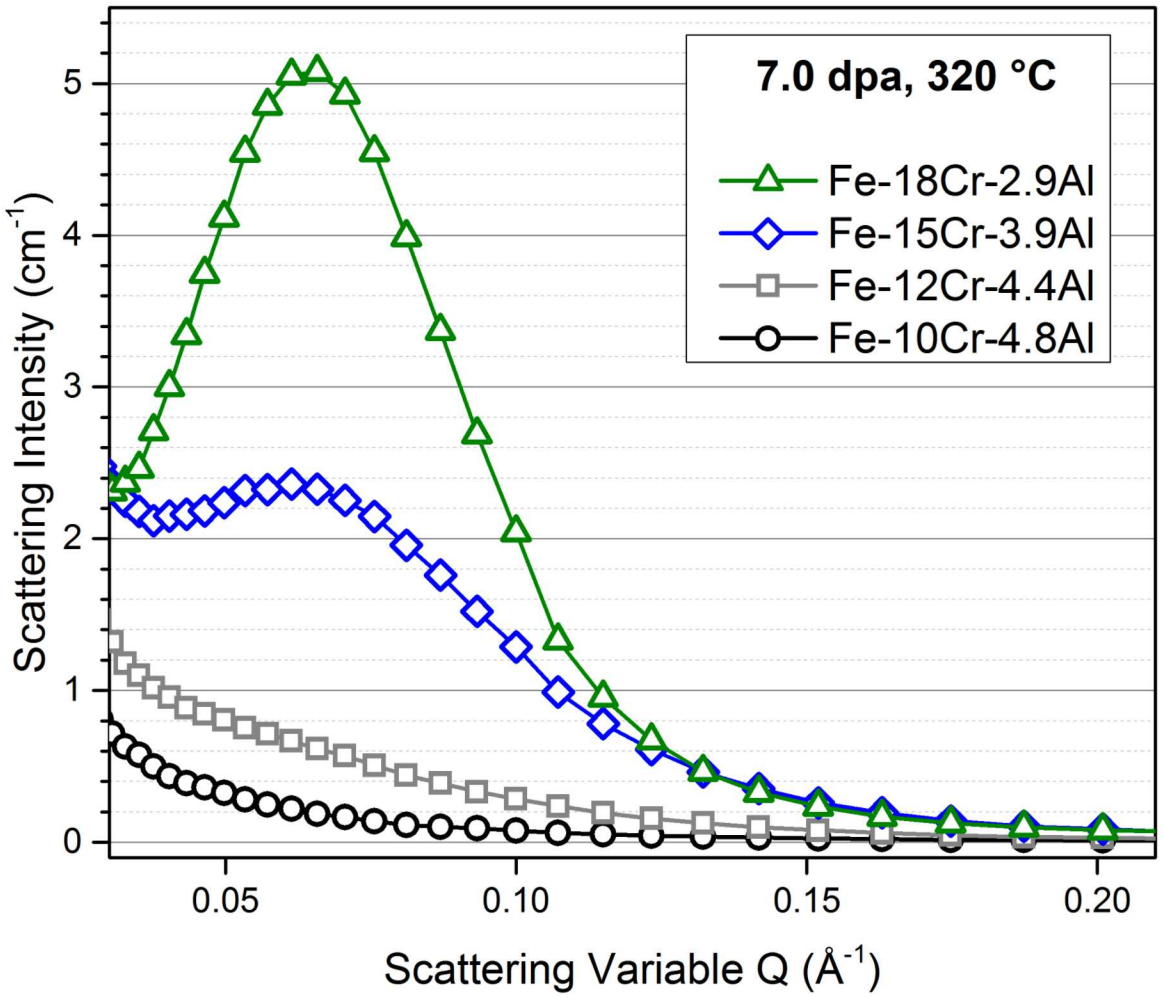

Irradiation Temperature Analysis

Inner Tensile

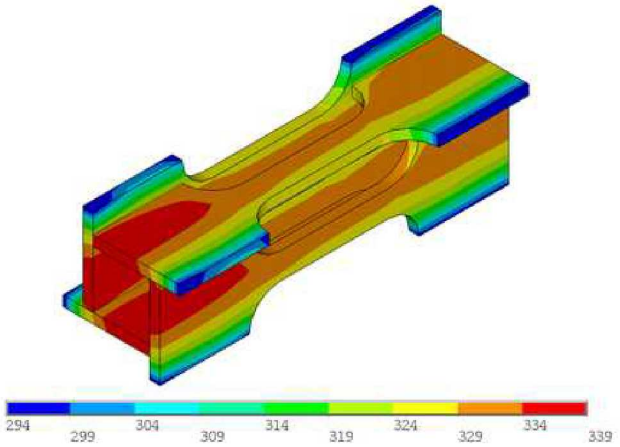

Middle Tensile

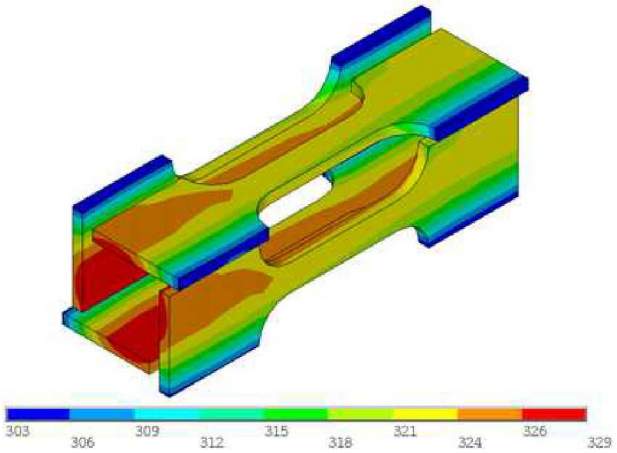

Outer Tensile

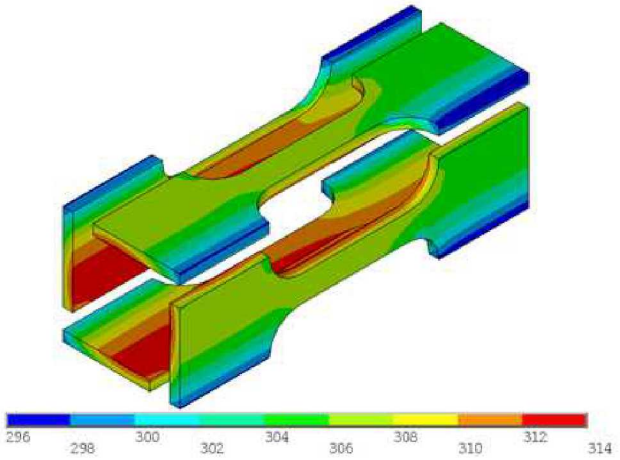

Sic Thermometry Bar

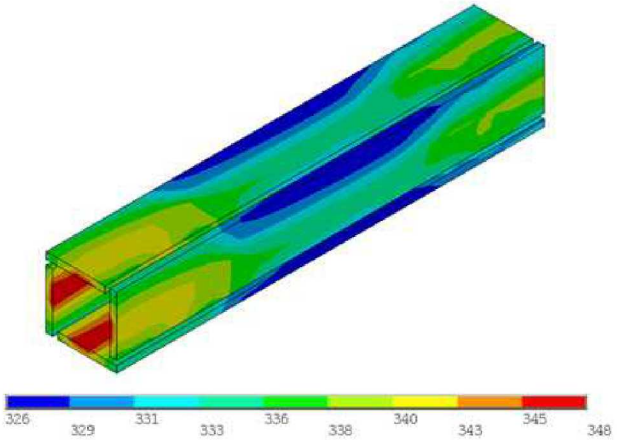

- Some thermal gradient expected in uninstrumented neutron-irradiation experiments
- Finite element analysis performed using ANSYS Workbench software using known HFIR heat generation rate and convection parameters
- Average temperatures within ~20 °C

Specimen	Specimen Temp (°C) Average (Min-Max)
Inner Tensile	328 (294-339)
Middle Tensile	321 (303-329)
Outer Tensile	307 (296-314)
SiC Thermometry	336 (328-344)

SANS Data Configuration

- Neutron irradiated SS-J tensile half specimens were encapsulated in Pb “piglets” to limit radioactivity while providing high quality SANS data

Specimen ID	Bare Specimen mR/hr γ on contact	Bare Specimen mR/hr γ at 30 cm	Shielded Specimen mR/hr γ on contact	Shielded Specimen mR/hr γ at 30 cm
OD01	2200	160	1100	120
OD03	2000	120	900	120
OD06	1800	100	1000	80

- SANS configuration:
  - GP-SANS Line at ORNL
  - ≳1 T saturated magnetic field
  - 3 detector configurations: $0.00658 \leq q\ (nm^{-1}) \leq 2.48$
  - Ambient air
  - 1D curves scaled to medium detector configuration

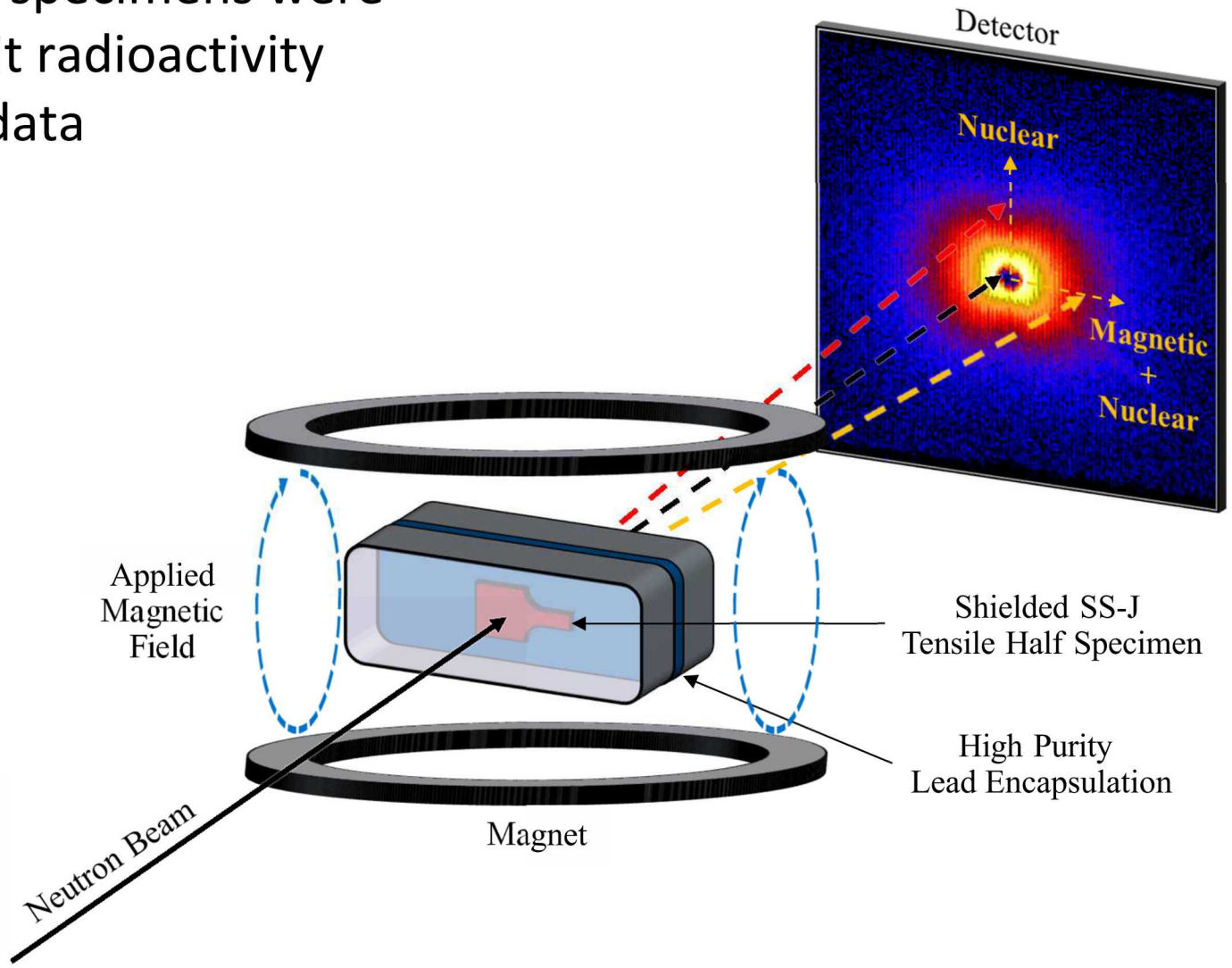

[1]Bressler et al., J Appl Crystallogr, 48(Pt 3) 2015, 962-969

SANS Data Analysis

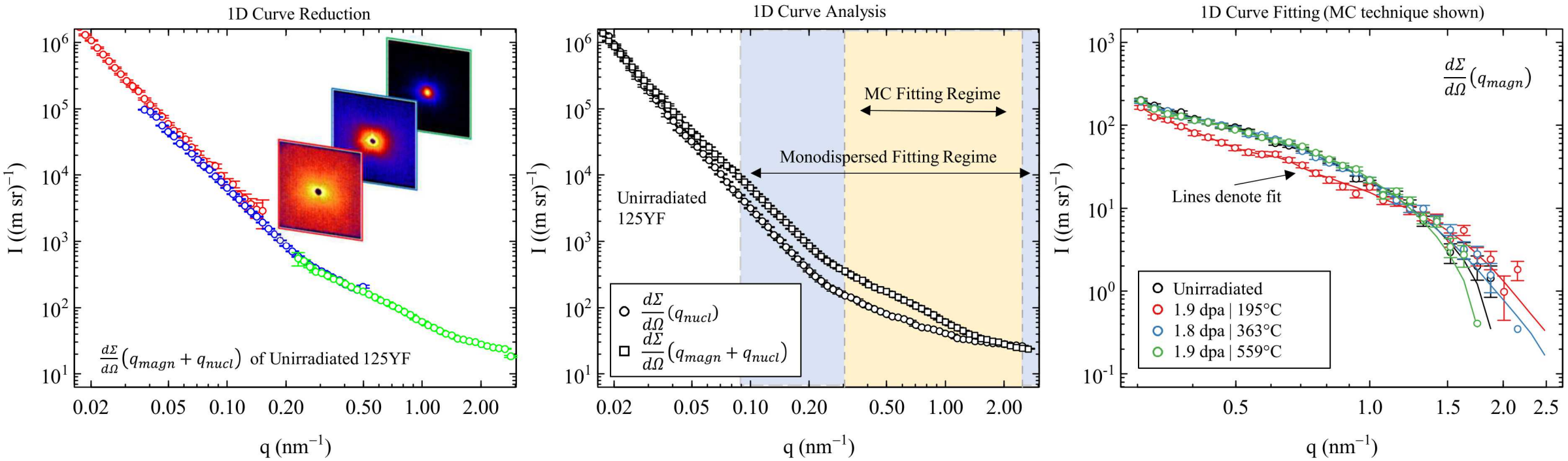

- Magnetic scattering contrast calculated as 1.55x10-11 Å^{-4} using normalized Fe-Cr-Al composition[1]
- A-ratios calculated assuming perfect crystals
- First order approximation of the magnetic scattering difference: $\frac{d\Sigma}{d\Omega}(q_{magn}) \approx \frac{d\Sigma}{d\Omega}(q_{nucl}) - \frac{d\Sigma}{d\Omega}(q_{magn}+q_{nucl})$
- Fitting on magnetic scattering difference completed using Monte Carlo regression analysis[2] and monodispersed spheres[3]

[1]Blau et al., Phys. Stat. Sol. (b) 81, 1977, 535 [2]Bressler et al., J Appl Crystallogr, 48(Pt 3) 2015, 962-969. [3]Pederson et al. Adv. Colloid Interface Sci. 70, 1997, 171-210.

Acknowledgements

- Primary funding provided by the U.S. Department of Energy (DOE), Office of Nuclear Energy, Advanced Fuel Campaign of the Fuel Cycle R&D Program and the U.S. DOE's Office of Science, Fusion Energy Sciences
- Use of CG-2 General Purpose SANS beamline at ORNL's HFIR facility sponsored by the U.S. DOE, Scientific User Facilities Division, Office of Basic Energy Sciences
- Use of Cameca LEAP 4000X HR at the Center for Advanced Energy Studies and at ORNL sponsored by the Nuclear Science User Facilities (NSUF) and the Center for Nanomaterials Science (CNMS), respectively
- This research was performed, in part, using instrumentation (FEI Talos F200X TEM) provided by the Department of Energy, Office of Nuclear Energy, Fuel Cycle R&D Program, and the Nuclear Science User Facilities.

125YF Dislocation Loop Microstructures

- Low temp irradiation resulted in high density of small, mostly black-dot loop defects
- Medium temp irradiation yielded lower density of larger, more well defined loop structures
- No loop structures observed in high temp irradiation

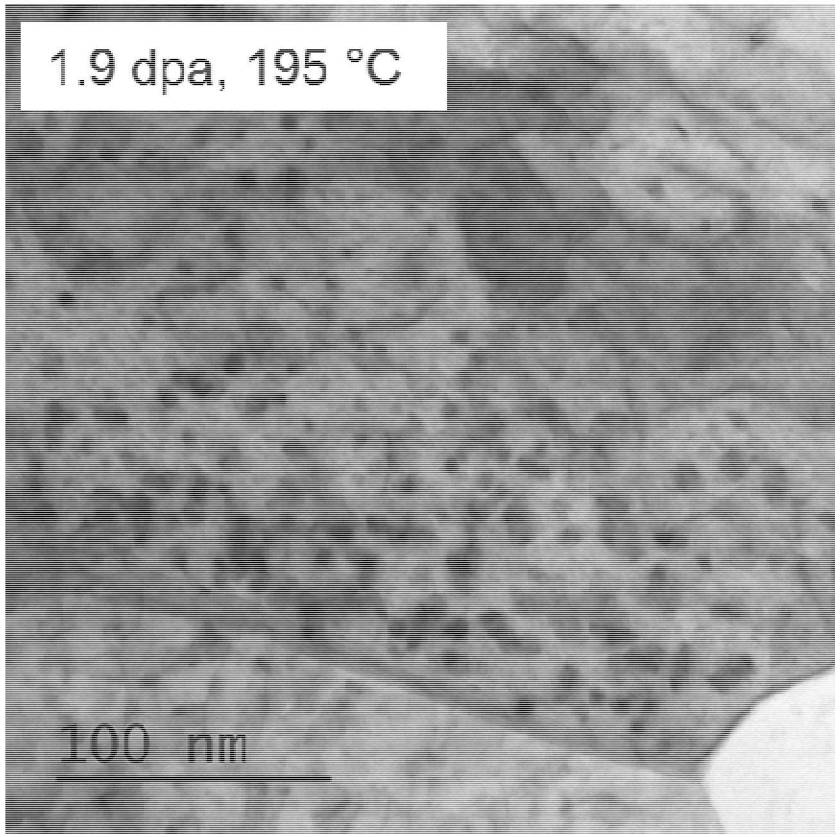

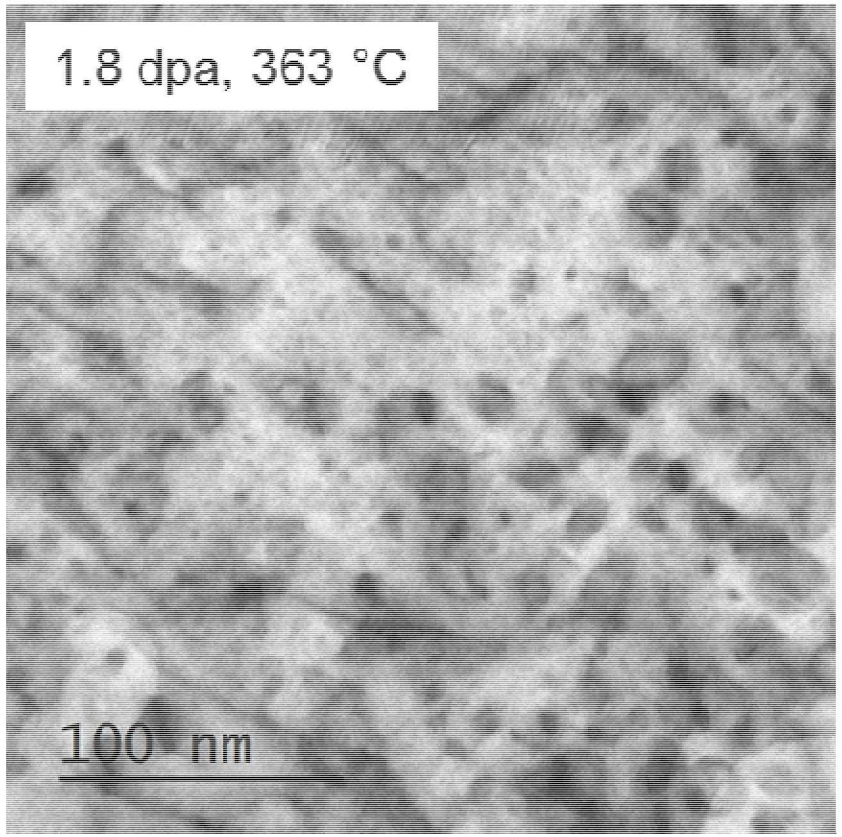

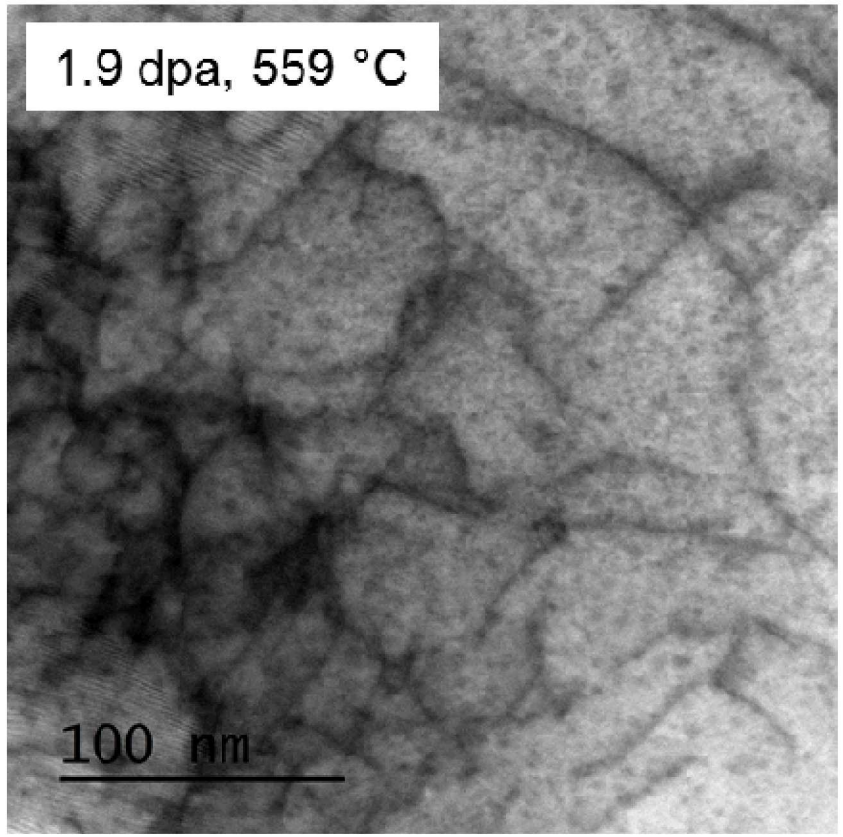

Comparison to non-ODS Alloys

- Higher density of smaller loops observed in ODS variant
- Smaller grain size may also contribute to observed effect

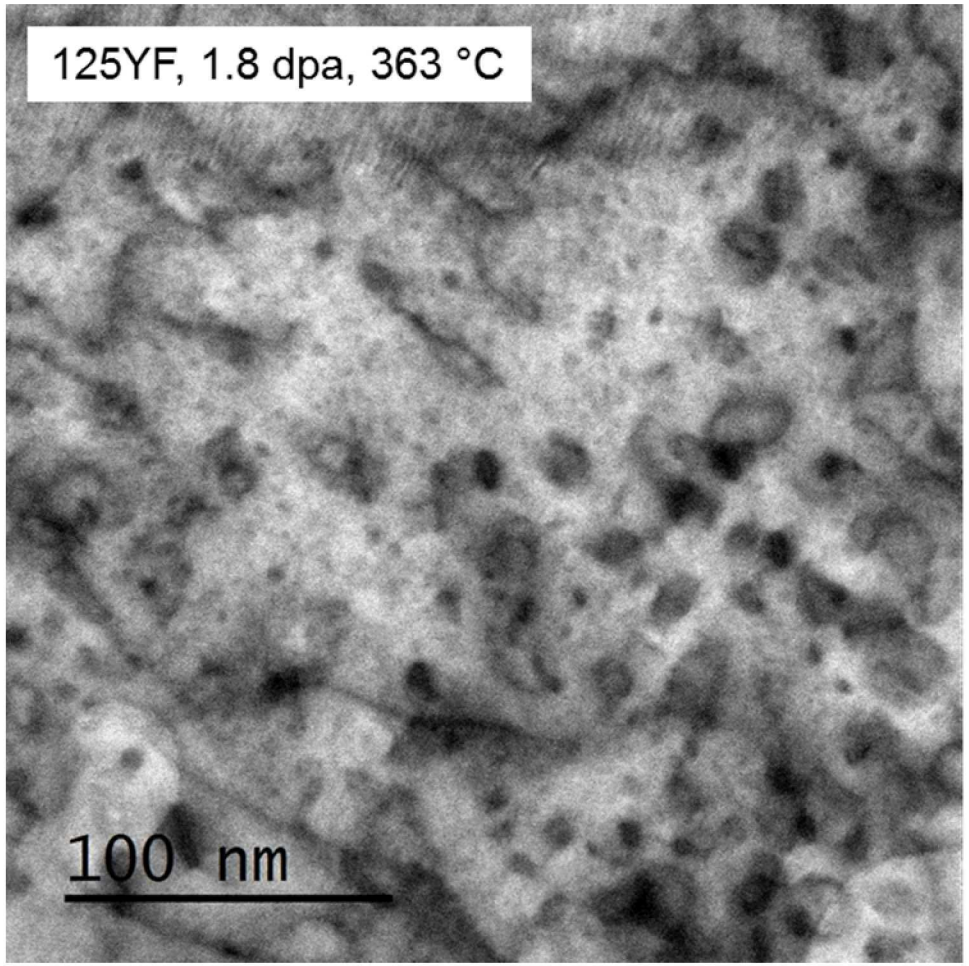

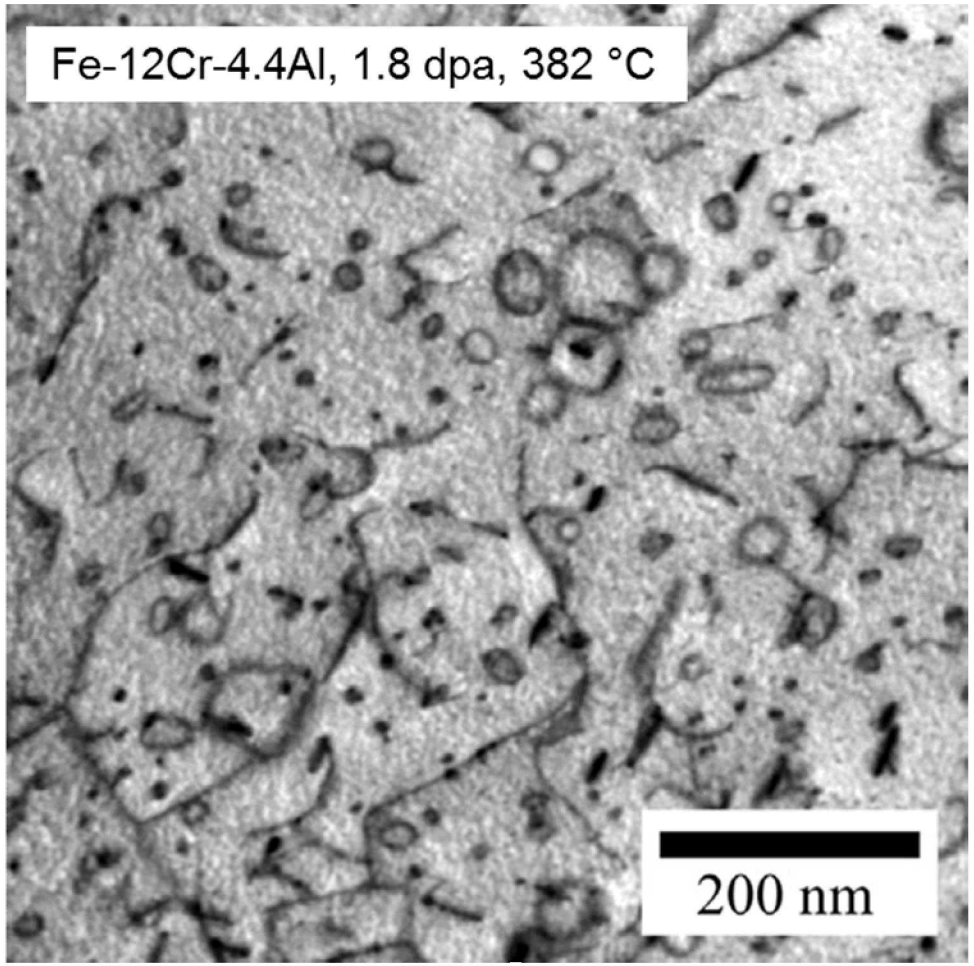

[1] Field, K. G., *et al.* (2015). Radiation tolerance of neutron-irradiated model Fe-Cr-Al alloys. *Journal of Nuclear Materials*. 465, 746-755.

Synthesis and Characterization of d-UO_2 Nanoparticles

- PED analysis not useful for determining exact phase stoichiometry
- Does appear to confirm that phase is indeed $UO_{2\pm x}$ as opposed to a more O-rich phase

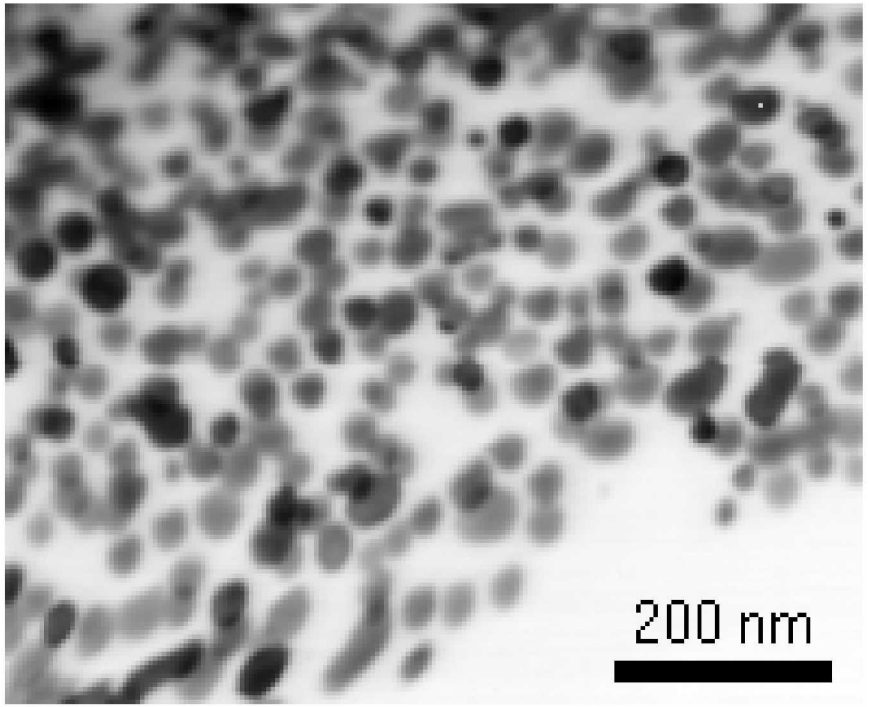

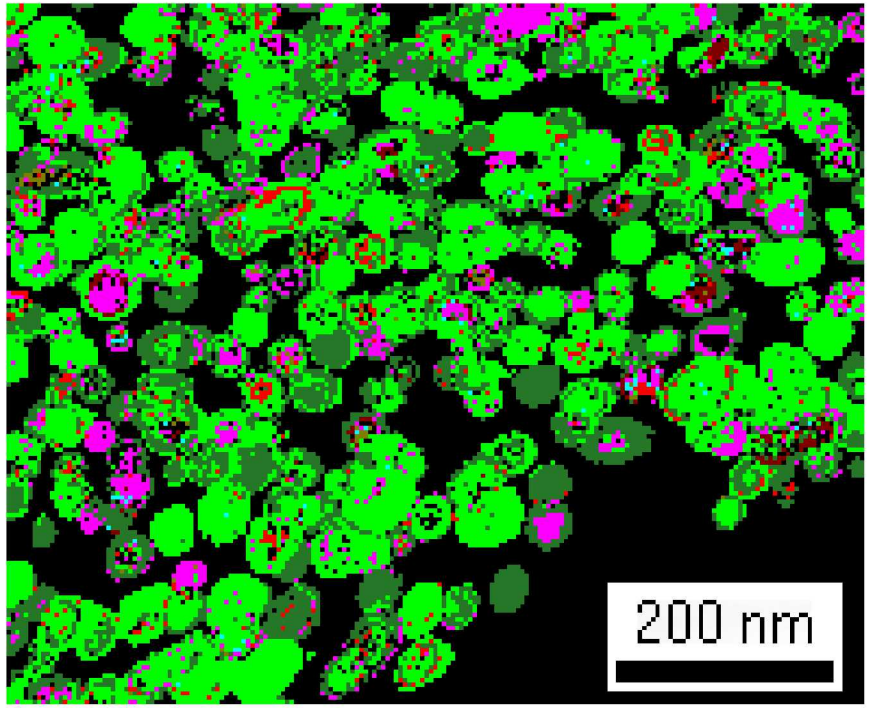

Fe-Cr-Al Alloys for Nuclear Systems

- Why is Fe-Cr-Al attractive as a LWR cladding material?
  - Exceptional high temperature oxidation resistance due to formation of passivating Al_2O_3 (up to 1200-1475 °C)
  - High strength, with potential for oxide-dispersion strengthened variants
  - Low swelling rates in irradiation environments
  - Potential for near-term deployment

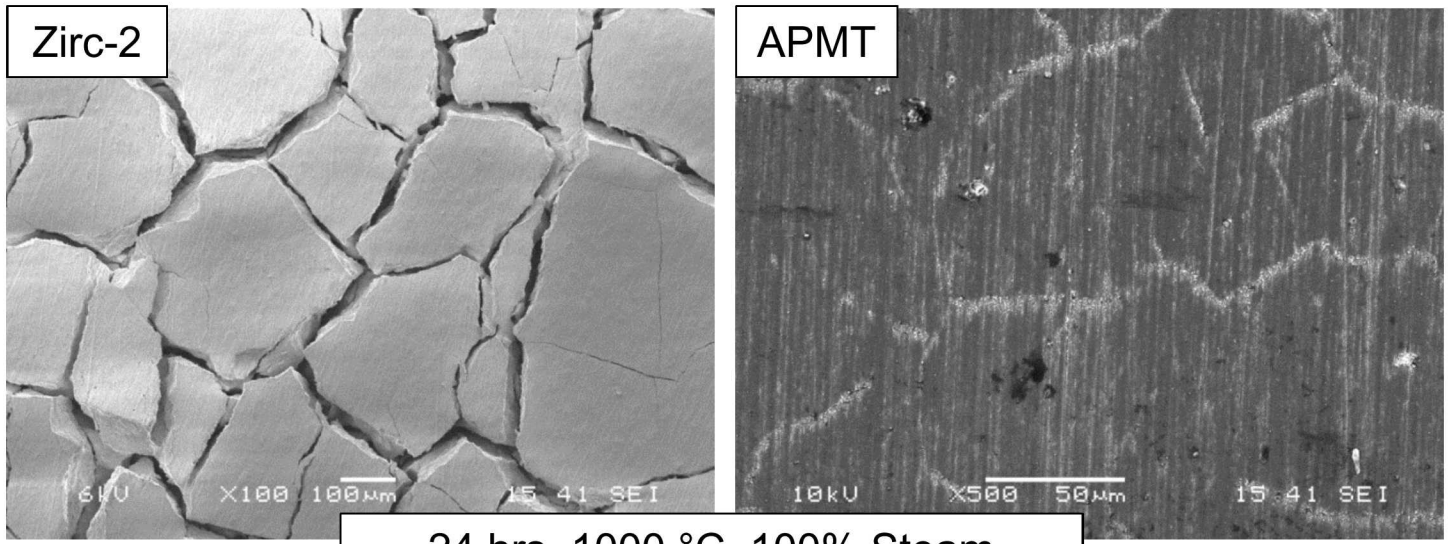

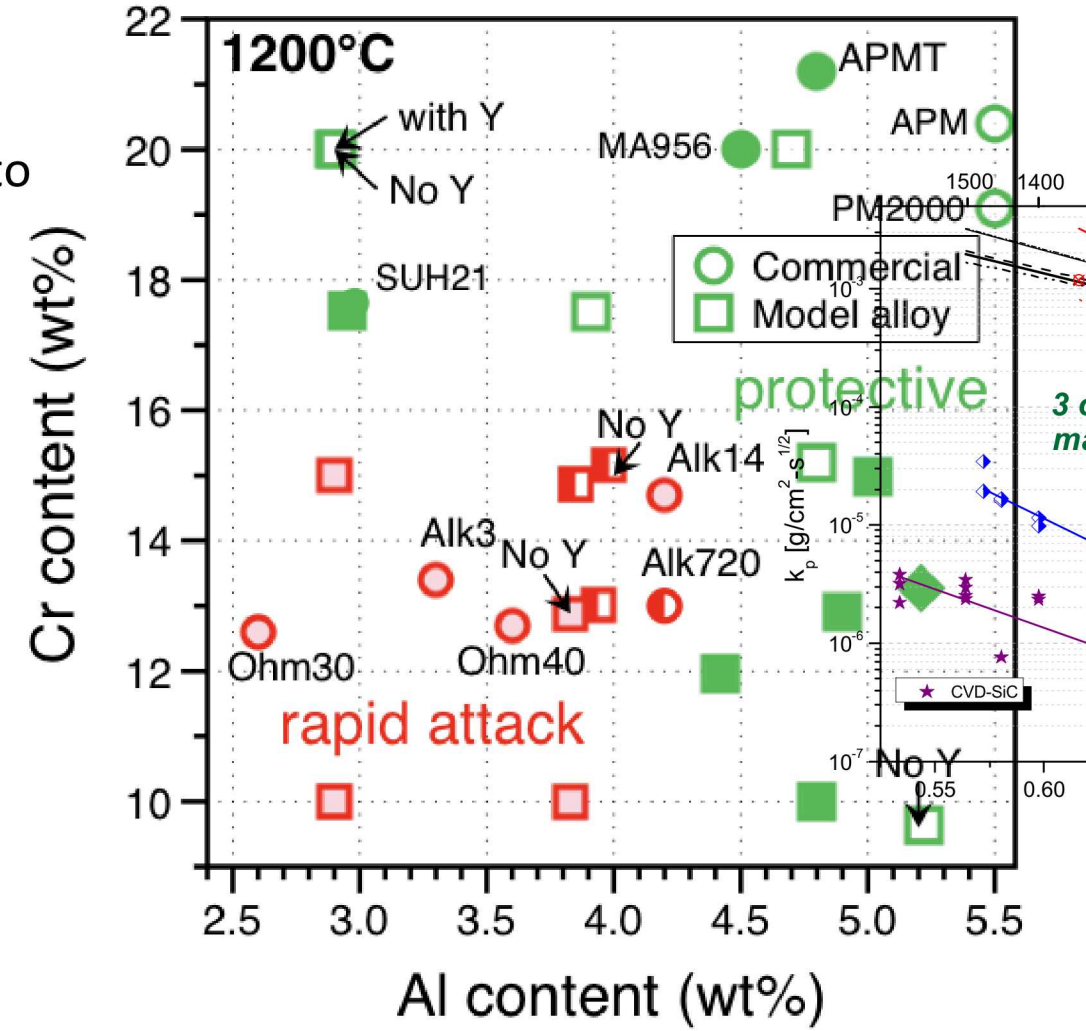

High temperature oxidation of model Fe-Cr-Al alloys exposed to steam at 1200 °C [1]

Images courtesy of Raul Rebak, GE Global Research

[1] Pint, B. A., Unocic, K. A., & Terrani, K. A. (2015). Effect of steam on high temperature oxidation behaviour of alumina-forming alloys. *Materials at High Temperatures*, *32*(1-2), 28–35.

Challenges for APT Analysis – Peak Deconvolution

- Overlapping peaks in the time-of-flight (TOF) spectrum need to be separated
  - Peak deconvolution is built into IVAS – based on natural isotopic abundances
  - Adjusted isotopic abundances generated using ORIGEN-2.2 Isotope Generation & Depletion software package[1]
  - Manually deconvolution can be performed on raw count info using calculated isotopic abundances following irradiation

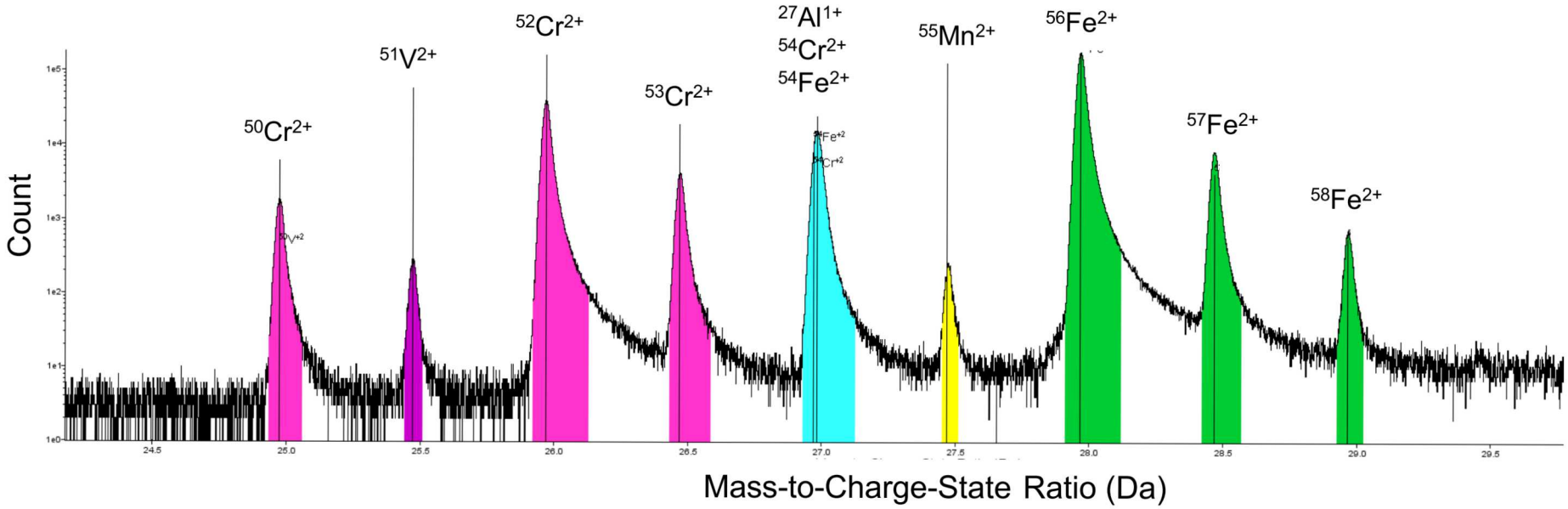

Adjusted isotopic abundances Generated by ORIGEN-2.2

Isotope	Nat. Abun.	Mod. Abun.
^{50}Cr	4.34%	3.69%
^{52}Cr	83.79%	83.68%
^{53}Cr	9.50%	8.52%
^{54}Cr	2.37%	4.11%
^{54}Fe	5.85%	5.71%
^{56}Fe	91.75%	89.32%
^{57}Fe	2.12%	4.52%
^{58}Fe	0.28%	0.36%
^{27}Al	100%	100%

[1] A.G. Croff, (2002). ORIGEN-2.2 [Computer software]. Retrieved from https://www.oecd-nea.org/tools/abstract/detail/ccc-0371

Challenges for APT Analysis – Aberration Artifacts

- Trajectory aberration effects are observed as regions of increased atomic density
  - Results in an artificial enrichment of Fe in the detected precipitate volume
  - Quantifying the magnitude of density variation allows for additional composition correction based on deviation from the expected atomic density

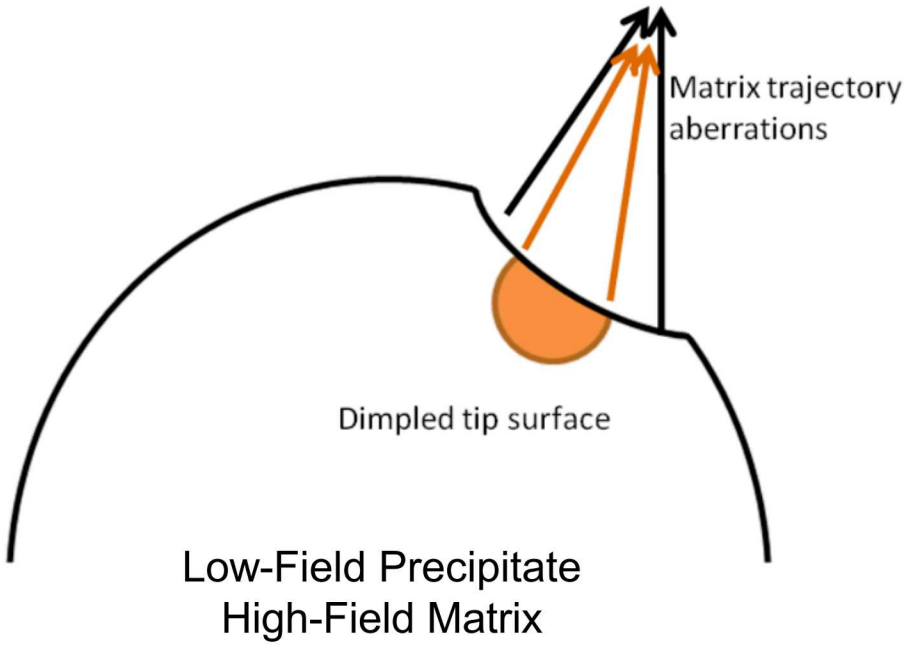

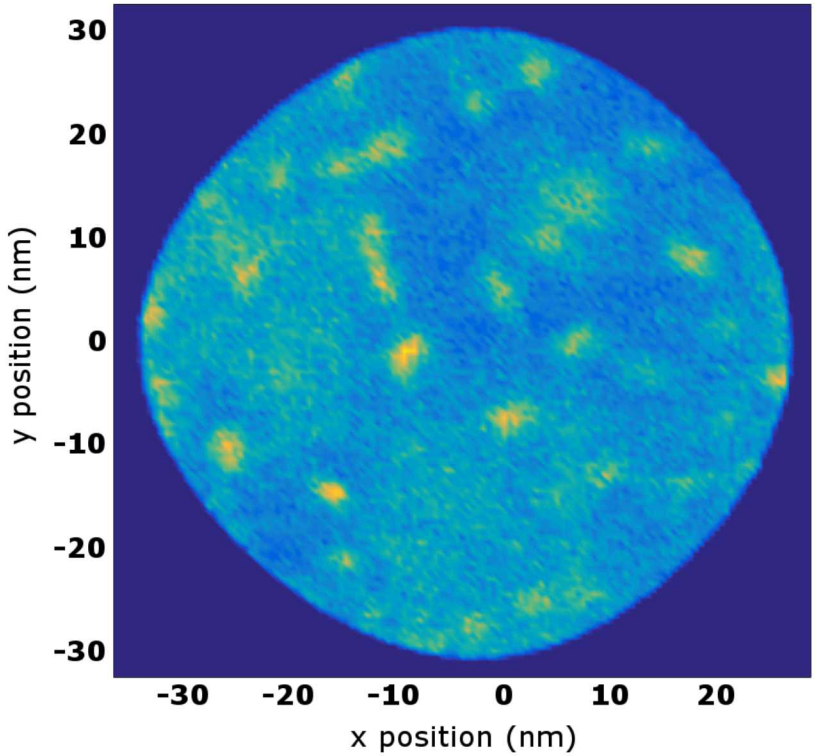

Atom Probe Tomography

- Destructive analysis – field evaporates atoms from cryo-cooled, sharp needle specimen using localized high voltage pulses coupled with focused laser pules
- Can reconstruct specimen geometry in 3D using ion time-of-flight (TOF) and position-sensitive detector – allows for detailed elemental analysis
- Most comprehensive α’ analysis method – yields data regarding phase morphology, distribution and composition

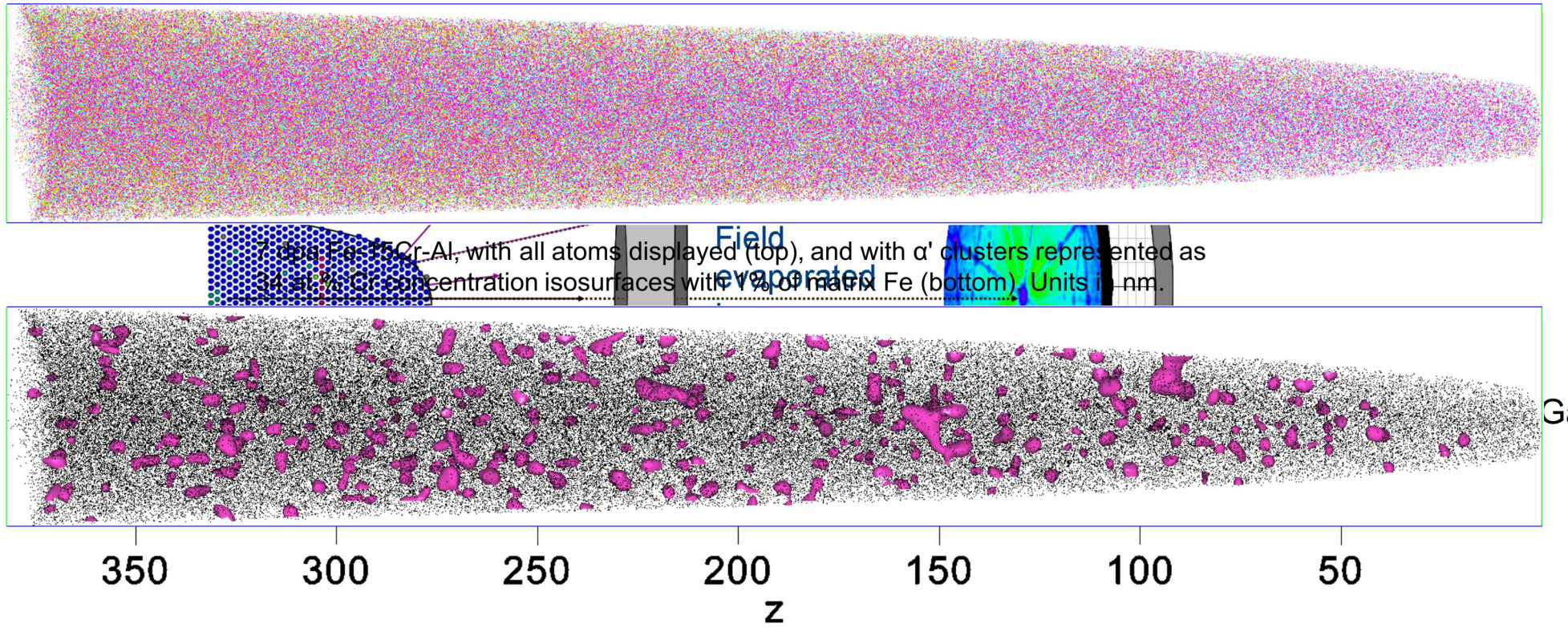

Application of Delaunay Triangulation Methods

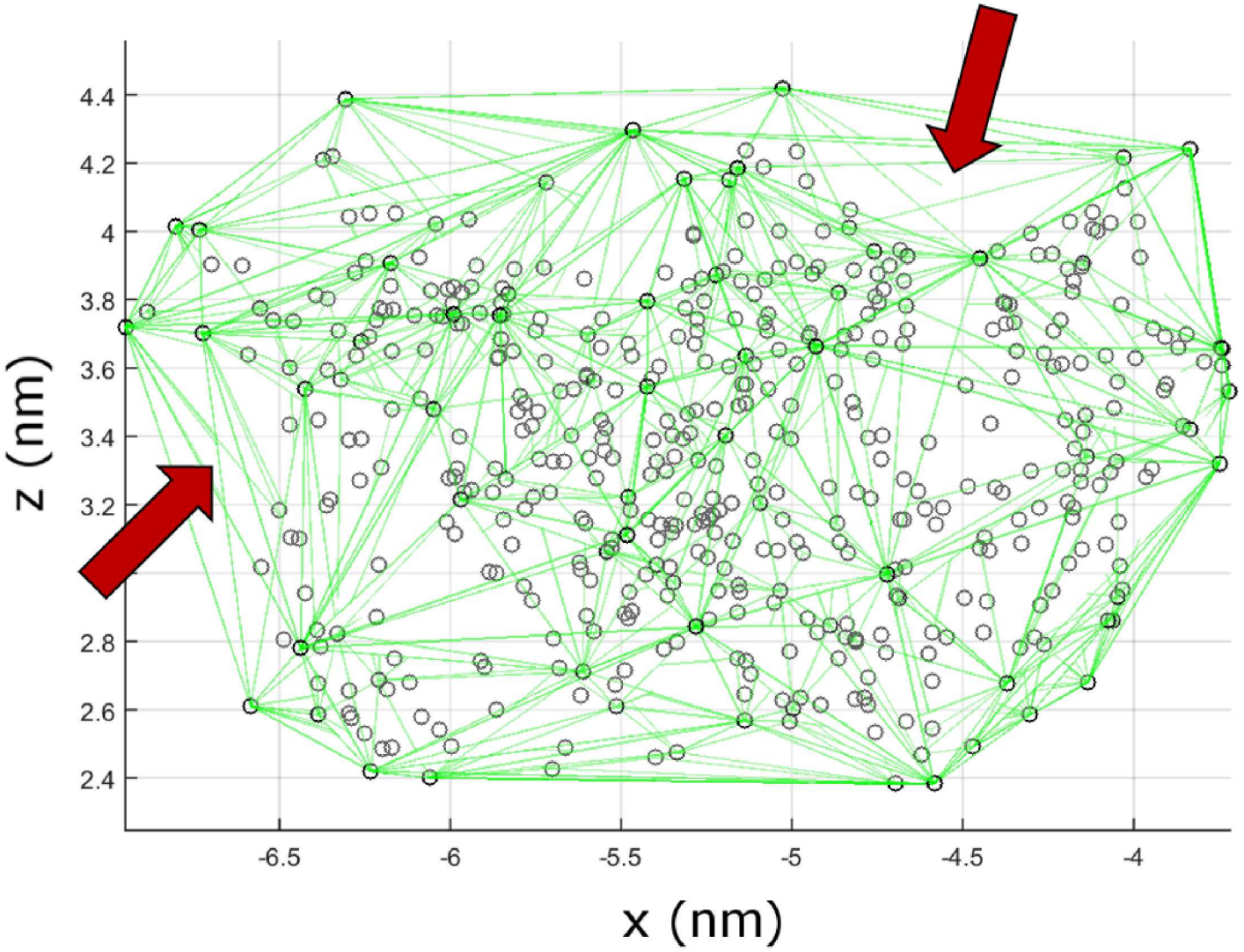

- Mesh cells “bridge” concave surfaces
- Overestimate cluster volume, underestimates cluster density, lower measured density ratio
- Correct by either:
  - Thresholding based on cell volume or Delaunay radius
  - Fitting to theoretical distribution

Application of Delaunay Triangulation Methods

- There exists a theoretical distribution for Delaunay circumsphere radii for a Delaunay triangulation of data resulting from a Poisson process (top right)

$$f(R_C) = \frac{32\pi^3\rho^3}{9} R_C{}^8 e^{-(4\pi\rho/3)R_C^3}$$

- Though randomness isn't a perfect assumption (lattice distances preserved), i is counter-balanced by imperfect spatial resolution of LEAP

- Reasonable fits are achieved to present data

- Density is able to be extracted analytically

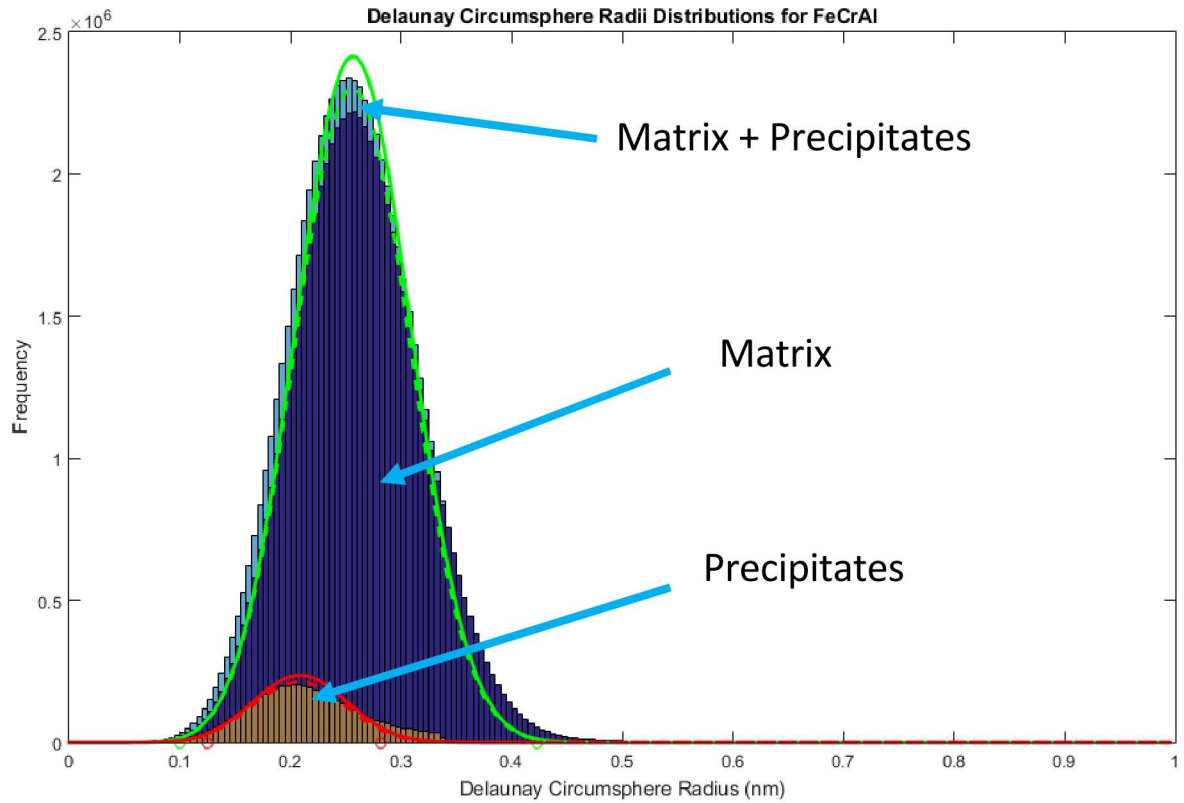

Lefebvre, W., Philippe, T., & Vurpillot, F. (2011). Application of Delaunay tessellation for the characterization of solute-rich clusters in atom probe tomography. *Ultramicroscopy*, *111*(3), 200–206. http://doi.org/10.1016/j.ultramic.2010.11.034

Summarized SANS Results for Fe-Cr-Al Alloys

Alloy	Irradiation Dose (dpa)	Irradiation Temp. (°C)	Number Density ($\times 10^{24}$ m^{-3})	Volume Fraction (%)	Average Radius (nm)
Fe-10Cr-9.3Al	0.8	355 ± 3.4	0.73	2.55	2.03
	1.8	382 ± 5.4	0.46	2.01	2.18
	7.0	320 ± 12.7	0.06	0.57	2.40
Fe-12Cr-8.7Al	0.3	334.5 ± 0.6	10.44	11.25	1.37
	1.8	382 ± 5.4	5.81	14.91	1.83
	7.0	320 ± 12.7	0.94	3.81	2.13
Fe-15Cr-7.7Al	0.3	334.5 ± 0.6	46.81	30.61	1.16
	1.8	382 ± 5.4	7.57	18.81	1.81
	7.0	320 ± 12.7	2.27	9.39	2.15
Fe-18Cr-5.8Al	0.8	355 ± 3.4	18.89	27.79	1.52
	1.8	382 ± 5.4	6.64	17.61	1.85
	7.0	320 ± 12.7	1.34	9.08	2.53

- Scattering contrast for specimens not analyzed by APT determined via extrapolation
- Trends from APT mostly preserved

Full SANS/EFTEM Comparison

Specimen ID	Irradiation Temp. (°C)	Number Density ($x10^{23}$ #/m^3)			Volume Fraction (%)			A-ratio (unitless)		Mean Radius (nm)		
		SANS MD	SANS Monte Carlo	EFTEM	SANS MD	SANS Monte Carlo	EFTEM	SANS MD	SANS Monte Carlo	SANS MD	SANS Monte Carlo	EFTEM
OD34	-	2.14±0.82	2.78±0.87	-	1.07±0.40	1.24±0.35	-	1.75±0.05	2.75±0.54	2.3±0.1	2.2±0.1 (unimodal)	-
OD01	195	5.02±2.80	1.54±0.54	1.04±0.24	0.96±0.45	1.01±0.33	0.43±0.28	1.31±0.08	2.06±0.37	1.7±0.2	2.5±0.1 (bimodal)	1.03±0.87
OD03	363	2.09±0.68	1.97±0.60	0.94±0.14	1.12±0.36	1.14±0.32	0.43±0.26	1.63±0.03	2.51±0.48	2.3±0.1	2.4±0.1 (unimodal)	1.27±0.90
OD06	559	1.39±0.80	1.89±0.61	0.49±0.34	0.72±0.41	1.24±0.37	1.56±1.93	1.96±0.11	2.32±0.40	2.3±0.1	2.5±0.1 (unimodal)	1.40±1.61

Experimental Goals

- Assess severity of α’ precipitation in neutron-irradiated model Fe-Cr-Al alloys using a correlative microscopy approach
  - Investigate how precipitation behavior varies with composition
  - Study evolution of precipitate morphology with dose
  - Determine effect of Al additions compared to binary Fe-Cr systems
  - Assist in developing structure/property relationships for radiation-induced hardening and embrittlement

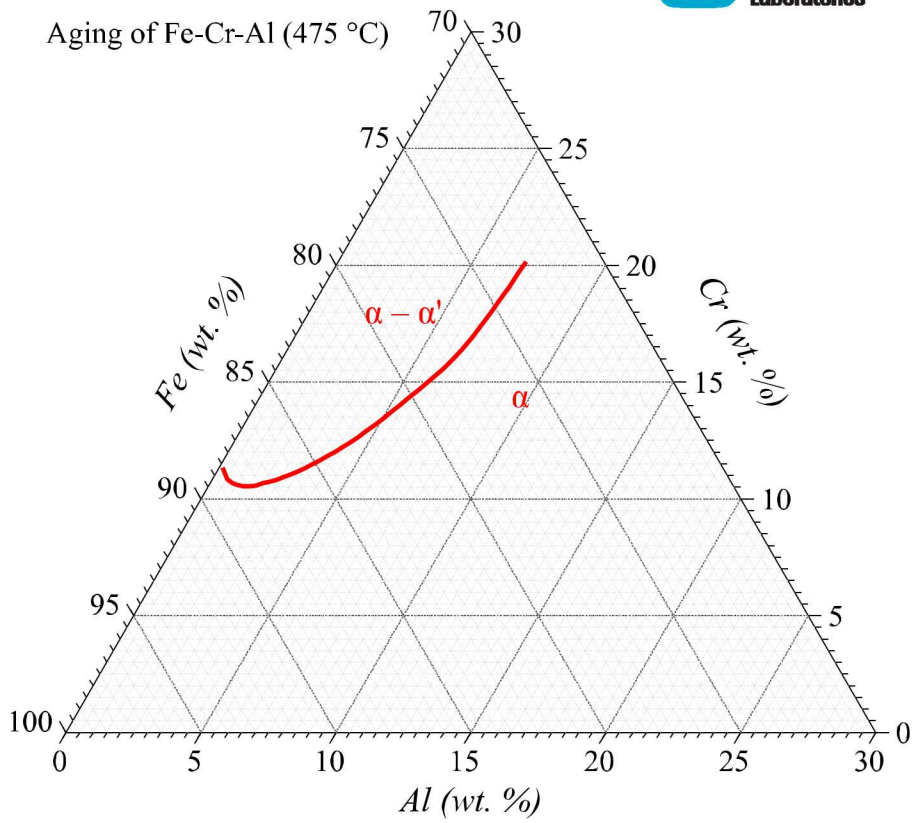

Ternary Fe-Cr-Al phase diagram showing destabilization of α' phase by bulk Al additions[1]

- **Develop a mechanistic understanding of the factors that influence precipitation in this alloy system in order to make informed design decisions regarding Fe-Cr-Al for accident-tolerant fuel cladding applications**

FCAY and FCAT Rabbits

PURPOSE: rapid screening of alloy irradiated tensile properties and microstructure

Specifications:

- SS-J2 and SS-2E flat sheet tensile specimen geometries
- Design temperatures of 200-550˚ C
  - Temperature monitored passively using SiC thermometry
- Modular; can accept any ratio of SS-J2 to SS-2E specimen configurations
- Robust, proven design over the past 4+ years

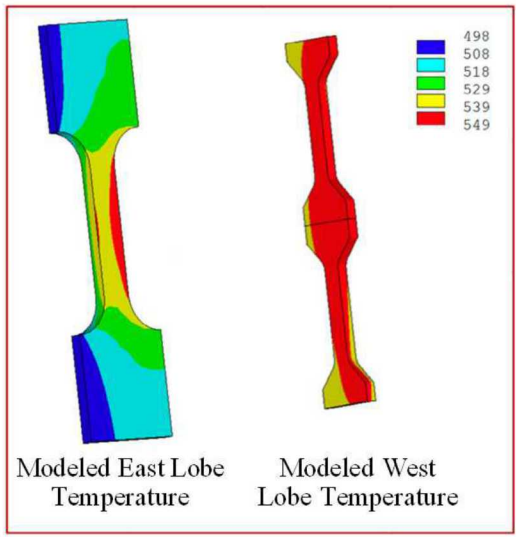

Example of specimen temperature gradients for 550°C irradiation

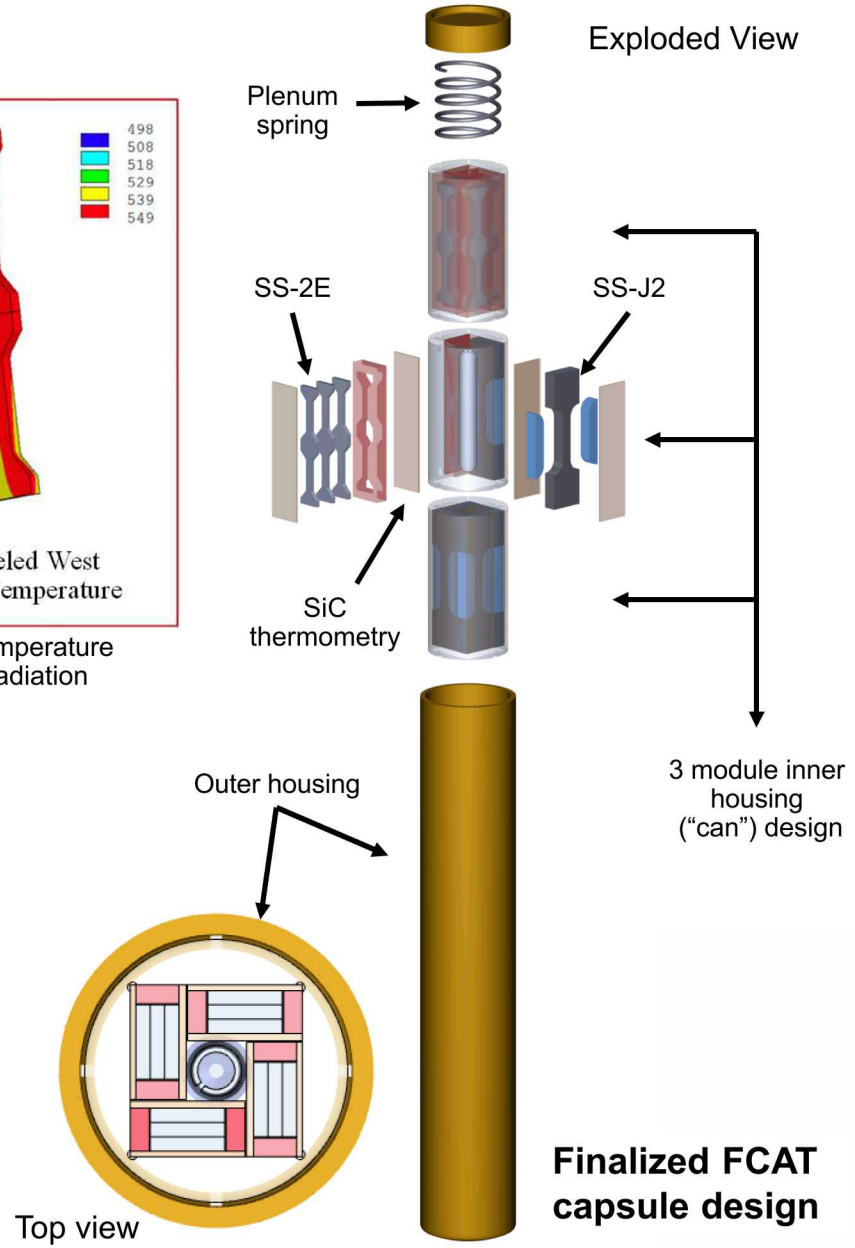

Finalized FCAT capsule design

FCAY and FCAT Rabbits

- Alloys studied:
  1. Model alloys (M): F1C5AY, B125Y, B154Y-2, B183Y-2
  2. Engineering grade alloys (E): C06M, C35M, C36M, C37M, C35MN, C35M10TC
  3. Commercial alloys (C): Kanthal APMT™, and Alkrothal 720
  4. ODS Alloys (O): 125YF

Capsule ID	Number Samples	Alloys	Exposure Time (hrs)	Neutron Flux (n/cm^{2}s) E > 0.1 MeV	Neutron Fluence (n/cm^2) E > 0.1 MeV	Dose Rate (dpa/s)	Dose (dpa)	Irradiation Temperature (°C)
FCAY-01	36	M+C	120	8.54×10^{14}	3.69×10^{20}	7.7×10^{-7}	0.3	334.5 ± 0.6
FCAY-02	36	M+C	301	8.54×10^{14}	9.25×10^{20}	7.7×10^{-7}	0.8	355.1 ± 3.4
FCAY-03	36	M+C	614	8.84×10^{14}	1.95×10^{21}	8.1×10^{-7}	1.8	381.9 ± 5.4
FCAY-04	36	M+C	2456	8.74×10^{14}	7.73×10^{21}	7.9×10^{-7}	7.0	319.9 ± 10.2
FCAY-05	36	M+C	4914	8.74×10^{14}	1.55×10^{22}	7.8×10^{-7}	13.8	340.5 ± 25.7
FCAT-01	45	E+O	548	1.10×10^{15}	2.17×10^{21}	9.6×10^{-7}	1.9	194.5 ± 37.9
FCAT-02	45	E+O	548	1.04×10^{15}	2.05×10^{21}	9.1×10^{-7}	1.8	362.7 ± 21.2
FCAT-03	45	E+O	548	1.10×10^{15}	2.17×10^{21}	9.6×10^{-7}	1.9	559.4 ± 28.1
FCAT-04	45	E+O	1754	1.10×10^{15}	9.32×10^{21}	9.6×10^{-7}	8.3	200*
FCAT-05	45	E+O	1754	1.04×10^{15}	8.81×10^{21}	9.1×10^{-7}	7.9	330*
FCAT-06	45	E+O	1754	1.10×10^{15}	9.32×10^{21}	9.6×10^{-7}	8.3	550*
FCAT-07	45	E+O	4032	1.10×10^{15}	1.82×10^{22}*	9.6×10^{-7}	16.3*	200*
FCAT-08	45	E+O	4032	1.04×10^{15}	1.73×10^{22}*	9.1×10^{-7}	15.4*	330*
FCAT-09	45	E+O	4032	1.10×10^{15}	1.82×10^{22}*	9.6×10^{-7}	16.3*	550*

*Target values

Note on Representation of APT Data

Left: 30 at.% Cr Concentration Isosurfaces

Center: Clusters from Maximum Separation Method

Right: Indexed Clusters from Max. Separation Method, 2 at.% Fe Matrix

- Variation in precipitate composition makes concentration isosurfaces not representative of measured cluster properties between conditions
- Indexed cluster diagrams allow for quantified precipitates to be easily distinguished

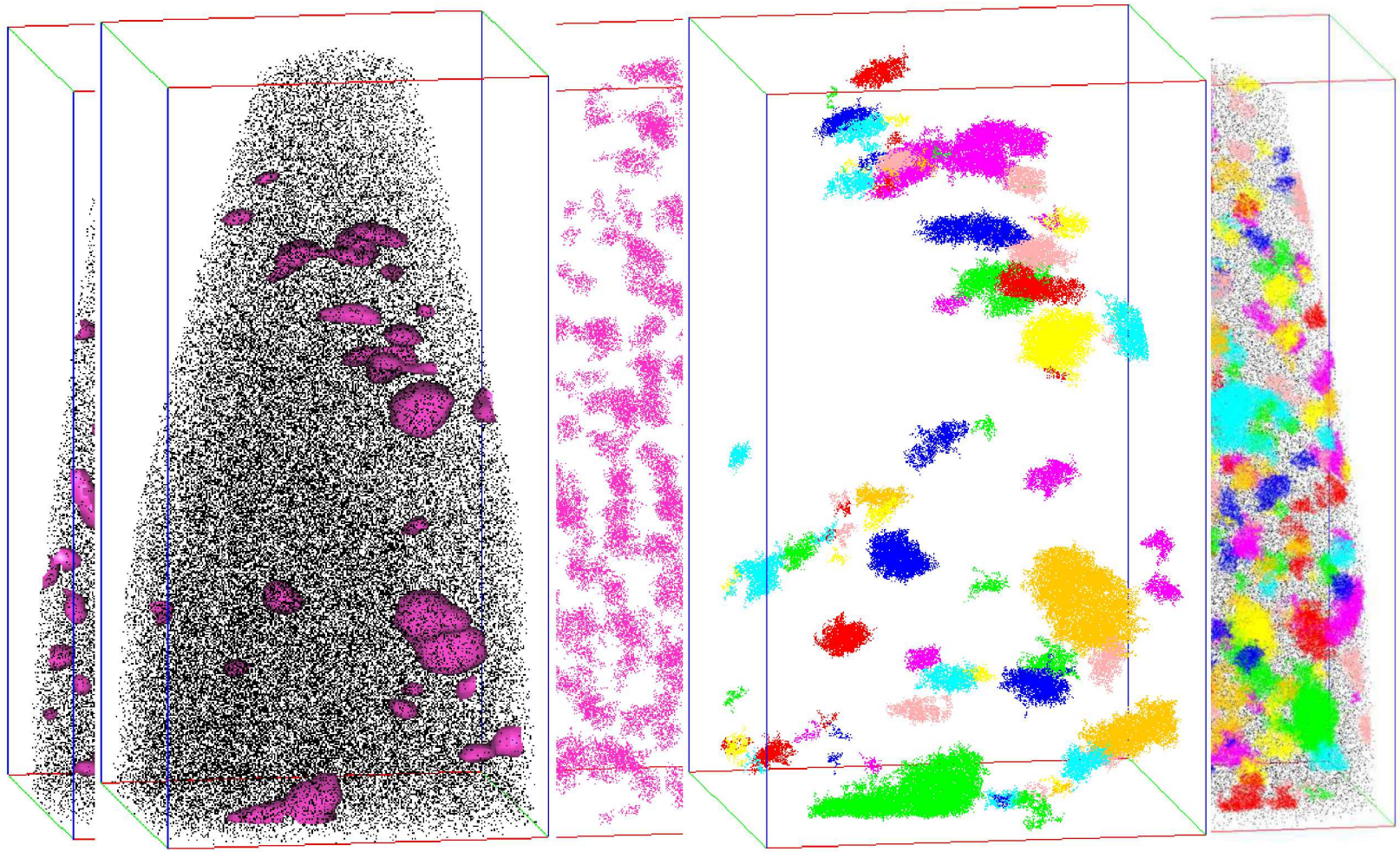

Fe-10Cr-9.8Al, 7 dpa, 320°C

Increasing Dose

Fe-18Cr-5.8Al

0.8 dpa, 355ºC	1.8 dpa, 382ºC	7 dpa, 320ºC
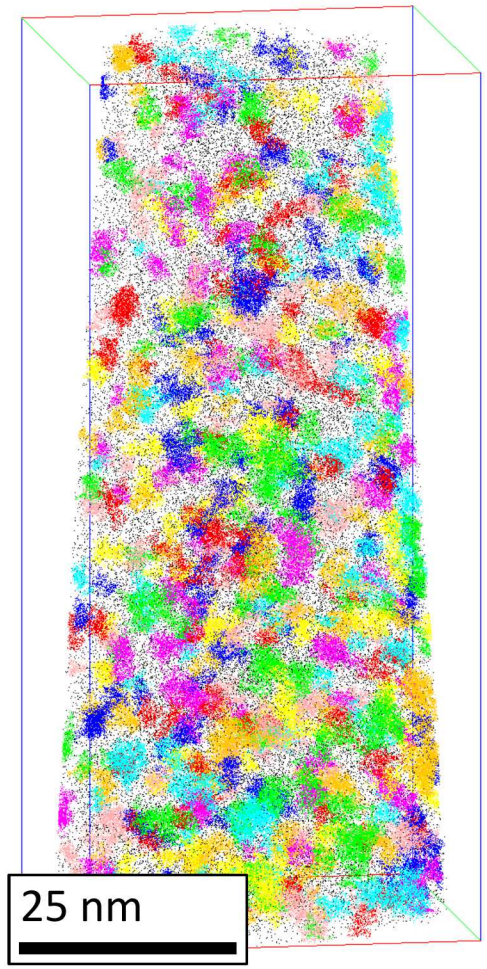	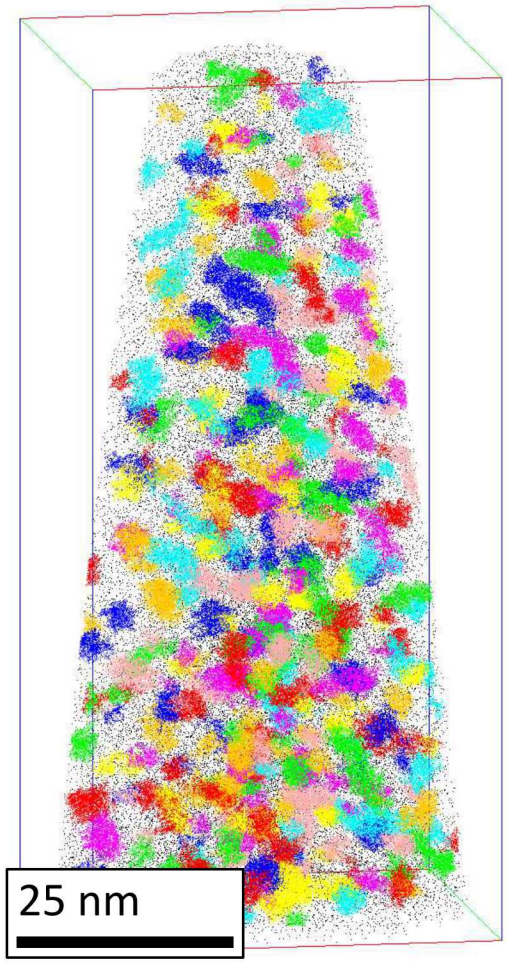	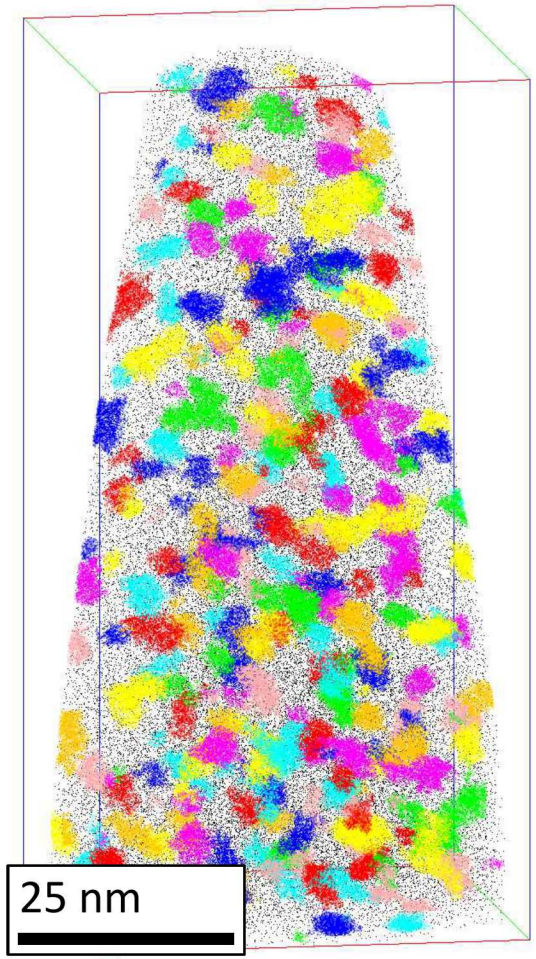
Total Volume Analyzed: 1.68×10^6 nm^3	Total Volume Analyzed: 1.16×10^6 nm^3	Total Volume Analyzed: 7.53×10^5 nm^3

Reconstructions cropped to 50x50x100 nm

Increasing Dose

Cr Atom Maps (40nm × 40nm × 20nm)

As-Received **0.8 dpa, 355ºC** **1.8 dpa, 382ºC** **7 dpa, 320ºC**

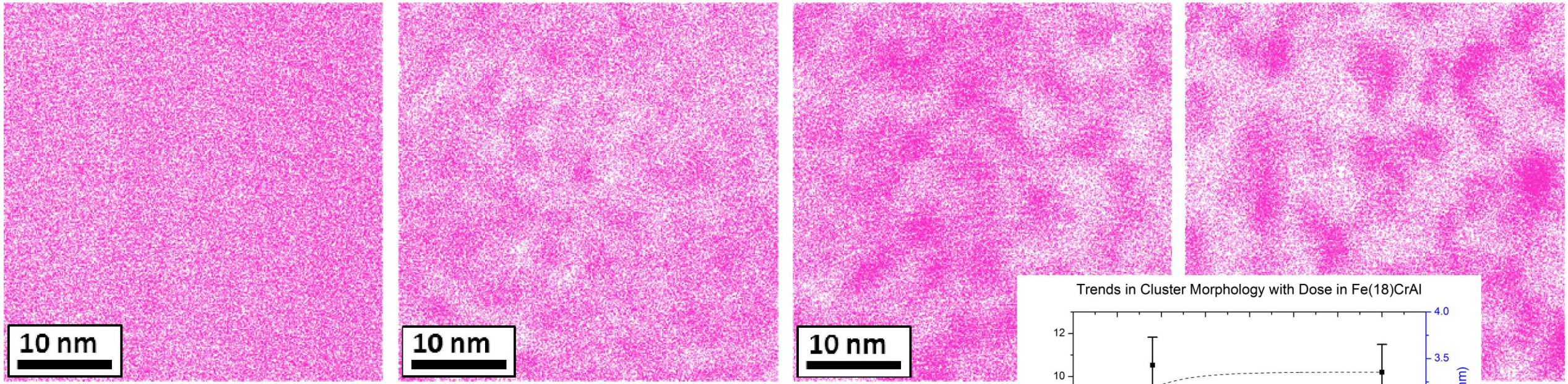

Fe-18Cr-5.8Al

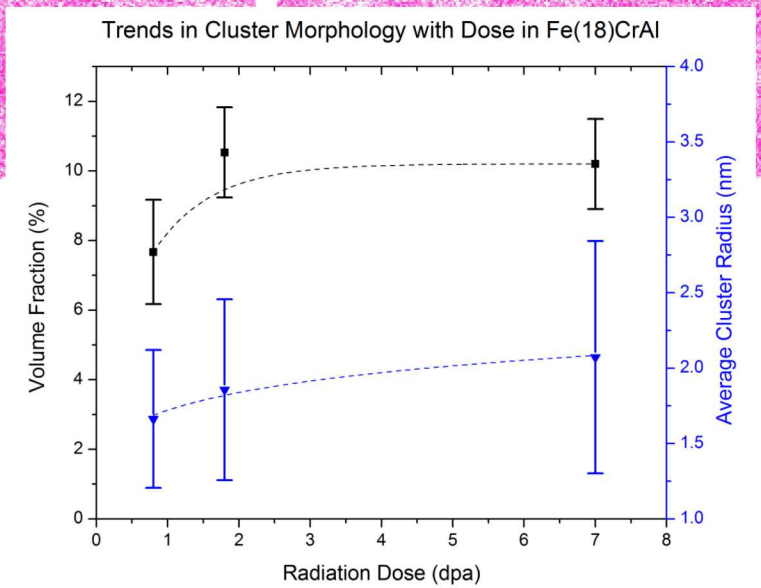

Key observations of dose evolution

- Precipitation observed in all irradiated specimens
- ↑ dpa leads to ↑ avg. cluster size, ↓ cluster number density
- Volume fraction saturates early, clusters continue to coarsen

Increasing Cr, Decreasing Al

Cr Atom Maps (40nm × 40nm × 20nm)

7dpa Fe-10Cr-9.3Al

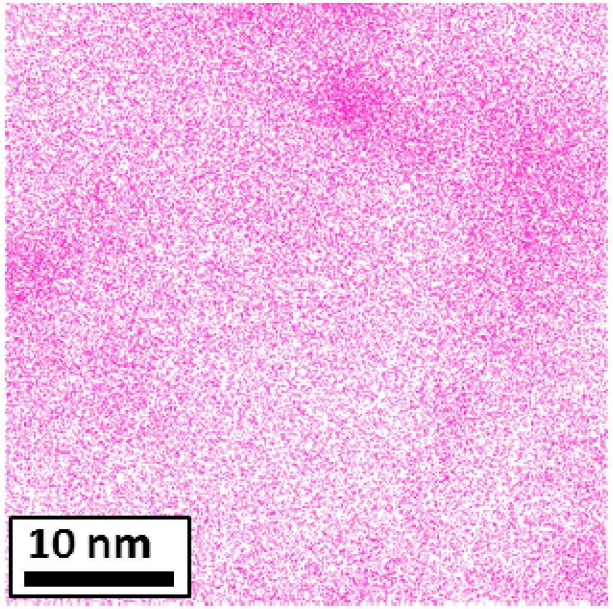

7dpa Fe-12Cr-8.7Al

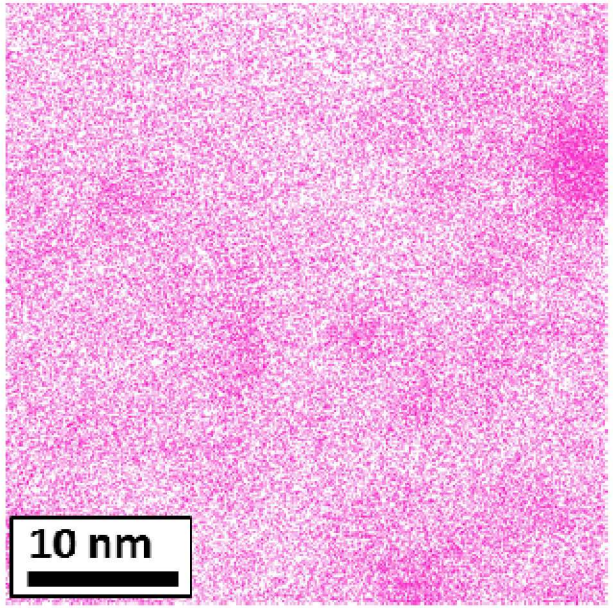

7dpa Fe-15Cr-7.7Al

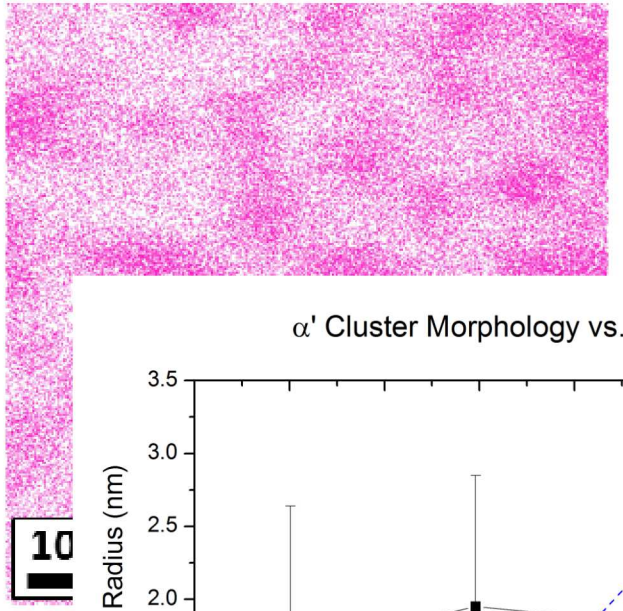

7dpa Fe-18Cr-5.8Al

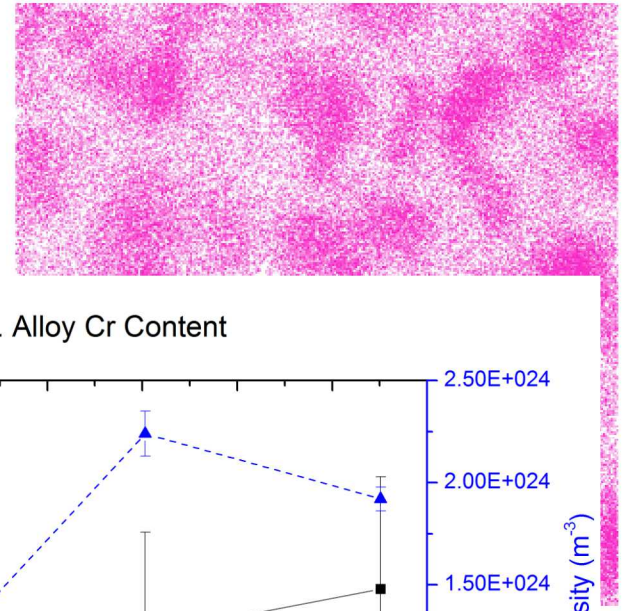

Key observations of composition dependence

- Precipitation in all compositions studied
- Volume fraction increases with increasing Cr
- ↑ Cr generally leads to ↑ cluster number density
- Large distribution of cluster sizes
- Al additions reduce Cr concentration of precipitates

Comparing APT & SANS

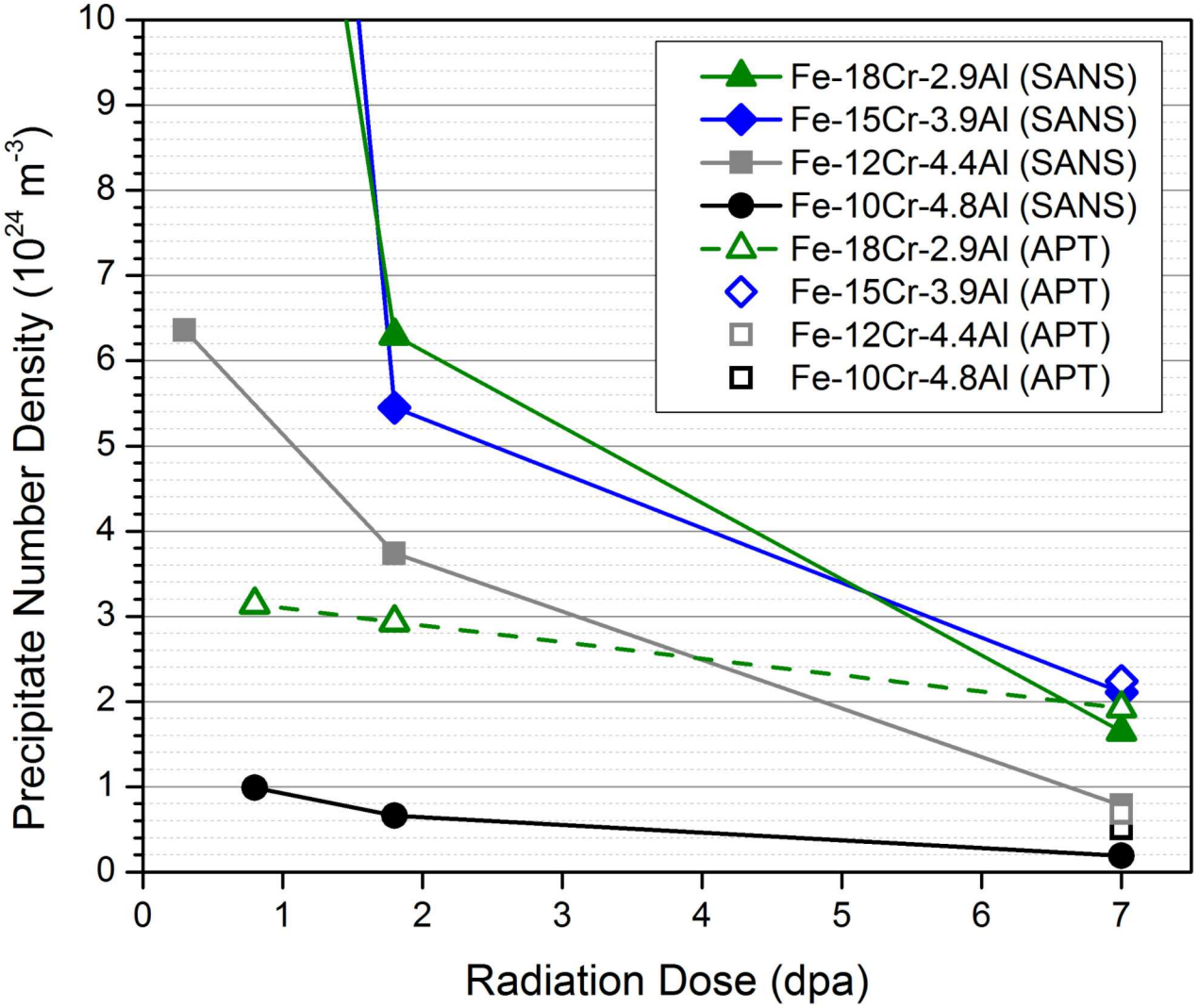

- Scattering contrast for specimens not analyzed by APT determined via extrapolation
- Trends from APT mostly preserved
  - Number density decreases with dose
  - Higher Cr content results in increased number density

Comparing APT & SANS

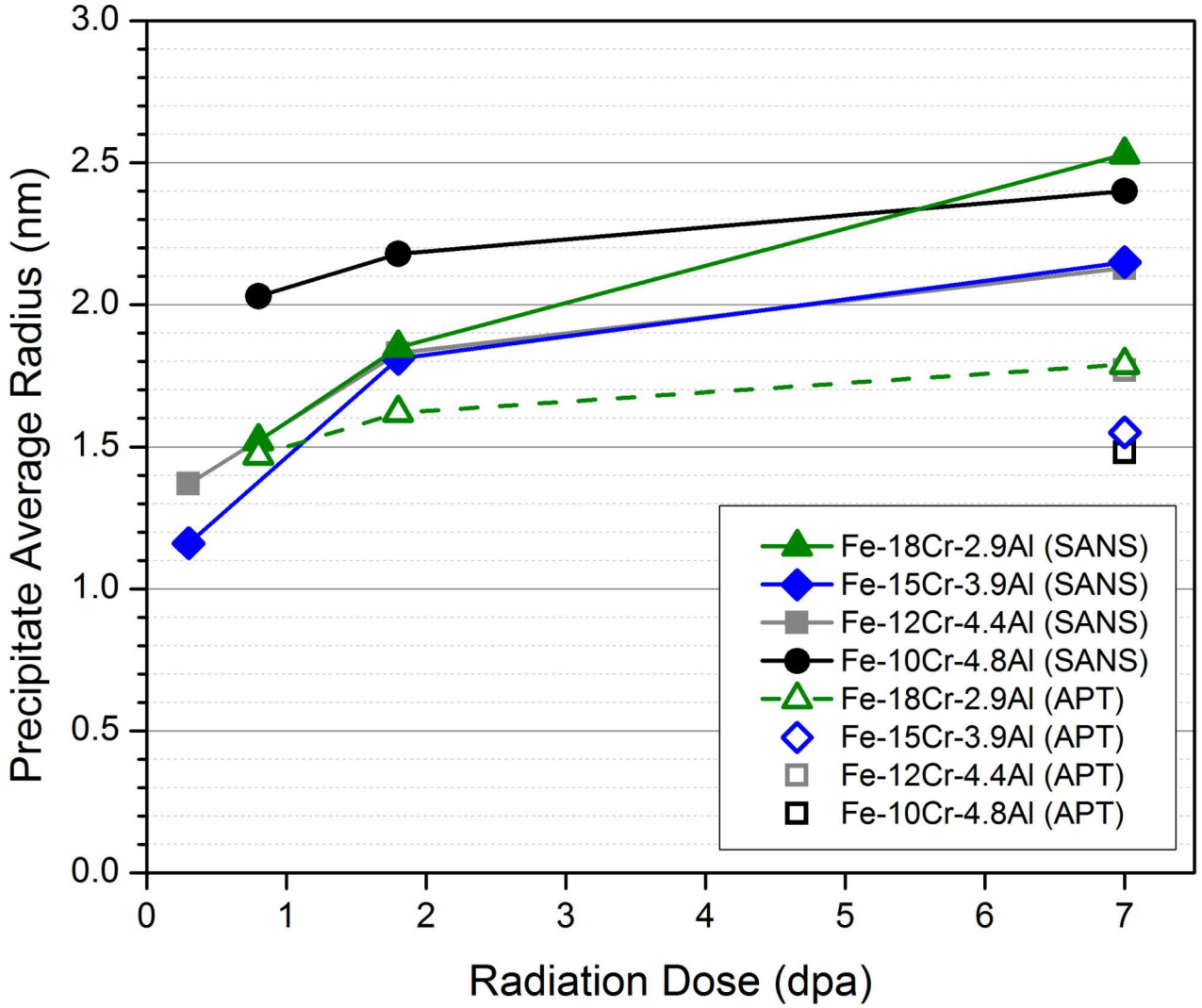

- Scattering contrast for specimens not analyzed by APT determined via extrapolation
- Trends from APT mostly preserved
  - Radius increases with dose as precipitates coarsen

Comparing APT & SANS

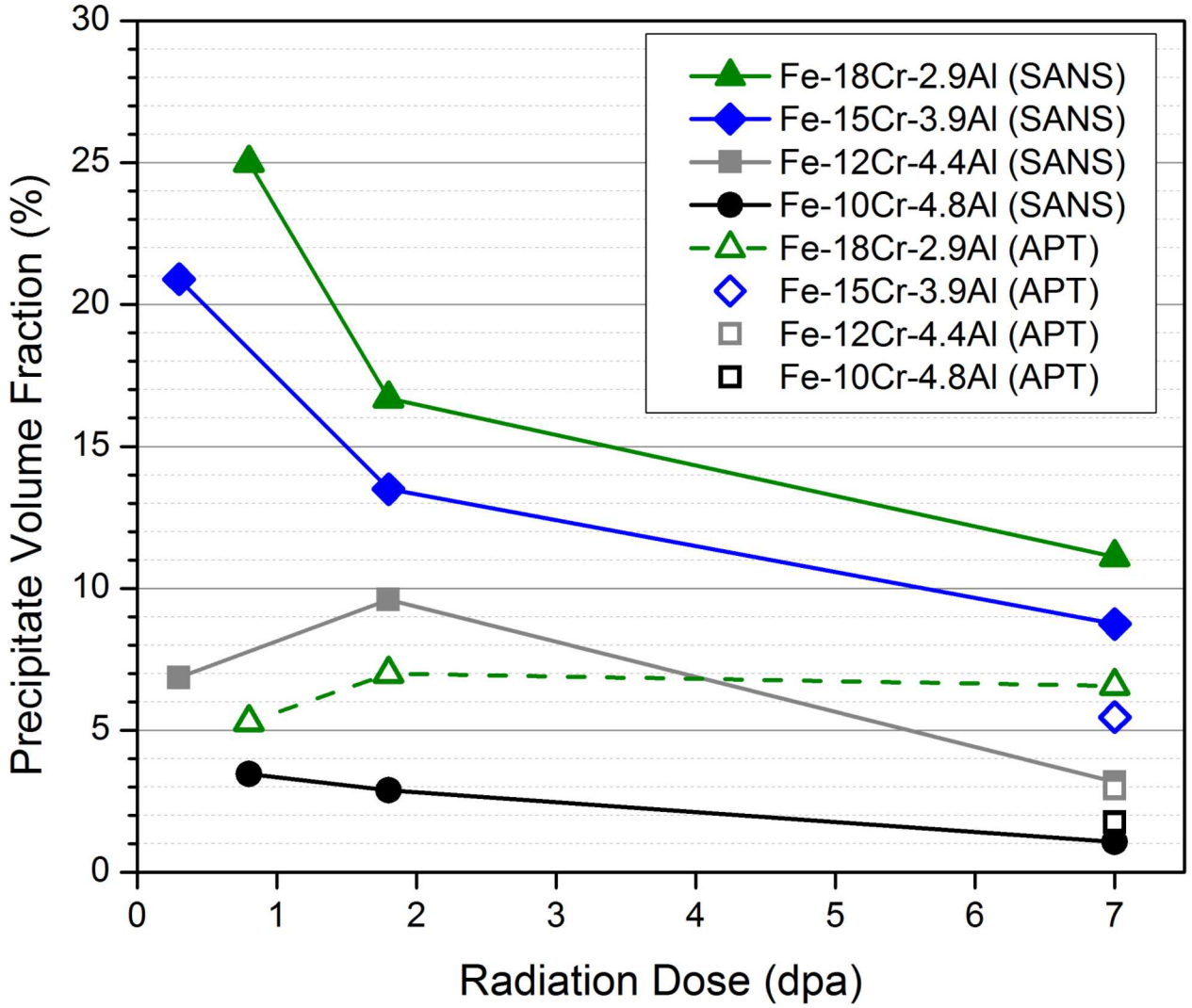

- Scattering contrast for specimens not analyzed by APT determined via extrapolation
- Trends from APT mostly preserved
  - Expect volume fraction to increase to saturation (APT data), not to decrease with dose
  - Trends with Cr content match
  - Attempting to reconcile by including polydispersity in the SANS model

Discussion – APT & SANS Correlation

- Despite significant effort, discrepancies remain in SANS & APT results arising from a variety of potential sources of error:
  - Different physical resolution limits
  - Artifacts in data due to aberrations (APT) or magnetic scattering effects (SANS)
  - Uncertainty in compositions/scattering length densities
  - Potentially oversimplifying assumptions in models used to fit SANS data

Discussion – LSW/UOKV Models for Precipitate Evolution

- Lifshitz, Slyozov, and Wagner (LSW) developed seminal model for diffusion-limited coarsening in binary alloys
- Umantsev, Olson, Kuehmann, and Voorhees (UOKV) extended this model to ternary systems
- Ultimately describes precipitate coarsening with aging time using a series of power laws:

$$\overline{R}_{\alpha'}(t) = K_R t^{1/3}$$

$$N_{\alpha'}(t) = K_N t^{-1}$$

$$\Delta C(t) = K_C t^{-1/3}$$

- Assumes:
  - spherical precipitates and constant volume fraction
  - terminal phase states are dilute solutions
  - stress-free matrix
  - negligible interparticle interactions

- Due to uncertainty in instantaneous and equilibrium phase compositions, we will focus on the first two relationships using the SANS data